Pro gradu -tutkielma, teoreettinen fysiikka
Examensarbete, teoretisk fysik
Master's thesis, theoretical physics

Various Aspects of Holographic Entanglement Entropy and Mutual Information

Jarkko Järvelä
2014-04-07

Ohjaaja | Handledare | Advisor
Esko Keski-Vakkuri

Tarkastajat | Examinatorer | Examiners
Kari Rummukainen
Esko Keski-Vakkuri

HELSINGIN YLIOPISTO
FYSIIKAN LAITOS

HELSINGFORS UNIVERSITET
INSTITUTIONEN FÖR FYSIK

UNIVERSITY OF HELSINKI
DEPARTMENT OF PHYSICS

HELSINGIN YLIOPISTO — HELSINGFORS UNIVERSITET — UNIVERSITY OF HELSINKI

Tiedekunta/Osasto — Fakultet/Sektion — Faculty	Laitos — Institution — Department
Faculty of Science	Department of Physics

Tekijä — Författare — Author
Jarkko Järvelä

Työn nimi — Arbetets titel — Title

Various Aspects of Holographic Entanglement Entropy and Mutual Information

Oppiaine — Läroämne — Subject
Theoretical physics

Työn laji — Arbetets art — Level	Aika — Datum — Month and year	Sivumäärä — Sidoantal — Number of pages
Master's thesis	April 2014	100

Tiivistelmä — Referat — Abstract

Entanglement entropy is a proposal to quantify quantum entanglement of two disjoint regions in a pure system. It is a relatively new topic and is developing rapidly. The current main motives to study it are its applications to studying quantum gravity, thermalization and phase transitions in condensed matter systems. Mutual information is a related quantity and it can be used to measure the amount of information two disjoint regions share.

The purpose of this thesis is to give an introduction to the general results of the field without considering specific systems. The two prominent approaches used are two-dimensional conformal field theory and the holographic entanglement entropy conjecture. The first approach is to calculate entanglement entropy using conformal field theory, the results of which are known to be exact although technically more difficult to derive and only available for $1+1$ dimensional systems. Both static and dynamic systems will be discussed. The results are reproduced and generalized to higher dimensions using holography. As a more recent topic, the holographic approach is used to rederive the entanglement entropy of systems with a Fermi surface using AdS/Vaidya metric with Lifshitz scaling and hyperscaling violation.

The final chapter of the thesis discusses mutual information in various static and dynamic cases considered in the previous chapters. For the first time, the evolution of mutual information is calculated in AdS/Vaidya metric with Lifshitz scaling and hyperscaling violation in the critical $\theta = d - 1$ case.

Avainsanat — Nyckelord — Keywords
holography, entanglement entropy, mutual information

Säilytyspaikka — Förvaringsställe — Where deposited
Kumpula campus library

Muita tietoja — övriga uppgifter — Additional information

HELSINGIN YLIOPISTO — HELSINGFORS UNIVERSITET — UNIVERSITY OF HELSINKI

Tiedekunta/Osasto — Fakultet/Sektion — Faculty	Laitos — Institution — Department
Matemaattis-luonnontieteellinen tiedekunta	Fysiikan laitos

Tekijä — Författare — Author
Jarkko Järvelä

Työn nimi — Arbetets titel — Title

Various Aspects of Holographic Entanglement Entropy and Mutual Information

Oppiaine — Läroämne — Subject
Teoreettinen fysiikka

Työn laji — Arbetets art — Level	Aika — Datum — Month and year	Sivumäärä — Sidoantal — Number of pages
Pro gradu -tutkielma	Huhtikuu 2014	100

Tiivistelmä — Referat — Abstract

Lomittumisentropia on yksi ehdotetuista tavoista mitata puhdastilasysteemin kahden osan välistä lomittumista. Aihe on verrattain tuore ja kehittyy nopeasti. Suurimmat syyt sen kiinnostavuudelle ovat sen sovellukset kvanttigravitaation, termalisaation ja tiiviin aineen systeemien faasimuunnoksen tutkimukseen. Keskinäisinformaatio on lomittumisentropiasta johdettu suure, joka nimensä mukaisesti mittaa, kuinka paljon yhteistä informaatiota kahden systeemin välillä on.

Tutkielman tarkoituksena on toimia johdatuksena alan yleisiin perustuloksiin paneutumatta liikaa yksittäisiin esimerkkeihin. Tärkeimmät työkalut ovat kaksiulotteinen konformikenttäteoria ja holografisen lomittumisentropian konjektuuri. Aiheen käsittely alkaa lomittumisentropian laskemisella konformikenttäteorioissa sekä ajasta riippumattomissa että riippuvissa systeemeissä, joiden tulokset ovat eksakteja, joskin teknisesti vaikeita, ja rajoittuvat avaruudellisesti yksiulotteisiin systeemeihin. Vastaavat tulokset johdetaan uudestaan holografisesta näkökulmasta ja yleistetään useampiulotteisiin systeemeihin. Tuoreempana lähestymistapana esitetään tapa johtaa Fermi-pintaisten kriittisten systeemien lomittumisentropia käyttämällä AdS/Vaidya-metriikka, johon on lisätty Lifshitz-skaalaus ja hyperskaalauksen rikkoutuminen.

Viimeinen luku käytetään keskinäisinformaation käsittelyyn aiemmissa luvuissa käsitellyissä systeemeissä. Uutena tuloksena määritetään keskinäisinformaation aikakehitys Lifshitz-skaalautuvassa ja hyperskaalausta rikkovassa AdS/Vaidya-metriikassa, jossa hyperviolaatioparametri on kriittinen, $\theta = d - 1$.

Avainsanat — Nyckelord — Keywords
holografia, lomittumisentropia, keskinäisinformaatio

Säilytyspaikka — Förvaringsställe — Where deposited
Kumpulan kampuskirjasto

Muita tietoja — övriga uppgifter — Additional information

Contents

Acknowledgements

Four years as a student is a long time and it definitely has left its mark on me. I have had the opportunity to meet various wonderful people without whom I would not be the person I am nor would I have reached this point. Thus, I feel that I must express my gratitude to some of these people.

First and foremost, I wish to thank my advisor, Esko Keski-Vakkuri, for introducing me to the subject of entanglement entropy and for his swift action when it was truly needed. Even more, I am happy to have shared many intriguing discussions with him and have him as my mentor. I cannot go without thanking Professor Kari Rummukainen for examining this thesis and also for the many illuminating discussions we have had.

For smaller contributions, I thank Lasse Franti for helping me understand some of the concepts in this thesis and sharing his code with which I calculated the results in the final chapter. I also thank Markus Hauru for helping me nail the graphical appearance of this thesis.

As James Howell put it, "All work and no play makes Jack a dull boy". Therefore, I wish to thank all of the friends I have made during these years. First, I thank my friends at Hiekkalaatikko for the numerous interesting debates and the even more numerous laughs we have shared. I also believe that the past years would not have been as enjoyable were it not for all the student organisations at the Kumpula campus, especially Resonanssi. Also, I thank my family for being the best family I could have had.

Last but definitely not the least, I thank Katriina for putting up with me and sharing many adventures with me.

Chapter 1

Introduction

1.1 The story so far

In the early 1970s, the role of black holes in thermodynamics of the universe was a puzzle for physicists. It was Jacob Bekenstein, who made the daring suggestion that the entropy of a black hole was proportional to the area of its event horizon,

$$S = \frac{A_{BH}}{4G_N}, \tag{1.1}$$

where A_{BH} is the area of the event horizon and G_N is the gravitational constant [1]. This relation is counterintuitive since entropy is usually proportional to the size, i.e. volume, of the system. As usual, the idea was met with reluctance at first. It was only after Stephen Hawking published his well-known results, which revealed that black holes should emit thermal black body radiation with a well defined temperature, that the idea of black hole entropy became accepted [2]. A later paper by 't Hooft, where he considered the entropy of the radiated particles, supported the idea of entropy being proportional to the area of the event horizon. 't Hooft also encountered a problem with UV divergence and he had to regulate the calculation by excluding the particles very close to the horizon [3].

The first idea of a *reduced density matrix*, obtained by tracing over the degrees of freedom corresponding to the space beyond the event horizon of the black hole, was suggested by Bombelli, Koul, Lee and Sorkin [4]. Physically this is equivalent to smearing out the space beyond the horizon to which we have no access anyway. They also calculated the entropy corresponding to the reduced density matrix for massive scalar fields in the case when half-space of R^3 is inaccessible. This work was independently extended by Mark Srednicki who considered a system of free massless scalar fields in flat spacetime with only an imaginary sphere accessible. In both cases, it turned out that the corresponding entropy is proportional to the area of the boundary between the accessible and inaccesible space and both needed UV regulation. This led Srednicki to propose that the entropy between two different subspaces is proportional to the area of the boundary separating them [5]. The entropy of the reduced density matrix became known as *entanglement entropy*. Soon after that, Holzhey, Callan and Wilczek considered two dimensional spacetime using conformal field theory and the so called replica trick by Susskind [6], and found that the entanglement entropy of an interval is proportional to the logarithm of its length [7].

The next boom on entanglement entropy came with Calabrese and Cardy who used the methods of $1+1$ dimensional conformal field theory to calculate entanglement entropy in numerous static and dynamic cases. Simultaneously entanglement entropy also raised interest in lattice models and other condensed matter systems [8, 9, 10, 11, 12]. The entanglement entropy has been evaluated for many one dimensional lattice systems and there has been a significant agreement with results from conformal field theories. Yet another new wave of interest for entanglement entropy began after Ryu and Takayanagi made the conjecture for holographic entanglement entropy inspired by the AdS/CFT duality. It transformed the complicated field theoretical calculations to considerably simpler analysis of minimizing surfaces in AdS space [13].

Recently there has been much interest in time evolution of entanglement entropy as a way to study thermalization of systems. In the case of holographic entanglement entropy, there has been evidence of phase transitions in its value. This has led to the application of entanglement entropy as a probe for phase transitions and confinement in confining gauge field theories [14, 15].

Perhaps the strongest and longest lasting source of driving force for entanglement entropy is to better understand the origin of black hole entropy and also quantum gravity itself. The black hole entropy has been proposed to be related to entanglement entropy. The holographic entanglement entropy could serve as a helpful tool to understand AdS/CFT duality [16].

1.2 Entanglement entropy

Entanglement is a fundamental property of quantum mechanical systems that has no classical equivalent. It is often discussed only qualitatively in introductory courses of quantum mechanics. The simple idea is that a measurement of one part of an entangled system affects the measurement of the other parts. Entanglement entropy is candidate for a quantitave measure of entanglement. I will now review the definition of entanglement entropy and a few of its most important properties.

Suppose we have a quantum mechanical system and the corresponding Hilbert space $\mathscr{H}$. In zero temperature, the system is in pure state $|\psi\rangle \in \mathscr{H}$ and thus has the density matrix $\rho = |\psi\rangle\langle\psi|$ and the total entropy of the system is zero. Divide the system into two parts, A and its complement $A^\complement$. This *bipartitioning* is depicted in both figures of (1.1), for the one dimensional lattice and for a two dimensional continuum theory. The original Hilbert space can now be written as $\mathscr{H} = \mathscr{H}_A \otimes \mathscr{H}_{A^\complement}$, i.e. as a tensor product of the Hilbert spaces of A and $A^\complement$. Now we can express all vectors of $\mathscr{H}$ with vectors of the subspaces.

$$|\psi\rangle = \sum_{i,j} a_{i,j} |\phi_i\rangle |\chi_j\rangle, \quad |\phi_i\rangle \in \mathscr{H}_A,\ |\chi_j\rangle \in \mathscr{H}_{A^\complement},\ a_{i,j} \in \mathbb{C}. \tag{1.2}$$

If the state cannot be expressed as a single tensor product of vectors of the subspaces, the system is entangled. The situation is similar for the density matrices of the subsystems. The reduced density matrix of A is defined as

$$\rho_A = \mathrm{Tr}_{A^\complement}\, \rho \tag{1.3}$$

where the trace is over the degrees of freedom of $A^\complement$. If the two subsystems are not entangled, the density matrix can be factorized $\rho = \rho_A \otimes \rho_{A^\complement}$ [17].

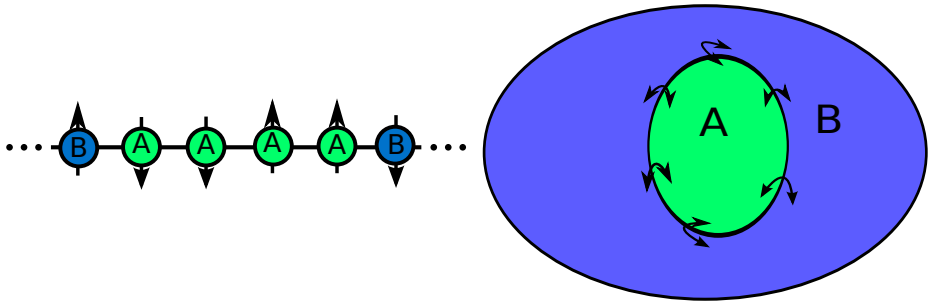

Figure 1.1: On the left side, bipartitioning of a one dimensional Ising model. On the right side, the bipartitioning of a continuum theory where the arrows imply that the most strongest correlations appear at the boundary causing UV divergence.

The entanglement entropy of A is defined as

$$S_A = -\mathrm{Tr}_A(\rho_A \log \rho_A) \geq 0 \tag{1.4}$$

where the trace is now over the remaining degrees of freedom. It is evident, that if the density matrix can be factorized, the entanglement entropy for both A and $A^{\complement}$ vanishes. A related quantity of interest is the so called *entanglement Rényi entropy* which is defined as

$$S_A^{(n)} = \frac{\log(\mathrm{Tr}_A[\rho_A^n])}{1-n} \tag{1.5}$$

where $n \geq 1$. The entanglement Rényi entropy shares many properties with entanglement entropy and, at the limit $n \to 1$, it converges to entanglement entropy [8].

Let us consider an example. The most simple example of entanglement is the creation of two spin-$\frac{1}{2}$ particles, A and B, through the decay of a scalar particle. Conservation of angular momentum requires that the two particles must have opposite spin along z-axis but does not specify, which particle has the positive spin along z-axis. Therefore, the state could be

$$|\psi\rangle = \sqrt{p}|\uparrow_z\rangle_A|\downarrow_z\rangle_B + \sqrt{1-p}|\downarrow_z\rangle_A|\uparrow_z\rangle_B$$

where $p \in [0,1]$. The reduced density matrix and entanglement entropy of A are now

$$\rho_A = \mathrm{Tr}_B(|\psi\rangle\langle\psi|) = p|\uparrow_z\rangle_A\langle\uparrow_z|_A + (1-p)|\downarrow_z\rangle_A\langle\downarrow_z|_A$$
$$S_A = -\mathrm{Tr}_A(\rho_A \log \rho_A) = -(p\log(p) + (1-p)\log(1-p)) \geq 0.$$

If p is either 0 or 1, the entanglement entropy is zero, and if $p = \frac{1}{2}$ we get maximum entanglement, log(2), which is intuitive. Thus, entanglement entropy has passed a test of reasonability. For all values of p, S_A equals S_B.

The equivalence of S_A and S_B is no accident. In fact, it applies for all pure states. This surprising result can be seen if we express the state as a Schmidt decomposition. All pure bipartite states can be expressed as

$$|\psi\rangle = \sum_i \sqrt{p_i}|\phi_i\rangle|\chi_i\rangle \tag{1.6}$$

where $\{|\phi_i\rangle\}$ and $\{|\chi_i\rangle\}$ are orthonormal bases of $\mathscr{H}_A$ and $\mathscr{H}_{A^{\complement}}$ respectively and $\sqrt{p_i}$ are the eigenvalues of ρ_A [17, 5]. This is known as the Schmidt decomposition and it is generally not unique. It

is clear that both ρ_A and $\rho_{A^\complement}$ have the same non-zero eigenvalues and thus their entanglement entropies are equivalent [5].

If we instead consider thermal states ($T \neq 0$), the state is no longer pure and the total entropy is non-zero. We still define the reduced density matrices and entropies of the subsystems as before, but the entropy is no longer a good measure for entanglement alone as it would include both the entanglement entropy and the thermal entropy of the subsystem. In addition, thermal entropy depends on the volume of the considered system so we will lose the equivalence of S_A and $S_{A^\complement}$ when the systems differ in volume.

Even if we consider a thermal state, there are still relations that apply to all cases. Let A, B and C be three separate subsystems. Then

$$S_{A\cup B} \leq S_A + S_B \tag{1.7}$$

where equality only applies if the density matrix of $A \cup B$ factorizes. This inequality is true even when A and B overlap [17]. This inequality is known as subadditivity.

For three subsystems, we can find a stronger inequality hence called strong subadditivity.

$$S_{A\cup B\cup C} + S_B \leq S_{A\cup B} + S_{B\cup C} \Leftrightarrow S_{D\cup E} + S_{D\cap E} \leq S_D + S_E \tag{1.8}$$

Here, D and E are arbitrary regions of the system. When D and E have no overlap, the inequality reduces to (1.7) [18].

There is also a third non-trivial inequality known as the Araki-Lieb inequality. If A and B are separate regions of space,

$$|S_A - S_B| \leq S_{A\cup B}. \tag{1.9}$$

Together with subadditivity, these two are sometimes called the triangle inequality [19].

We will later see a proof for these inequalities using the conjecture for holographic entanglement entropy.

1.2.1 Area law of entanglement entropy

Consider a $d+1$ dimensional spacetime. Let A be a fixed region of space and ∂A its boundary. In thermal cases, entropy scales like $S_A \sim \text{Vol}(A)$. When we consider zero temperature unbounded vacuum state, $\text{Vol}(A)$ or $\text{Vol}(A^\complement)$ would be infinite which would violate the equality of entanglement entropies if it scaled like volume. This led Srednicki to propose that the entanglement entropy must depend on the one thing that the regions of space have in common, their boundary, more specifically the area of the boundary. For $d = 3$ and a spherical region of radius R, Srednicki calculated the entanglement entropy for a free massless scalar field yielding

$$S_A = 0.30\frac{R^2}{a^2}$$

where a is the UV cutoff. This result led to the general proposal

$$S_A \sim \frac{\text{Area}(\partial A)}{a^{d-1}} \tag{1.10}$$

where a is the UV cutoff. This scaling property is understood as a reaffirmation that quantum fields are most strongly correlated at short distances i.e. near the boundary of the region [5]. This property was also depicted on the right side of figure (1.1), where the strongest correlations are indicated.

As always, things are never so simple in general. If $d = 1$, eq. (1.10) would imply that a single strip would have the same entanglement entropy independent of its length. This is not the case. If we consider a zero temperature conformal field theory and a single strip of length l on an infinite line, the entanglement entropy will be

$$S(l) = \frac{c}{3}\log\frac{l}{a} + c_1' \tag{1.11}$$

where c is the *central charge* of the theory and c_1' is a constant [7]. Logarithmic scaling has been confirmed explicitly for numerous one-dimensional lattice systems at their critical point such as the XY model [9, 12].

The general area law has been confirmed for many multidimensional systems [20]. Interestingly, the general area law is violated in some systems of higher dimension. It turns out that critical fermionic systems with a Fermi surface require an additonal logarithmic scaling i.e.

$$S_{\text{fermionic}} \sim \frac{l^{d-1}}{a^{d-1}}\log\left(\frac{l}{a}\right) \tag{1.12}$$

where l is a characteristic length of the system [21]. This can be interpreted heuristically that each point of the surface acts like a $1+1$ dimensional conformal field theory. Therefore, the entropy would be (number of points) $\times S_{\text{2D,CFT}}$.

As can be seen in all the results above, they are UV divergent and there is still no concensus on the method of renormalization [16]. The original formula for Bekenstein-Hawking entropy for black holes did not have such a feature. This problem persists in all quantum field theoretical calculations of entanglement entropy. However, there are other quantities related to entanglement entropy which are UV finite. When we have two regions of space, A and B, their *mutual information* is defined

$$I(A,B) = S(A) + S(B) - S(A\cup B). \tag{1.13}$$

When the two regions do not have an overlapping boundary, mutual information is finite. In addition, it is always non-negative as can be seen using the subadditivity property of entanglement entropy. Even more, mutual information satisfies the area law even in thermal cases [22].

Lastly, I define the *tripartite information*. For three separate regions of space, A, B and C, their tripartite information is defined

$$I_3(A,B,C) = I(A,B) + I(A,C) - I(A,B\cup C). \tag{1.14}$$

Unlike mutual information, this is UV finite even if the regions share boundaries. This quantity can take any sign and even be zero although, in field theories with no explicit time depencende, the value is always non-positive [22, 23].

1.3 Outline

In the next chapter, we will start with the tools of $1+1$ dimensional conformal field theory, construction of Riemann sheets and twist fields and then apply these to calculate, first, a few static cases of entanglement entropy in conformally invariant $1+1$ dimensional systems. We will extend these calculations to dynamical cases where we consider homogeneous global quenches and local quenches with one defect. The goal of the chapter is to establish the most significant and general results of entanglement entropy with semi-rigorous methods. These results can then be compared to the results of later chapters.

In the third chapter, we briefly introduce holography and AdS/CFT duality. The main idea is to introduce the Ryu-Takayanagi formula for calculations of holographic entanglement entropy using minimal surfaces. We then rederive the static results of chapter two and then apply the RT formula to higher-dimensional cases. In chapter four, we continue using holographic methods, extending our analysis to dynamical cases using the generalized RT formula, known as Hubeny-Rangamani-Takayanagi formula. We will attempt a rederivation of the dynamical results of chapter two using the infalling null-dust shell and falling particle geometries. In addition, we also consider higher dimensional cases. The entirety of the fifth chapter is dedicated to generalizations of the AdS metrics, by adding effects of Lifshitz scaling and hyperscaling violation. This will be applied to static cases and infalling null-dust shell geometry.

The sixth chapter will be spent on the various situations of mutual information and comparing the results of conformal field theories and the holographic approach. New results will be calculated for the hyperscaling violating Lifshitz-AdS-Vaidya metric.

Chapter 2

Two dimensional conformal field theory

Conformal field theories are field theories with *conformal symmetry*, that is, the action is invariant under coordinate transformations which locally rescale the metric

$$g_{\mu\nu}(x) \mapsto \Omega(x) g_{\mu\nu}(x) \tag{2.1}$$

where Ω is a positive function varying in spacetime. In more than two dimensions, these transformations are translations, scalings, rotations and the so called special conformal transformations.

Massless field theories often exhibit conformal symmetry and statistical systems at their classical and quantum critical points such as the XY model are also believed to be conformally invariant. Therefore, there is a vast amount of systems to which we can apply the tecniques conformal field theories. However, we are usually not interested in the specific content of the field theory. Often we deal with physical systems consisting of (quasi)-primary fields which rescale with the change of coordinates

$$\phi'(x') = \left|\frac{\partial x'}{\partial x}\right|^{\Delta} \phi(x), \tag{2.2}$$

where Δ is the scaling dimension of ϕ. This requirement alone fixes the 2 and 3-point functions of the theory and restricts the form of the 4-point functions greatly.

But it is the two dimensional systems in which the conformal field theory is most powerful. We can map the two dimensional spacetime to a complex plane where we treat the complex variables z and $\bar{z}$ as independent variables. It turns out that all holomorphic and anti-holomorphic functions are conformal transformations. This huge symmetry group is generated by the infinite dimensional Witt algebra which can be extended to the infinite dimensional Virasoro algebra.

The whole of this thesis could be spent discussing the details of conformal field theory barely scratching the surface of the topic. Hence, I assume the reader is somewhat familiar with the theory of two-dimensional field theories before reading further. If this is not the case, I can recommend the book by Di Francesco et al. [24] or the lecture notes by Ginsparg [25] and Cardy [26] for an illuminating introduction. For the most parts of this chapter, we will be following the review articles by Calabrese and Cardy [8, 27] and the references therein.

In this chapter, I will cover the basic and most illuminating examples of applications of conformal field theory. I will start with static examples of one interval in an infinite 1+1 dimensional

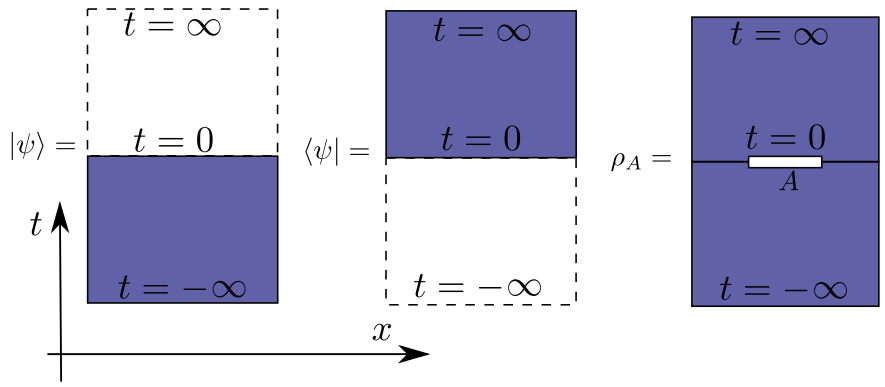

Figure 2.1: Pictorial depiction of vacuum functionals and the the reduced density matrix obtained by sewing the vacuum functionals along B.

system in zero temperature and generalize the results to finite length and finite temperature. Systems with a boundary will also be discussed. Then we will discuss dynamical examples with global and local quenches.

2.1 The replica trick, Riemann surfaces and twist fields

Consider an infinite straight line at zero temperature. Using Euclidean field theory, the vacuum state can be described by the vacuum state functional [28]

$$|\Psi(t_1,\phi_0)\rangle = \int_{\phi(-\infty,x)=0}^{\phi(t_1,x)=\phi_0(x)} [D\phi] e^{-S_E(\phi)}, \quad \langle\Psi(t_1,\phi_0)| = \int_{\phi_0(t_1,x)=\phi_0(x)}^{\phi_0(\infty,x)=0} [D\phi] e^{-S_E(\phi)} \tag{2.3}$$

where N is a normalization constant and S_E is the Euclidean action. The corresponding density matrix can be expressed using an ultraviolet regulator ε

$$\rho(t)_{\phi_1,\phi_2} = |\Psi(t,\phi_1)\rangle\langle\Psi(t,\phi_2)| \tag{2.4}$$

$$= \frac{1}{\mathcal{Z}(1)} \int_{\phi(-\infty,x)=0}^{\phi(\infty,x)=0} [D\phi] \prod_x \left[\delta(\phi(t-\varepsilon,x)-\phi_1(x))\delta(\phi(t+\varepsilon,x)-\phi_2(x))\right] e^{-S_E(\phi)}. \tag{2.5}$$

Pictorially, this is the same as making a cut at the complex plane along $t_E = t$ with a width 2ε. Ignoring the normalization constant $\mathcal{Z}(1)$, we obtain the partition function by taking a trace over all the possible fields. Pictorially, we would simply sew the cut back together [8]. See figure (2.1).

Now, we introduce a subset A, consisting of N disjoint intervals $[u_j, v_j]$ at fixed time $t_E = 0$. To obtain the reduced density matrix ρ_A, we integrate over the degrees of freedom in $A^{\complement}$. Pictorially, this is the same as sewing the cut in the complex plane back together only at $x \in A^{\complement}$. Unfortunately, there is no easy pictorial way to obtain the logarithm of ρ_A. Therefore, we focus on the integer powers of the reduced density matrix. As the density matrix is self-adjoint, it is diagonalizable with eigenvalues $\{\lambda_i\}$ and all its powers are also diagonalizable. As the eigenvalues are between zero and one, the powers of the density matrix are convergent and well-defined. We can make an analytical

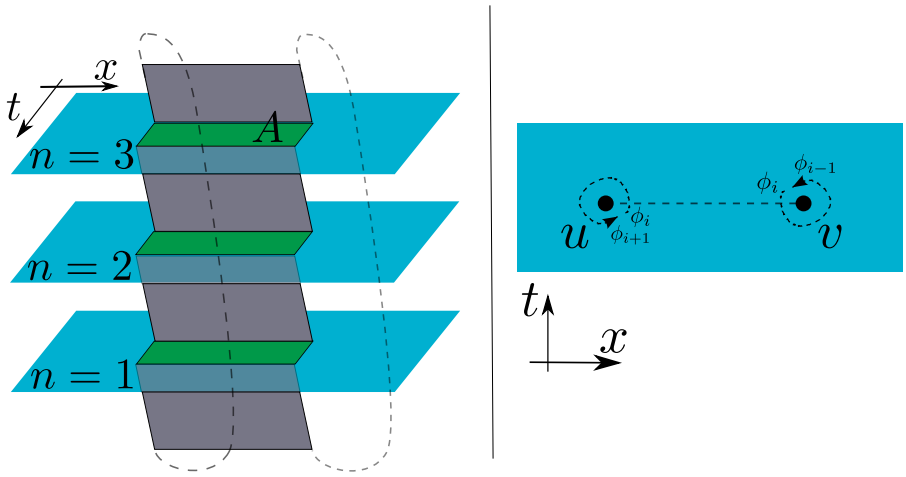

Figure 2.2: On the left side, we have the Riemann surface $\mathscr{R}_{1,3}$ obtained by sewing the sheets cyclically along A. Notice how you need to go around the branch point three times before ending up on the same sheet. On the right side, is the same situation when we map to the n sheet model where there are branch points and a branch cut between them. Passing the branch cut from below takes field ϕ_i to ϕ_{i+1}.

continuation of the discrete points n to complex plane with $\Re n > 1$. Taking a derivative with respect to n at $n = 1$, we obtain

$$-\frac{\partial}{\partial n}\mathrm{Tr}\rho_A^n = -\frac{\partial}{\partial n}\sum_i \lambda_i^n = -\log(\lambda_i)\lambda_i^n \to -\log(\lambda_i)\lambda_i \tag{2.6}$$

which is the expression for the entanglement entropy of A [8].

The powers of the reduced density matrix can be written as

$$[\rho_A^n]_{\phi_-,\phi_+} = [\rho_A]_{\phi_-,\phi_1}[\rho_A]_{\phi_1,\phi_2}\ldots[\rho_A]_{\phi_{n-1},\phi_+}, \tag{2.7}$$

where a sum over ϕ_i is implied. Pictorially, this is the same as having n copies of the field theory, and sewing the lower end of the cut to the upper end of the cut on the plane above i.e. having the boundary conditions $\phi_i(0-,x) = \phi_{i+i}(0+,x)$, where we identify 1 and $n+1$. We obtain a non-trivial *Riemann surface*, $\mathscr{R}_{N,n}$. This is depicted on the left side of figure (2.2). The trace can be expressed as

$$\mathrm{Tr}{\rho_A}^n = \frac{\mathscr{Z}_n}{\mathscr{Z}_1^n} \tag{2.8}$$

Where $\mathscr{Z}_n$ is the partition function on the Riemann surface [8].

The curvature on $\mathscr{R}_{N,n}$ is zero almost everywhere. However, the boundary points of A, u_i, v_i, have non-zero curvature. This is easily realized when we consider infinitesimal circles around various points of the Riemann surface. If we consider one around a boundary point, we do not end up at the same point. We are rather at the corresponding point of either the plane above or below the starting point. Thus, in the case of one interval, we need to do n such cirles to get back to our starting point. The boundary points thus have an anglular excess of $2\pi(n-1)$ which corresponds to a *conical singularity* at the boundary points. The corresponding curvature in the case of one interval is $R = 4\pi(n-1)\delta((0,\partial A))$ where the delta function is singular at the boundary points. This

approach can be used to obtain the expression for the entanglement entropy for the case of one interval as is done later in this chapter [28]. The case for more than one interval remains unsolved as the topology of multiple intervals is considerably more difficult [8].

We wish to focus more on the field theoretical aspect of this calculation. Therefore, consider the N intervals in the n-sheeted Riemann surface. Since we were originally considering flat space, no curvature is expected to be explicitly in the Lagrangian of our field theory on the Riemann surface. We are interested in the partition function on the Riemann surface,

$$\mathcal{Z}_{n,N} = \int D\phi \exp(-\int_{\mathcal{R}_{N,n}} \mathrm{d}^2 x \mathcal{L}_{E,n}(\phi)). \tag{2.9}$$

The field is defined on the entire Riemann surface. The manifold is a difficult setting to work in and we wish to simplify it by moving the theory to the complex plane. We do this by mapping $w = x + i\,t_E$ and introducing n mutually non-interacting field theories on the complex plane with a branch cut (corresponding to boundary conditions) at intervals of A at $t_E = 0$. See figure (2.2). Thus, the partition function can be rewritten as

$$\mathcal{Z}_{n,N} = \int \prod_{i=1}^{n} [D\phi_i] \prod_{x\in A} \delta(\phi_i(x,0-) - \phi_{i+1}(x,0+)) \exp(-\int_{\mathbb{C}} \mathrm{d}^2 x (\mathcal{L}_E(\phi_1) + \ldots + \mathcal{L}_E(\phi_n)). \tag{2.10}$$

The system has an internal global symmetry group generated by τ which maps ϕ_i to ϕ_{i+1} without changing the coordinates. Internal symmetries of field theories define what are known as *twist fields* [1] [8]. In this case, they generate branch-point twist fields associated with τ, Φ_n, and its inverse, Φ_{-n}. We can make the branch cuts manifest on a normal complex plane by setting the twist fields at the boundaries of each interval in A. Φ_n is set at the left boundaries, Φ_{-n} at the right boundaries. With twist fields, we can get rid of the branch points of the spacetime and implement them in the path integral with the twist fields. Consider a field theory on a complex plane with a branch-point twist field Φ_n inserted at u_i and Φ_{-n} at v_j. Taking a field of our original field theory, ϕ_k, around u_i clockwise causes it to obtain the value of ϕ_{k+1}. The same happens when we take the field around (v_j) counter-clockwise [8]. Thus, we have translated the branch-points into field theoretical language.

Hence, instead of setting the boundary conditions for our path integral, we can set the twist fields at the boundaries of A on the complex plane and calculate their expectation value. Thus, for the Riemann surface with N intervals and n sheets, the partition function can be expressed as

$$\mathcal{Z}_{n,N} \propto \langle \Phi_n(u_1,0)\Phi_{-n}(v_1,0)\cdots\Phi_n(u_N,0)\Phi_{-n}(v_N,0)\rangle_{\mathcal{L}^{(n)},\phi_i}, \tag{2.11}$$

where $\mathcal{L}^{(n)}$ indicates the Lagrangian of the n-copy model. Suppose we have a field operator $\mathcal{O}(x,t)$ on our Riemannian manifold. The expectation value of it is

$$\langle \mathcal{O}(x,t)\rangle_{\mathcal{R}_{N,n}} = \frac{\langle O_k(x,t)\Phi_n(u_1,0)\Phi_n(v_1,0)\cdots\rangle_{\mathcal{L}^{(n)},\phi_i}}{\langle \Phi_n(u_1,0)\Phi_n(v_1,0)\cdots\rangle_{\mathcal{L}^{(n)},\phi_i}}. \tag{2.12}$$

where O_k is the kth copy of $\mathcal{O}$ when the system is mapped to the n copy model on the complex plane. The operator $\mathcal{O}$ is copied n times on the complex plane, and the corresponding operator

[1] To grasp the main ideas of twist fields, I suggest the lecture notes by Ginsparg [25].

in the full n-copy model is $O^{(n)} = \sum_{k=1}^{n} O_k$ [8, 27, 29]. This causes the n-copy model to have every expectation value to be n times the expectation value of an ordinary conformal field theory on the complex plane.

We can transform the partition function into a useful form by diagonalizing the original fields in our Lagrangian [8, 28]. Introduce

$$\tilde{\phi}_j = \sum_{k=1}^{n} e^{i2\pi \frac{k}{n} j} \phi_k, \quad j = 0, 1, \ldots, n-1. \tag{2.13}$$

These are eigenvectors of τ and τ^{-1}; $\tau\tilde{\phi}_j = e^{i2\pi \frac{j}{n}}\tilde{\phi}_j$ and $\tau^{-1}\tilde{\phi}_j = e^{-i2\pi \frac{j}{n}}\tilde{\phi}_j$. Furthermore, we can factorize the mapping τ and the corresponding twist fields

$$\tau = \prod_{j=0}^{n-1} \tau_{j/n} \tag{2.14}$$

where $\tau_{j/n}\tilde{\phi}_{k,n} = \tilde{\phi}_{k,n}$ if $k \neq j$ and $e^{i2\pi \frac{j}{n}}\tilde{\phi}_j$ if $k = j$. The twist fields themselves, can be factorized. Each $\tau_{j/n}$ and its inverse have their corresponding twist fields $\Phi_{\pm j/n}$. The partition function factorizes similarly

$$\mathcal{Z}_n \propto \prod_{k=0}^{n-1} \langle \Phi_{k,n}(u_1,0)\Phi_{k,n}(v_1,0)\cdots\Phi_{k,n}(u_N,0)\Phi_{k,n}(v_N,0)\rangle_{\mathcal{L}^{(n)},\phi_i}. \tag{2.15}$$

2.1.1 Fermionic systems

Although never explicitly mentioned, the above discussion applies only for bosonic systems. If we consider fermionic systems, some of the details are changed a bit. This was considered in [30]. The first difference is in the calculation of the density matrix from the vacuum state functionals. In the calculations, antiperiodic boundary conditions must be applied i.e. the reduced density matrix is

$$[\rho_A]_{\psi_1\psi_2} = \frac{1}{\mathcal{Z}(1)} \int_{\psi(-\infty,x)=0}^{\psi(\infty,x)=0} [D\psi D\bar{\psi}] \prod_x [\delta(\psi(t-\varepsilon)+\psi_1(x))\delta(\psi(t+\varepsilon)-\psi_2(x))]\, e^{-S_E(\psi,\bar{\psi})}. \tag{2.16}$$

The construction of the Riemann surface proceeds identically except that for n-sheeted Riemann surface, going around the branch point n times, returns to the original sheet with the field multiplied by $(-1)^{n+1}$. Thus, the symmetry generator τ acts on the fields as $\tau\psi_i = \psi_{i+1}$ for $i < n$ and $\tau\psi_n = (-1)^{n+1}\psi_1$.

Diagonalizing the operator τ then gives the eigenvectors $\tilde{\psi}_k$ with eigenvalues $\exp(i\frac{2\pi k}{n})$, where $k = -(n-1)/2, -(n-3)/2, \ldots, (n-1)/2$ i.e. half-integers. The rest of the analysis is identical and we see a use of factorizing the partition function with fermions later in this section [30].

2.1.2 Analytic continuation of powers of the reduced density matrix

As I stated before, once we have found the integer powers of the reduced density matrix of A, we can analytically continue it to complex values with $\Re z \geq 1$. However, it is important that the continuation is unique to have a well-defined derivative with respect to n. The uniqueness is not self-evident and is yet to be proven but there are some convincing arguments for it [16].

In a general case, suppose we have a normalized density matrix, ρ with $\mathrm{Tr}\rho = 1$. If the matrix is finite dimensional, using triangle inequality, we can show for α with $\Re\alpha \geq 1$

$$|\mathrm{Tr}(\rho^\alpha)| \leq |\mathrm{Tr}(\rho)^\alpha| = 1. \tag{2.17}$$

Unfortunately, the same trick does not work with infinite dimensional matrices as we may encounter divergences. Suppose then that we have a regularized density matrix, ρ_ε with a regulator $\varepsilon > 0$ such that $\mathrm{Tr}(\rho_\varepsilon^\alpha) \leq 1$ with $\Re\alpha \geq 1$. This property then requires that our analytic continuation of the corresponding partition function is also bounded.

Suppose, that we have two analytic continuations of the partition function to complex values, $\mathcal{Z}_1$ and $\mathcal{Z}_2$. It is clear, that they must agree at integer values. This condition can be written as

$$\mathcal{Z}_1(\alpha) = \mathcal{Z}_2(\alpha) + \sin(\pi\alpha)g(\alpha), \quad \Re\alpha \geq 1 \tag{2.18}$$

where g is an analytic function. Our analytic continuation must be bounded. The sine function diverges at the imaginary infinity and therefore g must behave asymptotically as $|g(x+iy)| < e^{-\pi|y|}$. These conditions together with Carlson's theorem imply that g must be identically zero and thus the analytical continuation of the powers of the density matrix is unique [16, 31].

2.2 Entanglement entropy for a single interval: the static case

Consider the case of a single interval $A = [u, v]$ as subsystem in an infinite chain at zero temperature for a conformal field theory. To evaluate its entanglement entropy, we need to evaluate the expectation value of the stress energy tensor on the Riemann surface and then relate it to the one of the n-copy model. Consider the points of the Riemann surface, $w = x + it$, $\bar{w} = x - it$. We map the boundary points $(u + 0i, v + 0i)$ to $(0, \infty)$ using a *Möbius transformation* $\xi : \mathscr{R} \to \mathscr{R}$, $\xi(w) = (w-u)/(w-v)$. Furthermore, we can now uniformize the Riemann surface to the complex plane with $z : \mathscr{R} \to \mathbb{C}$, $z(\xi) = \xi^{1/n} = \left(\frac{w-u}{w-v}\right)^{1/n}$. The Möbius transformations are global conformal transformations and holomorphic. The mapping $z(\xi(w))$ is a conformal mapping in this case, as it maps the n sheeted Riemann surface with to the complex plane [8]. However, the $\xi^{1/n}$ mapping is not conformal on the complex plane or on the Riemann surface if we were still dealing with a finite interval.

Consider just the holomorphic part of the stress energy tensor. We know that $\langle T(z)\rangle_{\mathbb{C}} = 0$ as the complex plane has rotational, translational and scaling symmetry. Stress energy tensors transform in conformal mappings

$$T(w) = \left(\frac{dz}{dw}\right)^2 T(z) + \frac{c}{12}\{z, w\} \tag{2.19}$$

where c is the central charge of the theory and $\{z, w\} = \frac{z'''}{z'} - \left(\frac{3z''}{2z'}\right)$ is the *Schwarzian derivative*, which vanishes for Möbius transformations. Taking the expectation value of both sides, we get

$$\langle T(w)\rangle_{\mathscr{R}} = \frac{c}{12}\{z, w\} = \frac{c(1-n^{-2})}{24}\frac{(v-u)^2}{(w-u)^2(w-v)^2}. \tag{2.20}$$

Now we can relate this to the n-copy model stress energy tensor, $T^{(n)}$. Looking at equation (2.12), this is equivalent to

$$\langle T(w)\rangle_{\mathscr{R}} = \frac{\langle T_j(w)\Phi_n(u,0)\Phi_{-n}(v,0)\rangle_{\mathscr{L}^{(n)},\phi_i}}{\langle \Phi_n(u,0)\Phi_{-n}(v,0)\rangle_{\mathscr{L}^{(n)},\phi_i}}$$

for all j. Therefore, we need to multiply the right hand side of equation (2.20) with n, to obtain

$$\langle T^{(n)}(w)\Phi_n(u,0)\Phi_{-n}(v,0)\rangle_{\mathscr{L}^{(n)},\phi_i} = \frac{c(n-n^{-1})}{24}\frac{(v-u)^2}{(w-u)^2(w-v)^2}. \tag{2.21}$$

Now, we can evaluate the two-point functions of the twist fields. The twist fields Φ_n and Φ_{-n} have the same *conformal weights*. Therefore, the normalized expectation value is

$$\langle \Phi_n(z_1,\bar{z}_1)\Phi_{-n}(z_2,\bar{z}_2)\rangle = |z_1-z_2|^{-2h_n}|\bar{z}_1-\bar{z}_2|^{-2\bar{h}_n}, \tag{2.22}$$

where h_n and $\bar{h}_n$ are the conformal weights of the twist fields. The conformal Ward identity states that the expectation value of the stress energy tensor and primary fields for any conformal field theory is

$$\langle T(z)\phi_1(z_1,\bar{z}_1)\phi_2(z_2,\bar{z}_2)\cdots\rangle = \sum_i\left(\frac{h_i}{(z-z_i)^2}+\frac{1}{z-z_i}\frac{\partial}{\partial z_i}\right)\langle\phi_1(z_1,\bar{z}_1)\phi_2(z_2,\bar{z}_2)\cdots\rangle \tag{2.23}$$

We can apply this to calculate the expectation value of the stress energy tensor and two twist fields

$$\langle T^{(n)}(w)\Phi_n(u,0)\Phi_{-n}(v,0)\cdots\rangle_{\mathscr{L}^{(n)},\phi_i} = \frac{h_n}{(w-u)^2(w-v)^2(v-u)^{2h_n-2}(\bar{v}-\bar{u})^{2\bar{h}_n}} \tag{2.24}$$

With equation (2.21), we see that the conformal weight of the twist fields are $h_n = \bar{h}_n = \frac{c}{24}(n-n^{-1})$. Therefore, we can identify the scaling dimension of the twist fields as [8, 27]

$$\Delta_n = (h_n+\bar{h}_n) = \frac{c}{12}(n-n^{-1}). \tag{2.25}$$

We can now calculate the entanglement entropy of this single finite interval. Recalling our expression for the trace of the power of the reduced density matrix (2.8) and the partition function (2.11), we have

$$\begin{aligned} \mathscr{Z}_n &\propto \langle\Phi_n(u,0)\Phi_{-n}(v,0)\rangle_{\mathscr{L}(n),\phi_i} = |v-u|^{-2\Delta_n} \\ \mathrm{Tr}\rho_A^n = \frac{\mathscr{Z}_n}{\mathscr{Z}_1} &= c_n\left(\frac{v-u}{a}\right)^{c(n-1/n)/6} \end{aligned} \tag{2.26}$$

where a is a dimensional regulator to make the expression dimensionless, which corresponds to lattice spacing in discrete systems and c_n is an n dependent non-universal proportionality constant which requires the specific knowledge of the field theory to calculate. However, $c_1 = 1$ to normalize the reduced density matrix. Setting $l = |v-u|$, and differentiating with respect to n at $n = 1$, we obtain the entanglement entropy of a single interval of length l

$$S_A(l) = \frac{c}{3}\log\left(\frac{l}{a}\right)+c_1', \tag{2.27}$$

where c_1' is the derivative with respect to n of c_n. This remarkably simple expression has been obtained in numerous different ways in conformally invariant systems and has also been observed in quantum spin chains at critical point [7, 9, 10, 12, 29].

2.2.1 A single interval in finite length or finite temperature

The powerful symmetries of the two dimensional conformal field theory allow us to easily investigate systems with finite length or finite temperature. For conformal mappings $w(z)$ from one system to another, the correlation functions of primary fields scale according to

$$\langle \phi_1(w_1,\bar{w}_1)\phi_2(w_2,\bar{w}_2)\cdots\rangle = |z'(w_1)|^{\Delta_1}|z'(w_2)|^{\Delta_2}|\cdots|\langle \phi_1(z_1,\bar{z}_1)\phi_2(z_2,\bar{z}_2)\cdots\rangle. \tag{2.28}$$

The mapping $w(z) = \frac{\beta}{2\pi}\log(z)$ compactifies the temporal direction $t \sim t+\beta$ which corresponds to a system with temperature β^{-1}. It maps the whole complex plane to a cylinder with circumference β. The branch cut of the original sheets are now mapped to be parallel to the axis of the cylinder. We can now reuse our previous results, since the powers of reduced density matrix for a single interval still scale as the two-point functions of twist fields at the boundaries of interval on the cylinder. Plugging the mapping w into equation (2.28) and using our result (2.26), we arrive at an expression of mixed state entropy which is a combination of thermal entropy and entanglement entropy,

$$S_A(l,\beta) = \frac{c}{3}\log\left(\frac{\beta}{\pi a}\sinh\left(\frac{\pi l}{\beta}\right)\right) + c_1' = \begin{cases} \frac{c}{3}\log(\frac{l}{a}) + c_1' & \text{if } l \ll \beta \\ \frac{\pi c l}{3\beta} + c_1' & \text{if } \beta \ll l \end{cases}. \tag{2.29}$$

We see that as the temperature or the length of the interval decreases, the entropy approaches its zero temperature value, the entanglement entropy. On the other hand, if the temperature or the length of the interval grows, the entropy acts linearly and corresponds to the case of pure thermal entropy.

If we align the branch cut to be perpendicular to the axis of the cylinder, we get the entanglement entropy for a finite length system at infinite temperature. This is accomplished with the mapping $w(z) = \frac{L}{i2\pi}\log(z)$. It compactifies the spatial direction $x \sim x+L$ where L is the system length but leaves the temporal direction infinite. Plugging this into equation (2.28), we get

$$S_A(l,L) = \frac{c}{3}\log\left(\frac{L}{\pi a}\sin\left(\frac{\pi}{L}l\right)\right) + c_1'. \tag{2.30}$$

We notice that this expression is invariant when we map $l \mapsto L-l$ and that the asymptotic behavior is as expected. The entropy reaches its maximum at $l = L/2$. This knowledge can be used to our advantage when determining the central charge of a model using simulations with finite lattice size [8].

2.2.2 The case of finite temperature and finite length

The case of both finite temperature and finite system size is a considerably more difficult calculation. We need to consider a manifold with both the spatial and temporal directions compactified which corresponds to the topology of a torus. Conformal mappings from our original calculations do not help us here as the topology of a torus and a sheet are very different. In fact, conformal invariance is not enough and we need to know the full operator content to do the calculations. This has only been calculated in the case of free Dirac fermions in high and low temperature expansions [32]. I will only present the results.

It turns out that the relevant scale on the torus is the ratio of spatial and temporal periods $i\beta/L = \tau$ so we can set the inverse temperature as $-i\tau$ and the system length as 1. The powers of the reduced density matrices are calculated using the expression (2.15), where the two-point functions are

$$\langle \Phi_{k,n}(l,0)\Phi_{k,n}(0,0)\rangle_{\mathscr{L}^{(n)},\phi_i} = \left|\frac{2\pi\eta(\tau)^3}{\theta_1(l|\tau)}\right|^{4\Delta_k} \frac{|\theta_\nu(\frac{kl}{n}|\tau)|^2}{|\theta_\nu(0|\tau)|^2} \tag{2.31}$$

where $k = -\frac{N-1}{2},\ldots,\frac{N-1}{2}$ and $\Delta_k = \frac{k^2}{2N^2}$. The function η and θ are ellipictic functions where ν =2,3,4,1 is the sector of fermions. The authors of [32] presented the low and high temperature expansions of entanglement entropy for the case $\nu = 3$ corresponding to the (NS,NS) sector.

The expansions yield

$$\begin{aligned} S_{A,\text{high}} &= \frac{1}{3}\log\left(\frac{\beta}{2\pi}\sinh\left(\frac{\pi l}{\beta}\right)\right) + \frac{1}{3}\sum_{m=1}^{\infty}\log\left(\frac{(1-e^{2\pi l/\beta}e^{-2\pi m/\beta})(1-e^{-2\pi l/\beta}e^{-2\pi m/\beta})}{(1-e^{-2\pi m/\beta})^2}\right) \\ &+ 2\sum_{k=1}^{\infty}\frac{(-1)^k}{k}\frac{\frac{\pi lk}{\beta}\coth\left(\frac{\pi lk}{\beta}\right)-1}{\sinh(\frac{\pi l}{\beta})} \qquad (2.32) \\ S_{A,\text{low}} &= \frac{1}{3}\log\left(\frac{1}{2\pi}\sin(\pi l)\right) + \frac{1}{3}\sum_{m=1}^{\infty}\log\left(\frac{(1-e^{2\pi il}e^{-2\pi m\beta})(1-e^{-2\pi il}e^{-2\pi\beta m})}{(1-e^{-2\pi\beta m})^2}\right) \\ &+ 2\sum_{k=1}^{\infty}\frac{(-1)^{k-1}}{k}\frac{1-\pi lk\cot(\pi lk)}{\sinh(\pi k\beta)} \qquad (2.33) \\ & \qquad (2.34) \end{aligned}$$

We can see that the results for either finite temperature or finite length are reproduced in the first terms of the expansions. In the high temperature expansion, the secondary terms vanish as the system size grows and result (2.30) is recovered. Likewise, the low temperature expansion reduces to the result (2.29) as β grows. The absence of central charge is due to the fact that the free Dirac fermion theory has central charge $c = 1$ [32].

2.2.3 Systems with a boundary

So far, our systems have been either infinite or periodic. However, most physical systems have some kind of a boundary so it is natural to consider systems with one. The n-point functions of *boundary conformal field theory* are more difficult than those of ordinary CFT. Consider a semi-infinite chain. We can take the 1+1 dimensional theory to be in the upper half plane, where $z = t + ix$. We can no longer access the lower half plane and therefore the holomorphic and antiholomorphic parts of the theories do not decouple anymore. Instead, we consider the antiholomorphic part of the theory to be a mirror of the holomorphic part. This causes the 1-point functions of the boundary CFT to behave like 2-point functions of the ordinary CFT, which is still manageable, as the two-point functions are completely determined by the conformal invariance. However, the two-point functions of the boundary CFT behave as 4-point functions of the ordinary CFT, which require the knowledge of the specific field theory to determine completely [24].

Moving on, consider the interval $A = [0, l)$ on the semi-infinite system $[0,\infty)$. We can repeat the analysis we did before with the infinite system, only this time we have only one branch point at

$(0, il)$ thus requiring only one twist field. Thus, the partition function on the Riemann surface is proportional to $\langle \Phi_n(il,-il)\rangle_{\mathscr{L}^{(n)},\phi_i,\mathrm{UHP}}$, using the coordinates of the complex plane.

The uniformizing mapping is $z:\mathscr{R}\to$ Disc, $z(w)=[(w-il)/(w+il)]^{1/n}$ and the from the norm $|z(t+ix)|=[(t^2+(y-l)^2)/(t^2+(y+l)^2)]^{1/n}]\leq 1$ we can see that it maps the multi-sheeted upper-half plane to the unit disc $|z|\leq 1$. The expectation value of the holomorphic part of the stress energy tensor in the disc, $\langle T(z)\rangle_{\mathrm{Disc}}$, is still zero due to rotational invariance. We can use this to calculate the expectation value of the stress energy tensor of the Riemann surface [27],

$$\langle T(w)\rangle_{\mathscr{R}}=\frac{c}{12}\{z,w\}=\frac{c(1-n^{-2})}{24}\frac{(2l)^2}{(w-il)^2(w+il)^2}. \tag{2.35}$$

Like before, this is equivalent to the ratio

$$\langle T(w)\rangle_{\mathscr{R}}=\frac{\langle T^{(n)}(z)\Phi_n(il,-il)\rangle_{\mathscr{L}^{(n)},\phi_i,\mathrm{UHP}}}{n\langle \Phi_n(il,-il)\rangle_{\mathscr{L}^{(n)},\phi_i,\mathrm{UHP}}} \tag{2.36}$$

where the one-point function is now $\langle \Phi_n(z_1,\bar{z}_1)\rangle_{\mathscr{L}^{(n)},\mathrm{UHP}}=\langle \Phi_n(z_1)\Phi_n(\bar{z}_1)\rangle_{\mathbb{C}}=|z_1-\bar{z}_1|^{-\tilde{\Delta}_n}$. After the application of the conformal Ward's identity for one-point functions and some simple algebra, we see that $\tilde{\Delta}_n=\frac{c}{12}(n-n^{-1})$ and therefore

$$\mathcal{Z}_n \propto \langle \Phi_n(0+il,0-il)\rangle_{\mathscr{L}^{(n)},\mathrm{UHP}}=|i2l|^{-2\tilde{\Delta}_n} \tag{2.37}$$

$$\mathrm{Tr}\rho_A^n = \tilde{c}_n\left(\frac{2l}{a}\right)^{(c/12)(n-1/n)}, \quad S_A(l)=\frac{c}{6}\log\left(\frac{2l}{a}\right)+\tilde{c}_n'. \tag{2.38}$$

Here the $\tilde{c}_n$ are n dependent constants which depend on the specific theory we are considering [8]. We notice that this entanglement entropy is asymptotically half of the entropy for the infinite system which is due to the fact that we have only one boundary point between A and its complement.

Using the same arguments as before, the entanglement entropy for a semi-infinite system in zero temperature can easily be modified to the case of finite temperature or finite size. The calculations yield

$$S_A(l,\beta) = \frac{c}{6}\log\left(\frac{\beta}{\pi a}\sinh\left(\frac{2\pi l}{\beta}\right)\right)+\tilde{c}_1' \tag{2.39}$$

$$S_A(l,L) = \frac{c}{6}\log\left(\frac{2L}{\pi a}\sin\left(\frac{\pi l}{L}\right)\right)+\tilde{c}_1' \tag{2.40}$$

Using the constant c_1' from our previous calculations and $\tilde{c}_1'$ above, we can deduce that their difference corresponds to the boundary entropy $\tilde{c}_1'-c_1'/2=\log(g)$ associated with the boundary points between A and its complement [8].

2.2.4 The case of multiple intervals

In the case of multiple intervals in a conformally invariant system, we need to consider $2N$-point functions which cannot be evaluated without the full knowledge of the specific theory. The multi-interval cases cannot be conformally mapped to the complex plane due to their different genera making our methods, used for a single interval, useless here [33]. In the case of N intervals,

$[u_1, v_1], \ldots, [u_N, v_N]$, the powers of the reduced density matrix have the general form

$$\langle \Phi_n(u_1)\Phi_{-n}(v_1)\cdots\Phi_n(u_N)\Phi_{-n}(v_N)\rangle_{\mathscr{L}^{(n)},\phi_i,\mathbb{C}} = c_n^N \left(\frac{\prod_{j<k}(u_k-u_j)(v_k-v_j)}{\prod_{j,k}(v_k-u_j)} \right)^{(c/6)(n-1/n)} \mathscr{F}_{N,n}(\eta_i). \tag{2.41}$$

Here, $\mathscr{F}_{N,n}$, is a system specific function, and η_i are the $2N-3$ cross ratios. There is no simple way to determine these functions but it is known for some theories. In some cases, like massless fermions, the functions is just unity for all n and N, but for Luttinger liquids considered in [34], the expression is only known for integer n and $N = 2$. The case of multiple intervals is, in general, poorly understood [35]. We will return to the question of multiple intervals in the case of holographic entanglement entropy.

2.2.5 Non-critical models

Most of the time, systems are not at their critical point and thus not conformally invariant. However, if the system is close to the critical point, it is equivalent to introducing a small mass m to the field theory. The authors of [8, 27] were able to evaluate the entanglement entropy when A is the negative real line in an infinite system in a non-critical system. The correlation length is roughly the inverse of mass $\xi \sim m^{-1}$ and the entanglement entropy is

$$S_A = \frac{c}{6}\log\left(\frac{\xi}{a}\right). \tag{2.42}$$

When we consider a system consisting of separate intervals with length and separations much larger than the correlation length, they conjectured that the entanglement entropy would be

$$S_A = \frac{c\mathscr{A}}{6}\log\left(\frac{\xi}{a}\right) \tag{2.43}$$

where $\mathscr{A}$ is the number of boundary points between A and $A^{\complement}$. This behaviour has been confirmed for cases $\mathscr{A} = 1, 2$ [10, 12, 36, 37]. Correction terms for $l \ll \xi$ are also known and can be found in [29]. We give an alternate, slightly heuristic proof for this at the end of this chapter.

2.3 Entanglement entropy after a global quench

So far, we have only discussed static cases in thermodynamic equilibrium. But our observable world is hardly in any equilibrium and we need to consider dynamical cases. Entanglement entropy gives us a method to keep track of the state of equilibrium in the system. We expect that it is non-decreasing and reaches its maximum value when the system is in equilibrium.

For now, we will consider time evolution after a *global quench* [8, 38]. Suppose we have a one dimensional system at zero temperature. The state of the system can be controlled via a control parameter λ e.g. an external magnetic field and its time evolution is determined by the Hamiltonian $H(\lambda)$. We assume that the theory is conformal for all λ like in the case of massless $\lambda\phi^4$ theory. Suppose that the system is initally in its ground state $|\psi_0\rangle$ for λ_0. The control parameter is changed suddenly at $t = 0$ i.e. a global quench occurs. After the quench, the system evolves

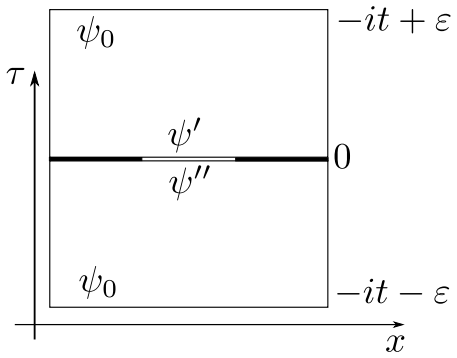

Figure 2.3: A path integral depiction of the reduced density matrix for the quenched field theory.

unitarily according to the Hamiltonian of the theory. Due to the sudden change of conditions, the original state should not evolve into the new ground state. Instead, the state is a superposition of the ground state and the excited states of the new Hamiltonian but it is still pure in the sense that the total entropy is zero. The scenario of the global quench corresponds to injection of energy all around the system.

The density matrix of the theory evolves unitarily for times after the quench

$$\langle\psi_1|\rho(t)|\psi_2\rangle = N_\varepsilon^{-1}\langle\psi_1|e^{-i(t-i\varepsilon)H(\lambda)}|\psi_0\rangle\langle\psi_0|e^{i(t+i\varepsilon)H(\lambda)}|\psi_2\rangle, \tag{2.44}$$

where we have introduced a regularization parameter ε to prevent ultraviolet divergence and a normalization constant N_ε. We can remove the parameter in the end if there are no divergences.

We switch to imaginary time formalism with $\tau_1 = it+\varepsilon$, $\tau_2 = -it+\varepsilon$ and identify the elements of ρ as two path integrals in imaginary time intervals $(-\tau_1, 0)$ and $(0, \tau_2)$. As an example

$$\langle\psi_1|e^{-\tau_1 H(\lambda)}|\psi_0\rangle = \mathcal{Z}(\tau)^{-1}\int [D\phi]\delta(\phi(x,0)-\psi_1(x))\delta(\phi(x,-\tau_1)-\psi_0(x))e^{-S_E(\phi)}, \tag{2.45}$$

where the Euclidean action $S_E(\phi)$ is solely in the new background and we have made a mathematically equivalent reinterpretation of the density matrix. For the other path integral, the boundary conditions are ψ_0 at $\tau=\tau_2$ and ψ_2 at $\tau=0$. We can combine the two path integrals into a single one as we did in our original static case (2.5). Pictorially, this is the same as having an infinite strip of width 2ε and ψ_0 as boundary conditions on both edges and then cutting along $\tau=0$. Like before, the trace is taken by sewing the edges along $\tau=0$ and the reduced density matrix for A is obtained by sewing along $\tau=0$ only at $x\in A^{\complement}$. This is depicted in figure (2.3). The integer powers of ρ_A^n are obtained by cyclically sewing the consecutive n strips along $\tau=0$ at $x\in A$ and [8]

$$\mathrm{Tr}\rho_A^n = \frac{\mathcal{Z}_n}{\mathcal{Z}_1^n}. \tag{2.46}$$

We consider the system to be at (or near) its quantum critical point and the size l and t to be much larger than the minimum distance (i.e. lattice spacing) of the system. Therefore, the bulk of the system can be described by bulk RG fixed point theory (i.e. a CFT). The boundary conditions, on the other hand, will flow to some fixed boundary state. Thus, we can replace $|\psi_0\rangle$ by RG invariant $|\psi_0^*\rangle$. Technically, the changes to leading order can be taken into account by changing the boundary

Figure 2.4: The mapping of strip geometry to upper-half plane. Notice, how the argument of the points in the UHP is determined completely by the imaginary part of the strip points and how the radius of the UHP points is determined by the real part of the strip points.

times $\tau_1 \to \tau_1 + \tau_0$ and $\tau_2 \to \tau_2 + \tau_0$. Now, we can set $\varepsilon \to 0$ and consider the strip width to be $2\tau_0$. The parameter τ_0 is called the extrapolation length in the context of boundary critical behaviour and describes the RG distance to the RG invariant state. It is expected to be of the order of typical time scale of the Hamiltonian [8].

2.3.1 One interval after a global quantum quench in an infinite system

Once again, the case of one interval can be calculated analytically. Let the interval be of length $l \in [-l/2, l/2]$ at $\tau = \tau_1$. We carry out the calculations assuming that τ_1 and τ_2 are real and then analytically continue them to their complex values in the end. Assuming that the Hamiltonian is in its quantum critical point, we can treat the systems as conformally invariant. The partition function of the Riemann surface can once again be expressed with the the twist fields in the n copy model

$$\mathcal{Z}_n \propto \langle \Phi_n(w_u, \bar{w}_u)\Phi_n(w_v, \bar{w}_v)\rangle_{\text{strip}}, \tag{2.47}$$

where $w_u = -l/2 + i\tau_1$ and $w_v = l/2 + i\tau_1$ are the positions of the boundary points on the strip.

We do not know the form of the correlation functions in the strip geometry itself but they can be deduced using the correlation functions of the upper-half plane discussed in the case of systems with boundaries. The upper-half plane is mapped to the infinite strip with the conformal mapping $w(z) = \frac{2\tau_0}{\pi}\log(z)$ [38]. This is sketched in figure (2.4). Therefore, we can use conformal invariance and boundary CFT to calculate

$$\begin{aligned}\langle \Phi_n(w_u, \bar{w}_u)\Phi_n(w_v, \bar{w}_v)\rangle &= |w'(z_u)\,w'(z_v)|^{-2\tilde{\Delta}_n}\langle \Phi_n(z(w_u), \bar{z}(w_u))\Phi(\bar{z}(w_v), \bar{z}(w_v))\rangle_{\text{UHP}} \\ &= \left(\frac{\pi}{2\tau_0}\right)^{2\tilde{\Delta}_n}\left(\frac{e^{\pi l/(2\tau_0)} + e^{-\pi l/(2\tau_0)} + 2\cosh(\pi t/\tau_0)}{(e^{\pi l/(4\tau_0)} - e^{-\pi l/(4\tau_0)})^2\cosh^2(\pi t/(2\tau_0))}\right)^{\tilde{\Delta}_n}\tilde{\mathcal{F}}_n(x),\end{aligned} \tag{2.48}$$

where we have analytically continued $\tau_1 \to -\tau_0 + it$. Here $\tilde{\Delta}_n = c(n - 1/n)/12$ is the scaling dimension of the twist fields calculated previously for the upper-half plane geometry, $x = (z_{u\bar{u}}z_{v\bar{v}})/(z_{u\bar{v}}z_{\bar{u}v})$ is the four point ratio and z_{ij} is the separation of the points on the upper half plane geometry. The function $\tilde{\mathcal{F}}_n$ depends on the specific theory and is the reason why four-point functions are generally hard to evaluate. However, as t and l are much larger than τ_0, we see that

$$x \to \frac{e^{\pi t/\tau_0}}{e^{\pi l/(2\tau_0)} + e^{\pi t/\tau_0}} \sim \begin{cases} 0 & \text{if } t < l/2 \\ 1 & \text{if } t > l/2 \end{cases}. \tag{2.49}$$

Fortunately, the asymptotic behaviour of $\tilde{\mathcal{F}}$ is well known near these points. When $x \sim 1$, the points are deep in the bulk in the half-plane geometry and then $\tilde{\mathcal{F}}(1) \sim 1$. On the other hand, when $x \sim 0$ the points are near the boundary in the upper-half plane geometry, $\tilde{\mathcal{F}}(0) \sim 1$. Thus, we may safely ignore the additional unknown function [8].

Taking the limit $\tau_0 \to 0$, the expression for two-point function reduces to

$$\langle \Phi_n(w_u, \bar{w}_u)\Phi_n(w_v, \bar{w}_v)\rangle_{\text{strip}} = \left[\frac{\pi}{2\tau_0}\frac{\text{Max}(e^{\pi l/(2\tau_0)}, e^{\pi l/(2\tau_0)})}{e^{\pi l/(2\tau_0)}e^{\pi l/(2\tau_0)}}\right]^{2\tilde{\Delta}_n} \tag{2.50}$$

We remember that the two-point function is proportional to the trace of the powers of reduced density matrix. Therefore, taking the derivative of expression (2.50) at $n = 1$, we get the time evolution of entanglement entropy

$$S_A(l,t) = -\frac{c}{3}\log(\tau_0) + \begin{cases} \frac{\pi c t}{6\tau_0} & \text{if } t < l/2 \\ \frac{\pi c l}{12\tau_0} & \text{if } t > l/2 \end{cases}. \tag{2.51}$$

We notice that the entanglement entropy grows linearly for times $t < l/2$ and reaches a constant value after the critical time $t_c = l/2$ which is linear in l i.e. an extensive quantity. In our result, there is a sharp cusp at the critical time. In more physical situations, the cusp is rounded around the critical time with radius $\sim \tau_0$ [8].

If we do not make the assumption $\tau_0 \ll t$, but instead assume $\tau_0 \gg t$, we will see a quadratic increase of the entanglement entropy at the early times

$$S_A(l,t) = \frac{c\pi^2}{24\tau_0^2}t^2 - \frac{c}{3}\log\left(\frac{\pi}{2\tau_0}\right). \tag{2.52}$$

The behaviour of the entanglement entropy is drastically different from our previous results where the entanglement entropy depended logarithmically on l. The final value is more like the expression for thermal entropy in result (2.29) with $\beta_{\text{eff}} = 4\tau_0$. This is due to the fact that we made a sudden change in the control parameter λ which caused the system to be moved away from the ground state. The physical interpretations is that A reaches a quasi-static thermal state and the remaining infinite system $A^{\complement}$ acts as a heat bath. It has been shown in [41] that the effective temperature of the final state also appears when evaluating two-point functions making it a physically relevant parameter. However, the final state is still a pure state with vanishing entropy as the time evolution was done unitarily. As pointed out in [17], the fact that the time evolution of the whole system is unitary does not imply that it is unitary in a subsystem. Had we done the change of control parameter adiabatically, the system would have remained arbitarily close to its ground state and the entanglement entropy would have retained its logarithmic form.

Time evolution of entanglement entropy has also been studied for solvable one dimensional lattice models at their critical point, such as the XY model, and they exhibit behaviour very similar to the result above. The linear growth before the critical time appears to be a universal feature at least for large l and the critical time is approximately at $t_c \sim l/2$. However, most lattice models do not reach their asymptotic value immediately after the critical time. They seem to approach it only asymptotically. This issue will be addressed later [11, 39, 40].

2.3.2 Time evolution for a semi-infinite chain

To combine what we have learned so far, we can evaluate the time evolution of entanglement entropy for a single interval in a semi-infinite system. This time, the geometry of the system is a semi-infinite strip where the bounded imaginary time axis is on the real axis and the position axis is on the imaginary axis. For simplicity, we consider the interval to be starting from the boundary of the system.

As before, we form the Riemann surface in a cyclic fashion along the interval. This time, there is only one branch point so we are interested in the one-point function on the semi-infinite strip to which the partition function is proportional. The mapping $z(w) = \sin\left(\frac{\pi w}{2\tau_0}\right)$ takes the semi-infinite strip to the upper-half plane geometry mapping the corner points $\pm\tau_0$ to ± 1 [41]. Thus, the one-point function on the strip is

$$\langle \Phi_n(\tau_1 + il, \tau_1 - il)\rangle = \left(\frac{\pi}{2\tau_0}\right)^{2\tilde{\Delta}_n} \frac{(\cosh^2(\pi l/(2\tau_0)) - \sin^2(\pi\tau_1/(2\tau_0)))^{\tilde{\Delta}_n}}{(2\sin(\pi\tau_1/(2\tau_0))\sinh(\pi l/(2\tau_0)))^{2\tilde{\Delta}_n}}. \tag{2.53}$$

Inserting $\tau_1 = it - \tau_0$ and assuming $l, t \gg \tau_0$, we get

$$\mathrm{Tr}\rho_A^n = c_n \left(\frac{\pi}{8\tau_0}\right)^{2\tilde{\Delta}_n} \left(\frac{e^{\pi l/\tau_0} + e^{\pi t/\tau_0}}{e^{\pi(t+l)/\tau_0}}\right)^{\tilde{\Delta}_n}, \quad S_A(t,l) = -\frac{c}{6}\log(\tau_0) + \begin{cases} \frac{\pi c t}{12\tau_0} & \text{if } t < l \\ \frac{\pi c l}{12\tau_0} & \text{if } t > l \end{cases} \tag{2.54}$$

We notice many similarities with the result for time evolution in the infinite system and the entanglement entropy for the semi-infinite system. The entropy grows linearly at first at half speed but after the critical time, which is $t_c = l$ this time, the entropy reaches a constant value, which is the same as the one for the infinite system.

2.3.3 Time evolution for multiple intervals

As the boundary theory specific function $\tilde{\mathcal{F}}$ could be disregarded for one interval, so can it be forgotten for multiple intervals to reasonable accuracy. This calculation has been done in [38] and we simply quote the result as we will need it later. Let the spatial region be $A = [u_1, u_2] \cup \ldots \cup [u_{2N-1}, u_{2N}]$, i.e. N disjoint intervals. We can freely translate the intervals such that their center of mass is at the origin i.e. $\sum_{i=1}^{2N} u_i = 0$. In this case, the time evolution of entanglement entropy is approximately

$$S_A(t) \approx S_A(\infty) + \frac{\pi c}{12\tau_0} \sum_{i,j}^{2N} (-1)^{i-j} \mathrm{Max}(u_i - t, u_j + t). \tag{2.55}$$

Here, $S_A(\infty)$ is the final entanglement entropy corresponding to the sum of the individual lengths of the intervals multiplied with the constant $\frac{\pi c}{12\tau_0}$. From the result, we see that the sum vanishes as $t \to \infty$ if N is finite or u_k are bounded. If the u_k are not bounded, we could construct a system in which the entanglement entopy has a saw-tooth like behaviour [38].

2.3.4 Physical interpretation via creation of quasiparticles

Many of the features of the time evolution can be understood with a semi-classical toy model. The original state $|\psi_0\rangle$ is a mixture of the ground state and excited states of the Hamiltonian $H(\lambda)$. The

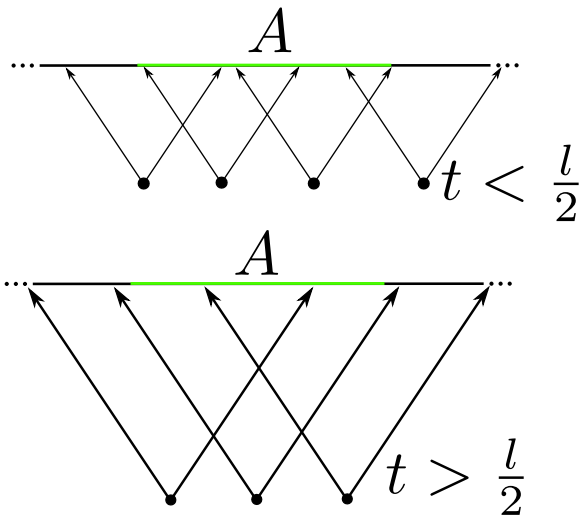

Figure 2.5: The quasiparticle image when the particles propagate at maximum speed, $v = 1$. At late times, some quasiparticles have already swept over the whole region A.

change of control parameter λ can then be considered as a global injection of energy in the system. This excess energy is dispersed by emission of pairs of *quasiparticles*, which are formed everywhere. This then leads to the thermalization of the system. Quasiparticles produced at the same point are entangled but those that are created apart, are not entangled. We assume that at $t = 0$, all over the system, pairs of particles are created with momenta p' and p'' with cross-section $f(p', p'')$, one left moving and one right moving. After emission, the particles move classically with energy E_p and their speed is $v_p = dE_p/dp$. When two particles, emitted at the point x, reach two different points at time t', all the points between $x + v_{p'}t'$ and $x + v_{p''}t'$ are entangled. The maximum speed of particles is limited by special relativity, $|v_p| \leq 1$ [8]. This is depicted in figure (2.5).

As to entanglement entropy, the above discussion implies that the entangled quasiparticles increase entanglement entropy whenever they are in different regions simultaneously and that it is extensive. Therefore, we can make a crude approximation of the time evolution of entanglement entropy between A and its complement.

$$S_A(t) \approx \int_A \mathrm{d}x' \int_{A^{\complement}} \mathrm{d}x'' \int_{-\infty}^{\infty} \mathrm{d}x \int \mathrm{d}p' \mathrm{d}p'' f(p', p'') \delta(x'' - x - v_{p''}t) \delta(x' - x - v_{p'}t) \tag{2.56}$$

Now, assume that we have an infinite system and A is a single interval of length l. We can simplify the expression by realizing that the entanglement to the right of A is the same as to the left of A. Therefore, we can multiply the integral by two and neglect the axis left of A. Also, we can now set

$p'' > 0,\ p' < 0.$

$$\begin{aligned} S_A(t) &\approx 2\int_0^l \mathrm{d}x' \int_l^\infty \mathrm{d}x'' \int_\infty^0 \mathrm{d}p' \int_0^\infty \mathrm{d}p'' f(p',p'')\delta(x''-x'-(v_{-p'}+v_{p''})t) \\ &= 2\int_0^l \mathrm{d}x' \int_\infty^0 \mathrm{d}p' \int_0^\infty \mathrm{d}p'' f(p',p'')\theta(x'+(v_{-p'}+v_{p''})t-l) \\ &= 2t\int_\infty^0 \mathrm{d}p' \int_0^\infty \mathrm{d}p'' f(p',p'')((v_{-p'}+v_{p''})t)\theta(l-(v_{-p'}+v_{p''})t) \\ &\quad + 2l\int_\infty^0 \mathrm{d}p' \int_0^\infty \mathrm{d}p'' f(p',p'')\theta((v_{-p'}+v_{p''})t-l). \end{aligned} \tag{2.57}$$

Here, θ is the Heaviside step-function. Before the critical time $t_c = l/2$, the second integral vanishes as $|v_p| \leq 1$ and the entanglement entropy grows linearly. After the critical time, the second integral begins contributing and is eventually the only term that is non-zero. However, as there are conformal field theories with quasiparticles slower than the maximum speed, the terms vary smoothly instead of abruptly at the critical time as the CFT results predicted [38]. This simple toy model provides us with a natural explanation as to why the entanglement grows linearly but doesn't reach a constant value immediately after the critical time. This non-abrupt behaviour has been shown in some lattice models [39, 38]. The cross-section f has been calculated for the XY model in [39].

We could have varied the control paramater λ locally leading to inhomogeneous quenches. This case has been calculated analytically and can be found in [42].

2.4 Entanglement entropy after a local quench

We now move on to another kind of quench. We consider once again an infinite one dimensional chain. This time, the system is divided in two so that the two sides are both in their own ground states and not entangled with each other. We then choose a subsystem A and consider the time evolution of its entanglement entropy after we remove the decoupling. The physical situation corresponds to the case, when we inject energy to an infinite system at one location i.e. a *local quench*. This problem cannot be solved using the methods for global quench as the system is not translationally invariant and the boundary condition does not flow into a RG invariant state (i.e. conformally symmetric) [43].

However, we can still use the path-integral approach we used for global quenches. Consider the expression (2.44). We can reinterpret it as a path integral with boundary conditions $|\psi_0\rangle$ at $\tau = \pm\varepsilon$ and discontinuous arbitrary boundaries at some imaginary time τ. To impose the boundary between the two semi-infinite systems, we modify the Euclidean geometry by inserting a slit along the imaginary time axis for $\tau > +\varepsilon$ and $\tau < -\varepsilon$. We impose conformal boundary conditions at the slit. For the rest of the calculation we will consider τ to be real and $|\tau| < \varepsilon$. After the calculations, we will analytically continue it to it [43, 44].

Once again, the geometry of the slitted plane is too difficult to handle straightforwardly so we must map it to something more familiar. This can be done with the conformal mapping to right

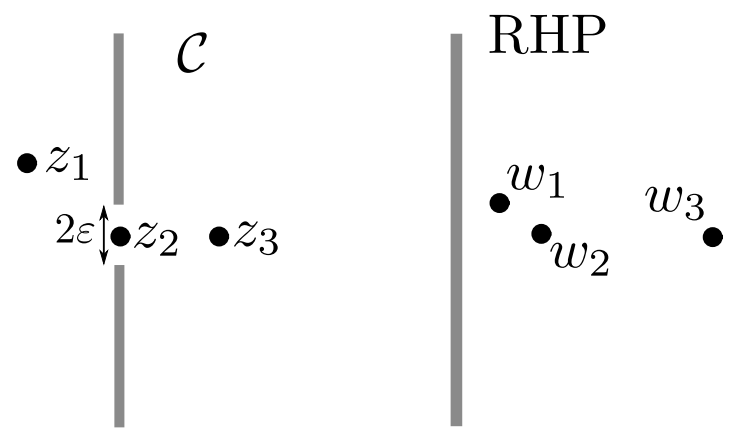

Figure 2.6: The mapping of the split complex plane to right-half plane. Here $z_1 = -1 + i$, $z_2 = 0$ and $z_3 = 1 + i$ and $\varepsilon = 0.5$.

half plane ($\Re w > 0$) $z \mapsto w$ and with the inverse

$$w(z) = \frac{z}{\varepsilon} + \sqrt{\left(\frac{z}{\varepsilon}\right)^2 + 1}, \quad z(w) = \varepsilon \frac{w^2 - 1}{2w}. \tag{2.58}$$

Here the square root is understood with a branch cut at the negative real axis [43, 45]. The mapping is depicted in figure (2.6).

2.4.1 The case of semi-infinite interval

The explicit calculations is done for the cases of semi-infinite A. We consider the quench point to be situated at $x = 0$. At first, we consider $A = (-\infty, 0]$ and consider the evolution of entanglement entropy after the two disjoint regions are connected. We can construct the Riemann surfaces as we have done before. We can see, based on our previous calculations, that we need only consider one-point functions of twist fields Φ_n to evaluate the entanglement entropy. In the right half plane, the one point functions are calculated $\langle \Phi_n(w, \bar{w}) \rangle_{\text{RHP}} = (2\Re w)^{-\tilde{\Delta}_n}$ [43].

We evaluate the one-point function of at $z_1 = i\tau$ on the Riemann surface of the slit geometry.

$$\begin{aligned} \text{Tr}\rho_A^n &= \tilde{c}_n \langle \Phi_n(i\tau, -i\tau) \rangle = |w'(z(i\tau))|^{\tilde{\Delta}_n} \langle \Phi_n(w(i\tau)) \Phi_n(w(-i\tau)) \rangle_{\text{RHP}} \\ &= \left(\frac{1}{\sqrt{\varepsilon^2 - \tau^2}} \right)^{\tilde{\Delta}_n} \left(\frac{a}{2\sqrt{1 - \tau^2/\varepsilon^2}} \right)^{\tilde{\Delta}_n} \end{aligned} \tag{2.59}$$

where $\tilde{\Delta}_n = c(n - 1/n)/12$ and a is a number with dimesion of length to fix the overall dimension. After analytically continuing $\tau = it$, the entanglement entropy is

$$S_A(t) = -\frac{\partial}{\partial n} \text{Tr}\rho_A^n = \frac{c}{6} \log\left(\frac{t^2 + \varepsilon^2}{2a\varepsilon} \right) + \tilde{c}_1' \tag{2.60}$$

When $t \gg \varepsilon$, the expression simplifes to

$$S_A(t) = \frac{c}{3} \log\left(\frac{t}{\varepsilon} \right) + k_0. \tag{2.61}$$

Here $k_0 = \frac{c}{6} \log\left(\frac{\varepsilon}{2a}\right) + \tilde{c}_1'$, which we can set to zero by requiring that $S_A(t = 0) = 0$ which requires that we fix $a = \varepsilon \exp(6\tilde{c}_1'/c)/2$.

Now, we consider the case of $A = (-\infty, l]$, where the region overlaps the quench point. We evaluate the one-point function at $z_2 = l + i\tau$.

$$\varepsilon w_2 = l + i\tau + \rho e^{i\theta}, \text{ with } \theta = \frac{1}{2}\arctan\left(\frac{2l\tau}{\varepsilon^2 - \tau^2 + l^2}\right), \tag{2.62}$$

$$\rho_0 = \sqrt[4]{(\varepsilon^2 - \tau^2 + l^2)^2 + 4l^2\tau^2)} \tag{2.63}$$

$$\varepsilon |w'(z_1)| = \left|\frac{\rho_0 e^{i\theta} + w}{\rho_0 e^{i\theta}}\right| = \frac{\sqrt{(l + \rho_0\cos(\theta))^2 + (\tau + \rho_0\sin(\theta))^2}}{\rho} \tag{2.64}$$

$$\mathrm{Tr}\rho_A^n = \tilde{c}_n \left(\frac{a\sqrt{(l + \rho\cos(\theta)) + (\tau + \rho\sin(\theta))^2}}{2\rho_0(l + \rho_0\cos(\theta))}\right)^{\tilde{\Delta}_n} \tag{2.65}$$

The expression looks daunting but we can take $l, t \gg \varepsilon$ after analytically continuing $\tau = it$. After some complex algebraic manipulations, we see that $\rho_0 \to \sqrt{|l^2 - t^2|}$, $\rho_0\cos(\theta) \to \max(l, t)$ and $\rho_0\sin(\theta) \to i\min(l, t)$ for zeroth order of ε. Inserting these (with higher order corrections) to the equation above, we get the entanglement entropy

$$S_A(t, l) = \begin{cases} \frac{c}{6}\log\left(\frac{2l}{a}\right) + c_1', & \text{if } t < l \\ \frac{c}{6}\log\left(\frac{t^2 - l^2}{\varepsilon}\right) + k_0, & \text{if } t > l \end{cases} \tag{2.66}$$

where k_0 is as above. At early times, we see that the entropy corresponds to the case of finite interval at the boundary of a semi-infinite system. Likewise, at late times, the latter expression simplifies to the expression (2.61). The critical time in this case is $t_c = l$, i.e. the slope of the entanglement entropy changes abruptly at this point [43].

2.4.2 The case of finite intervals

Often, we are more interested in the case of finite intervals. The calculations above can be generalized by using two-point functions. Unfortunately, we need to concern ourselves with the additional function $\tilde{\mathscr{F}}_{n,N}$ appearing for two-point functions of the right half plane. The explicit calculations have been carried out in [43, 44] and we will simply quote their results.

For the interval $A = [0, l]$, the entanglement entropy is

$$S_A = \begin{cases} \frac{c}{3}\log\left(\frac{t}{a}\right) + \frac{c}{6}\log\left(\frac{l}{\varepsilon}\right) + \frac{c}{6}\log\left(4\frac{l-t}{l+t}\right) + 2\tilde{c}_1' + \tilde{\mathscr{F}}_{1,2}'(\eta), & \text{if } t < l \\ \frac{c}{3}\log\left(\frac{l}{a}\right) + 2\tilde{c}_1', & \text{if } t > l \end{cases} \tag{2.67}$$

We see that at early times, the first term simply corresponds to the entanglement entropy after a local quench in a semi-infinite interval and the second term corresponds to the entanglement entropy of a interval in a semi-infinite system, which is quite natural. The third term is the non-trivial cross term. We also see, that the theory specific function $\tilde{\mathscr{F}}$ makes its appearance during the time evolution. After the critical time $t_c = l$, the expression is almost the same as for a finite interval in an infinite system with the exception of boundary entropy $\log g = 2\tilde{c}_1' - c_1'$ and the theory specific boundary function can also be ignored in this regime [8].

On the other hand, for $A = [l_2, l_1]$ where $l_1 > |l_2| > 0$, the entanglement entropy is for $t, l_1, |l_2| \gg \varepsilon$

$$S_A = \begin{cases} \frac{c}{6}\log\left(\frac{2l_1}{a}\right) + \frac{c}{6}\log\left(\frac{2|l_2|}{a}\right) + 2\tilde{c}_1' + \tilde{\mathscr{F}}_{1,2}'(\eta) & \text{if } l_2 < 0, t < |l_2| \\ \frac{c}{6}\log\left(\frac{(l_1-l_2)^2}{(l_1-l_2)^2}\frac{4l_1|l_2|}{a^2}\right) + 2\tilde{c}_1' + \tilde{\mathscr{F}}_{1,2}'(\eta) & \text{if } l_2 > 0, t < l_2 \\ \frac{c}{6}\log\left(\frac{(l_1-l_2)(l_1-t)}{(l_1-l_2)(l_1+t)}\frac{4l_1(t^2-l_2^2)}{\varepsilon a^2}\right) + 2\tilde{c}_1' + \tilde{\mathscr{F}}_{1,2}'(\eta) & \text{if } |l_2| < t < l_1 \\ \frac{c}{3}\log\left(\frac{l_1-l_2}{a}\right) + 2\tilde{c}_1' & \text{if } t > l_1 \end{cases} \tag{2.68}$$

It is immediately seen that the theory specific function haunts us once again for the time evolution regimes. It can be disregarded only after the subsystem has reached equilibrium i.e. $t > l_1$. We notice that the first equation corresponds to the sum of two cases of semi-infinite systems with a finite interval at the boundary. The second equation corresponds to the entanglement entropy of a finite interval $[|l_2|, |l_2| + l_1]$ of a semi-infinite system. In the third equation, we see that the time variable is only connected to l_2 and not to l_1. This is consistent with our previous results as the entanglement from the discontinuity has only reached the nearer left boundary of A. The final equation corresponds to the entanglement of interval $[l_2, l_1]$ in an infinite system with an extra boundary entropy term [8, 44].

It is notable, that the entanglement entropy is not a monotonous function of time. For example, in the case of $A = [0, l]$, the entanglement entropy has a maximum value at $t = l(\sqrt{5}-1)/2$ if we ignore the contribution of the derivative of $\tilde{\mathscr{F}}_{1,2}$.

Interestingly, as pointed out in [44], if we consider the symmetric case i.e. $-l_2 = l_1 \equiv l$, the entanglement entropy is constant, $S_A = c/3\log(l/a) + 2\tilde{c}_1'$. This can be understood with the quasiparticle picture explained below.

Multiple intervals

The case of multiple intervals has been considered in [44]. They only considered intervals with equal length. We will just quote their results as we will need them later in chapter 6. For the symmetric case, where $A = [-(d/2 + l), -d/2]$ and $B = [d/2, d/2 + l]$, the entanglement entropy is

$$S_{A\cup B} = \frac{c}{3}\log\left(\frac{dl^2(2l+d)}{a^2(d+l)^2}\right) + 4\tilde{c}_1' + \tilde{\mathscr{F}}_{1,4}'(\{\eta_i\}). \tag{2.69}$$

The universal part is constant in time, in accordance with the result for a single symmetric interval. The universal part is the sum of entanglement entropies for single intervals of length l at distance d from the boundary.

For the case of two asymmetric intervals, but still on the opposite sides, there are five different regimes of evolution, the first and the last one corresponding to the regime of constant entanglement entropy, the first corresponding to the non-interacting case and the last corresponding to the interacting case. Let $A = [-(d - x + l), -(d - x)]$ and $B = [x, x + l]$ where x is the distance of B from the boundary and d is the distance between the two intervals. Assuming that $x < d - x + l$, the

entanglement entropy in two other regimes is given by

$$S_{A\cup B}(d-x<t<x) = \frac{c}{6}\log\left[\frac{16xdl^3(l+d-x)(l+x)(l-d+2x)(t^2-(d-x)^2)(x-t)(l+d-x-t)(l+x+t)}{a^4\varepsilon(2x-d)(l+2d-2x)(l+2x)^2(l+d)(x+t)(l+d-x+t)(l+x-t)}\right] +4\tilde{c}_1' + \tilde{\mathscr{F}}'_{1,4}(\{\eta_i\}), \tag{2.70}$$

$$S_{A\cup B}(x<t<d-x+l) = \frac{c}{6}\log\left[\frac{4d^2l^2(l+d-x)(l+x)(l^2-(d-2x)^2)}{a^4(l+2d-2x)(l+2x)(l+d)^2}\right] + 4\tilde{c}_1' + \tilde{\mathscr{F}}'_{1,4}(\{\eta_i\}). \tag{2.71}$$

The entanglement entropy in the final region, $d-x+l<t<x+l$, is given to great accuracy by replacing t in (2.70) with $(d+l)/2-t$. This is due to the fact that the time evolution of entanglement entropy is almost symmetric about $t=(d+l)/2$. The universal terms are depicted in figure (2.7).

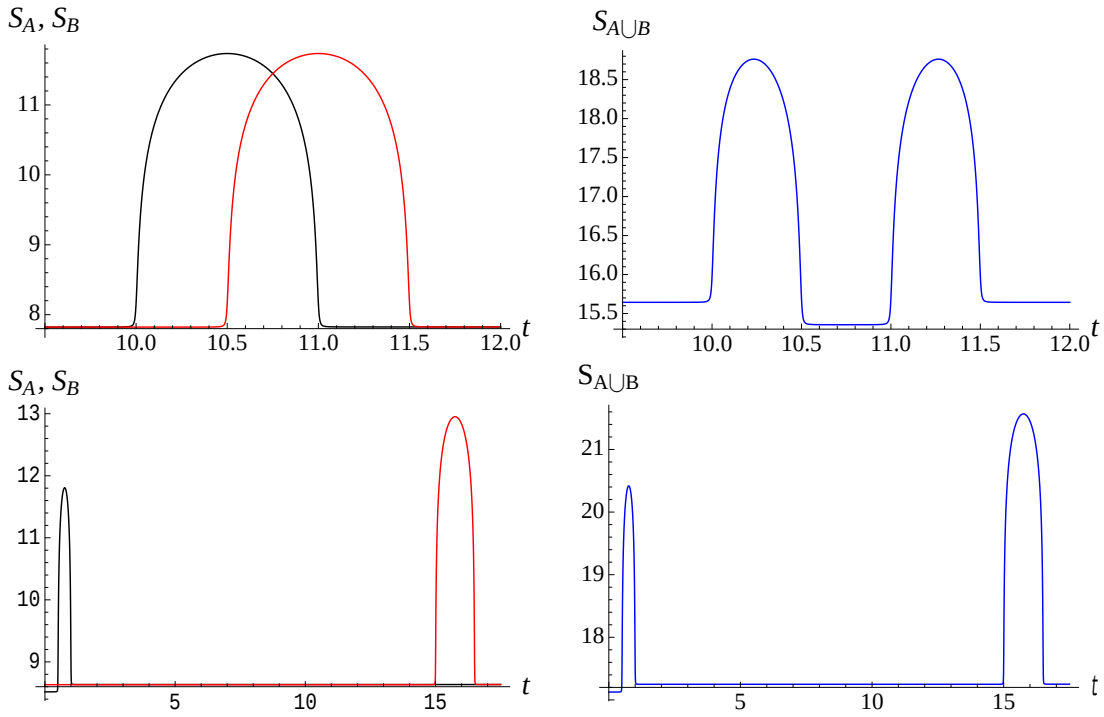

Figure 2.7: On the upper line, we have the entanglement entropies corresponding to two asymmetric intervals, $A=[-11,-10]$ and $B=[10.5,11.5]$ with $\varepsilon=0.01$. On the lower line, we have the entropies corresponding to two intervals on the same side of the defect with some overlap with the defect. Here $A=[-0.1,1]$ and $B=[15,16.5]$. These figures originally appeared in [44]

It is also possible to calculate the entanglement entropy for two intervals on the same side of the defect, but the width of the page is not enough to write the solution. Fortunately, it is given to good accuracy by just summing the contributions of the two individual intervals together. The longer the distance, the better the agreement. This is depicted in the lower line of figure (2.7). This phenomenon is easily understood by considering the quasiparticle picture given below.

The case of multiple discontinuities

Perhaps the most interesting setting would be to consider a finite interval that is disconnected from the two semi-infinite systems. Unfortunately, no general conformal mapping of the corresponding slit geometry to the right half plane is known. Even the vastly simpler problem of one semi-infinite system with a single discontinuity can not be solved generally. The conformal mapping to right half plane is known, but the inverse mapping does not have a closed expression making analytic consideration fruitless.

This has been considered in [43]

2.4.3 Physical interpretation of time evolution after a local quench

Like in the case of global quenches, local quenches, too, can be considered through creation of quasiparticles. This time, quasiparticles are only created at the discontinuity site. This can be understood as an injection of energy into a single point with the energy injected proportional to τ_0^{-1}. The excess energy is then dispersed as emisson of quasiparticles resulting in zero temperature CFT [43]. In the CFT models, the particles emitted travel at the maximum propagation speed, i.e. the speed of sound or speed of light, $|v_s| = 1$ along the lightcone. The pair of particles emitted at the same time are entangled and when they reach points x' and x'' at time t, the two points become entangled. The behaviour of critical time is easily understood with this picture as entanglement remains constant until a one of the pair of quasiparticles reaches A and the other reaches B. This becomes even more evident when we consider the symmetrical case $A = [-l, l]$. The entanglement entropy remains constant as the pair of particles are always in the same subsystem.

The quasiparticle interpretation gains even more ground when we consider the *stress energy tensor* of the system as is done in [44]. We can use the conformal mapping to right half plane as a starting point to evaluate the expectation value of the stress energy tensor in the slit geometry. Then, we can analytically continue $\tau \to it$ and get $\langle T_{tt}(x,t)\rangle = \langle T_{xx}(x,t)\rangle = \langle T_{ww}(x-t) + T_{\bar{w}\bar{w}}(x+t)\rangle$. All in all, we get

$$\langle T_{tt}(x,t)\rangle = \langle T_{xx}(x,t)\rangle = \frac{c\varepsilon^2}{16\pi}\left(\frac{1}{((x-t)^2+\varepsilon^2)^2} + \frac{1}{((x+t)^2+\varepsilon^2)}\right) \tag{2.72}$$

$$\langle T_{tx}(x,t)\rangle = \langle T_{xt}(x,t)\rangle = -\frac{c\varepsilon^2}{16\pi}\left(\frac{1}{((x-t)^2+\varepsilon^2)^2} - \frac{1}{((x+t)^2+\varepsilon^2)}\right) \tag{2.73}$$

or

$$\langle T_{\pm\pm}(x_\pm)\rangle = \frac{c}{16\pi}\frac{\varepsilon^2}{(x_\pm^2+\varepsilon^2)^2}, \quad \langle T_{\pm\mp}\rangle = 0, \tag{2.74}$$

where $x_\pm = x \pm t$ are the light cone coordinates. We can see, that the energy density, $\langle T_{tt}\rangle$, is concentrated on the lightcone.

2.5 Four dimensional conformal field theory

Before we dwell into holography, we will shortly discuss entanglement entropy in four dimensional conformal field theories.

2.5.1 Weyl anomaly

Despite the power of 1 + 1 dimensional conformal field theory, the calculation of entanglement entropy in higher dimensions is much more difficult and so far, no exact results are known. There are however other methods to compute the entanglement entropy but these involve choosing a specific theory with its Lagrangian making the calculations less appealing. Despite the difficulty, there have been some general analytic results for general conformal field theories, especially in 3 + 1 dimensional CFTs.

In renormalization group theory, the RG fixed points of a quantum field theory are massless, scale invariant theories, often conformal field theories. Much of the power of 1 + 1 dimensional CFT comes from the *c-theorem* [47]. It states that for all 2D quantum field theories, there is a positive real function depending on the coupling constants, C, that decreases monotonically under renormalization group flows and takes the value of central charge at the RG fixed points. Perhaps even more important is that it that the theory has a well-defined quantity, the central charge. The entanglement entropy was found to be proportional to the central charge and it turns out that the degrees of freedom of a quantum field theory is also proportional to the central charge, implying that entanglement entropy and degrees of freedom are proportional, naturally. In odd dimensional cases, the concept of central charge has not been succesfully defined, but in even-dimensional spacetimes the situation is not so dim due to the existence of Weyl anomaly [28].

The stress energy tensor of a theory is defined as the functional derivative of the action with respect to the metric i.e.

$$T^{\mu\nu} = \frac{4\pi}{\sqrt{g}} \frac{\delta S}{\delta g_{\mu\nu}}, \tag{2.75}$$

where g is the determinant of the component matrix of the metric. In classical conformal field theories, the stress energy tensor has vanishing trace. However, due to quantum effects, the expectation value of the stress energy tensor becomes non-zero in even-dimensional spacetimes. This is known as the *Weyl anomaly* and in 1 + 1 dimensional CFT, the expectation value is

$$\langle T^{\mu}_{\mu} \rangle = -\frac{c}{12} R, \tag{2.76}$$

where R is the scalar curvature and c the central charge. This relation can be used to define the central charge of 1 + 1 dimensional field theories. In the previous chapter, we shortly mentioned that the introduction of Riemann surfaces introduced conical singularities on the n copy model and this can be used to calculate the entanglement entropy of the theory [24].

For four dimensional CFTs, the Weyl anomaly is

$$\langle T^{a}_{a} \rangle = -\frac{c}{8\pi} W_{\mu\nu\rho\sigma} W^{\mu\nu\rho\sigma} + \frac{a}{8\pi} \tilde{R}_{\mu\nu\rho\sigma} \tilde{R}^{\mu\nu\rho\sigma}, \tag{2.77}$$

where W and $\tilde{R}$ are the Weyl tensor and the dual of the curvature tensor, respectively. The contracted tensors can be written as

$$W_{\mu\nu\rho\sigma} W^{\mu\nu\rho\sigma} = R_{\mu\nu\rho\sigma} R^{\mu\nu\rho\sigma} - 2R_{\mu\nu} R^{\mu\nu} + \frac{1}{3} R^2, \tag{2.78}$$

$$\tilde{R}_{\mu\nu\rho\sigma} \tilde{R}^{\mu\nu\rho\sigma} = R_{\mu\nu\rho\sigma} R^{\mu\nu\rho\sigma} - 4R_{\mu\nu} R^{\mu\nu} + R^2. \tag{2.79}$$

The coefficients a and c are sometimes called the central charges of the four dimensional CFT. It is believed that a could have its own version of the two dimensional c theorem, sometimes called the a theorem [28].

2.5.2 Entanglement entropy

Now, let our manifold be the $d+1$ dimensional M_1 and let the region A be our spatial region of interest and suppose that it has the length scale l. To calculate the entanglement entropy using the above, we first need to construct the generalized n-sheeted manifold, M_n, corresponding to the bipartition of the spatial region. From the theory of conformal field theories, it is known that variation of the length scale affects the partition function introducing the stress energy tensor. Thus, using this, we get

$$\begin{aligned} l\frac{l}{dl}\log\left[\mathrm{Tr}_A\rho_A^n\right] &= 2\int d^{d+1}x g_{\mu\nu}\frac{\delta}{\delta g_{\mu\nu}}\left[\log\mathcal{Z}_n - n\log\mathcal{Z}_1\right] \\ &= -\frac{1}{2\pi}\left\langle\int d^{d+1}x\sqrt{g}T^\mu_\mu\right\rangle_{M_n} + \frac{n}{2\pi}\left\langle\int d^{d+1}x\sqrt{g}T^\mu_\mu\right\rangle_{M_1}. \end{aligned} \tag{2.80}$$

We wish to consider spacetimes that were originally flat, thus the latter integral vanishes. In this case, the entanglement entropy has the relation [28, 7]

$$l\frac{d}{dl}S_A = \frac{1}{2\pi}\lim_{n\to1}\frac{\partial}{\partial n}\left\langle\int d^{d+1}x\sqrt{g}T^\mu_\mu\right\rangle_{M_n}. \tag{2.81}$$

Now, in the case of a two-dimensional CFT, we had

$$R = 4\pi(1-n)\left[\delta^{(2)}(x-u)+\delta^{(2)}(x-v)\right] \tag{2.82}$$

for one interval. Plugging this into the Weyl anomaly expression and the equation above, we have

$$l\frac{d}{dl}S_A = \frac{c}{3}. \tag{2.83}$$

Integrating, we get the logarithmic behaviour. Even more, we could have assumed that the theory has a small mass, m. In this case, we could have repeated the calculations above for one conical singularity and replaced l with $m^{-1}=\xi$, the correlation length. This would then give us the expression for entanglement entropy of a semi-infinite interval in a massive theory (2.43) [28],

$$S_A = \frac{c}{6}\log\frac{\xi}{\varepsilon}.$$

In even dimensional manifolds, the *Euler number* is given by integrating the *Euler density* over the whole manifold. In two dimensional spacetimes, the Euler density is proportional to the scalar curvature i.e.

$$\chi[M_n] = \frac{1}{4\pi}\int_{M_n} d^2x\sqrt{g}R = 2(1-n). \tag{2.84}$$

Interestingly, the Euler density for four dimensions is the latter term in the Weyl anomaly for 4D CFTs [16].

Moving on, an equation entanglement entropy for 4D CFTs can be written as

$$l\frac{d}{dl}S_A = \gamma_1\frac{\mathrm{Area}(\partial A)}{\varepsilon^2}+\gamma_2. \tag{2.85}$$

Here, ε is the UV regulator and γ_1 and γ_2 are numerical constants. The divergent first term comes from the integral over the square Weyl tensor which diverges at the boundary, ∂A, due to the behaviour of the square of scalar curvature. The first term show explicitly on the most divergent term as γ_1 also depends on the UV regulation. The Euler density term produces the Euler number of the n-sheeted manifold and is thus finite. The term γ_2 includes contribution from this and also the non-divergent and the universal terms from the Weyl tensor integration. Therefore, γ_2 is universal (i.e. does not depend on the cutoff) and it could also be measured physically. All in all, the entanglement entropy becomes

$$S_A = \frac{\gamma_1}{2}\frac{\text{Area}(\partial A)}{\varepsilon^2} + \gamma_2 \log\frac{l}{\varepsilon} + S_{A,\text{finite}}, \tag{2.86}$$

where the last term contains finite contributions to the entanglement entropy [48].

We conclude this section with the notion that there is no simple nor straightforward way to calculate entanglement entropy in more than two dimensions. Nevertheless, the above results have been found true in other approaches to entanglement entropy concerning specific theories. We will see the logarithmic contribution emerge later on with spherical regions in even dimensional spacetimes.

Chapter 3

Holographic entanglement entropy

This chapter will focus on the holographic approach to entanglement entropy and introduce the one of the most important formulas in this field: the Ryu-Takayanagi formula. This allows us to evaluate entanglement entropy using methods of general relativity and it is straightforwardly generalized to higher dimensions.

3.1 Briefly on the holographic principle and AdS/CFT correspondence

The *holographic principle* is an idea, that all information of a gravitational physical system inside a spatial region is encoded on the surface surface of the region. The original idea was proposed by 't Hooft [49] in 1993 and the work was extended by Susskind [50]. The reasoning behind this unintuitive idea is fairly simple and I shall review it here.

Consider a three-dimensional spatial region with volume V. We wish to know what is the number of degrees of freedom inside V. Suppose that the system consists of n spin-$\frac{1}{2}$ particles each of which have two degrees of freedom. In this case, $N = 2^n$. Now, let each site of V be occupied by such a particle. We assume that the particles form a lattice with spacing l_p i.e. the Planck length. The maximal entropy inside the region would be $S \sim \log(N) = \log(2)\, V / l_p^3$. This is the intuitive result from classical thermodynamics.

However, this system can very well be a black hole and its horizon can extend beyond the region V. The entropy of black holes, with horizon area A, is given by the Bekenstein-Hawking formula

$$S = \frac{A}{4G} \sim \frac{A}{l_p^2}. \tag{3.1}$$

Suppose that we could have a region V which would have greater entropy than a black hole which would barely fit inside V but V does not have the energy to form it. If we then add a tiny amount of energy inside V, such a black hole could form and it would have smaller entropy than the region in which it was born. This would violate the second law of thermodynamics. This thought experiment was originally made by Bekenstein who concluded that a black hole would maximize the entropy inside a spatial region V. 't Hooft took one step further and claimed that the gravitational physics inside a spatial region V could be perfectly described by the non-gravitational physics on

its boundary. This is the holographic principle and can be straightforwardly generalized to arbitrary spatial dimension d [49].

The first realization of the holographic formula was formulated by Maldacena in 1997 in [51, 52, 53]. The results state that a ten-dimensional type IIB string theory in $AdS_5 \times S^5$ is dual to the $\mathcal{N} = 4$ Super Yang-Mills theory with the gauge group $SU(N)$ in the large N limit in the four-dimensional Minkowski spacetime. In other words, the bulk fields of the weak coupling limit of a string theory, i.e. a supergravity theory, in AdS_5 space has a one-to-one mapping to the operators of the strong coupling limit of a conformal field theory in four dimensions. The group $SO(2,4)$ is the isometry group of four-dimensional CFT and AdS_5, and $SO(6)$ is the isometry group of R-symmetries in the $\mathcal{N} = 4$ Super Yang-Mills theory and S^5. The degrees of freedom corresponding to S^5 decouple from those of AdS_5 in the weak coupling limit and can be removed by dimensional reduction [54].

This is known as the *AdS/CFT duality* which is perhaps the most important discovery of physics in 20 years. The idea has passed numerous tests. The origins of this correspondence is in string theory but it has been applied to many other fields for quite some time. In fact, many of its applications need no understanding of string theory [55]. There are many forms of this duality where the dual theories and regimes of validity vary. The form that we will need is the following. A $d+1$-dimensional quantum field theory in flat space has a dual gravitational theory in AdS_{d+2} background.

The $d+2$ dimensional Anti de-Sitter spacetime is defined as follows. It is a hypersurface in $\mathbb{R}^{(2,d+1)}$ and has the metric induced by it. The defining equation and the metric are

$$-X_0^2 - X_{d+2}^2 + X_1^2 + \ldots + X_{d+1}^2 = -R^2, \quad ds^2 = -dX_0^2 - dX_{d+2}^2 + dX_1^2 + \ldots + dX_{d+1}^2 \tag{3.2}$$

where R is the radius of curvature. AdS_{d+2} is the homogeneous solution to the Einstein field equations with negative cosmological constant, Λ, defined with the action

$$S_g = \frac{1}{16\pi G^{(d+2)}} \int \mathrm{d}^{d+2}x\sqrt{-g}[\mathscr{R} - 2\Lambda], \quad \Lambda = -\frac{d(d+1)}{2R^2}. \tag{3.3}$$

Here $G^{(d+1)}$ is the $d+2$-dimensional gravitational constant and $\mathscr{R}$ is the scalar curvature [56].

Naturally, we can parametrize the $d+2$ X_μ's with $d+1$ parameters. The most useful one is the *Poincaré parametrization* which casts the metric into the form

$$ds^2 = R^2 \frac{dz^2 - dt^2 + dx_i dx_i}{z^2}, \quad i = 1, \ldots, d \tag{3.4}$$

Here $z > 0$. It is evident that there is a boundary at $z = 0$ and the dual CFT is defined at the d+1 dimensional hypersurface $z = \varepsilon$, where ε is an UV regulator corresponding to the UV regulator of the CFT. This is depicted in figure (3.1) for AdS_3. Poincaré coordinates are not defined on the whole of AdS space [54].

Another useful parametrization are the *global coordinates*. Unlike Poincaré coordinates, they are well-defined on the whole of AdS space. With them, the metric takes the form

$$ds^2 = R^2(-\cosh^2(\rho)dt^2 + d\rho^2 + \sinh^2(\rho)d\Omega_d^2). \tag{3.5}$$

In these coordinates, $\rho \geq 0$. This time, the CFT is defined on the $\rho = \rho_0$ hypersurface where ρ_0 is some IR regulator [54]. Unlike the Poincaré coordinates, the corresponding CFT is compact.

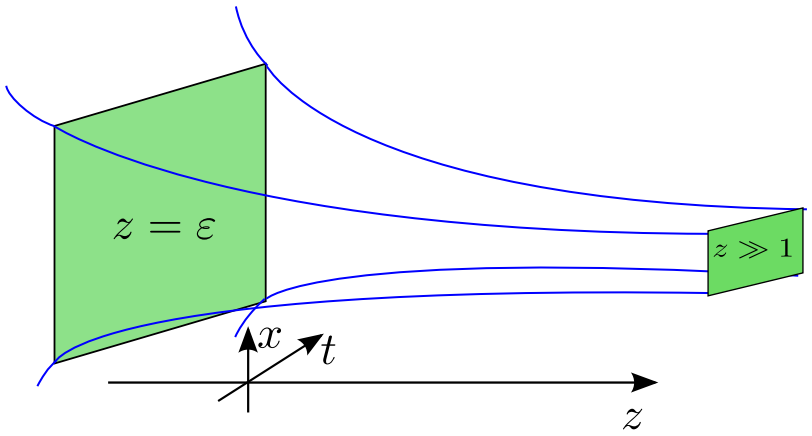

Figure 3.1: A depiction of AdS Poincaré space. The metric diverges as $z \to 0$. The field theory lives on the boundary $z = \varepsilon$.

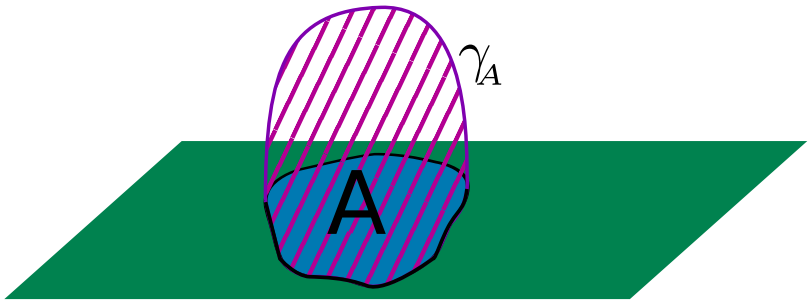

Figure 3.2: A sketch of a minimal surface for a $2+1$-dimensional field theory. The surface extends to the bulk AdS space in the z direction.

The pure AdS space corresponds to CFT at zero temperature. Adding a black hole to the geometry for large z would result in a finite temperature CFT at the boundary. Even more, if we add an IR regularization $\xi > z$, the corresponding theory on the boundary will describe a near-critical system where the correlation length is finite [28].

3.2 Holographic entanglement entropy

3.2.1 Ryu-Takayanagi formula

Partly inspired by the connection of thermal entropy in CFT and black hole entropy in [53], Ryu and Takayanagi proposed a realization of AdS/CFT duality in evaluation of entanglement entropy in [13]. Suppose that there is a time independent $d+1$ dimensional CFT on the boundary of an asymptotically AdS_{d+2} space, $\mathbb{R} \times M$, where we assume that the manifold M is either S^d or $\mathbb{R}^d$. We choose a constant time d dimensional region A in M. We know that the AdS dual is time independent and that there is a natural foliation with spacelike surfaces, $AdS_{d+2} = \mathscr{M} \times \mathbb{R}$. Therefore, there is a region $\mathscr{A}$ in $\mathscr{M}$, on the boundary of which A is.

The *Ryu-Takayanagi formula* for *holographic entanglement entropy* proposes that the entanglement entropy of A can be calculated with the formula

$$S_A = \frac{\text{Area}(\gamma_A)}{4G^{(d+2)}}. \tag{3.6}$$

Here γ_A is the constant time areawise minimal d-dimensional surface in the AdS_{d+2} dual which shares its boundary with A i.e. $\partial(\gamma_A) = \partial A$. The area is to be understood as the d dimensional volume. When $d = 1$, it is to be understood as the length of minimal geodesics and when $d = 2,3$ it is to be understood as the area of a minimal 2-surface or the volume of a 3-surface, respectively. $G_N^{(d+2)}$ is the gravitational constant in $d+2$ dimensions.

This formula is also conjectured to apply for all other quantum field theories with a gravity dual. However, there is no straightforward method to find such gravity duals which is why we will be concentrating only on the few known duals of conformal field theories.

The interpretation for the Ryu-Takayanagi formula is as follows. Entanglement entropy is defined as the entropy of some region after smearing out the rest of the system. In this case, the observer in A has no access to the information in B and sees 'blackness' in the direction of B. In gravitational theories in AdS space, such fuzziness is produced by introducing a horizon γ_A which covers B. For such a surface, $\partial\gamma_A = \partial A = \partial B$, and the area of the horizon, γ_A, is the upper bound for the entanglement entropy or 'blackness'. The minimality requirement is to find the strictest bound for the entanglement entropy. We will see that the upper bound is satisfied exactly for two-dimensional conformal field theories and therefore it is believed that it will also be satisfied in higher dimensions.

In pure AdS space, $\gamma_A = \gamma_B$, which immediately implies the equivalence of entanglement entropies of A and its complement for zero temperature CFTs.

3.2.2 The proof of RT formula

There is no rigorous proof for the Ryu-Takayanagi formula. There is a heuristic proof by Fursaev first presented in [57]. Unfortunately, the proof is flawed as shown in [58]. However, there is a rigorous proof for spherical entangling surfaces as shown in [59].

The main idea of Ryu and Takayanagi and Fursavev was to extend the calculation of $\mathrm{Tr}\rho_A^n$ with twist functions considered in chapter 2 to higher dimensions. We construct manifolds M_n similar to Riemann surfaces and consider it as an n copy model in M, the manifold where the conformal field theory is defined. At the boundary of the spatial region ∂A, there is a angular excess $\delta = 2\pi(n-1)$ and a conical singularity $R = 4\pi(n-1)\delta^{(d+1)}(\partial A)$.

According to AdS/CFT duality, the partition functions of the conformal field theory on the boundary and the gravitational theory in the bulk AdS space are equal,

$$\int [D\phi] e^{-S_{\mathrm{CFT}}(\phi)} = \int [Dg] e^{-S_{\mathrm{gr}}(g)}. \tag{3.7}$$

The integral on the right-hand side is taken over all metrics that produce the curvature of the field theory on the boundary. The gravitational action is roughly

$$S_g = -\frac{1}{16\pi G_N^{(d+2)}} \int_{\mathscr{M}} \mathrm{d}^{d+2}x\sqrt{g}R - 2\Lambda + \cdots \tag{3.8}$$

where $\mathscr{M}$ is the bulk AdS space on the boundary of which is the CFT. The idea by Fursaev was to extend the conical singularity to the bulk AdS space, $R = 4\pi(n-1)\delta^{(d+2)}(m_A)$, where m_A is some surface which shares its boundary with A. He then considered different metrics that would

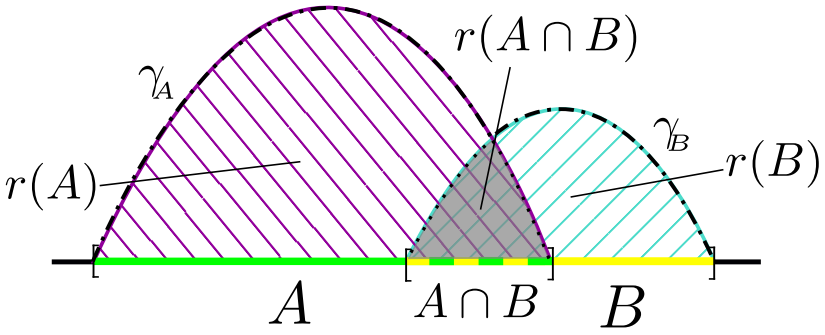

Figure 3.3: A graphical proof of the strong subadditivity property of holographic entanglement entropy. The dot-dashed and dotted lines are surfaces for $A \cup B$ and $A \cap B$, respectively.

reproduce the conical singularity at the boundary. After making the assumption that there is one dominant metric that minimizes the action and contributes most to the partition function, he arrived at the result

$$\log(\mathcal{Z}_{\mathrm{gr},n}) = -I_{\mathrm{gr},n}[\bar{g}] \approx \frac{\mathrm{Area}(\gamma_A)}{4G_N^{(d+2)}}(n-1) + \cdots \tag{3.9}$$

where γ_A is the minimizing surface. Now, differentiating the logarithm of the partition function with respect to n at $n = 1$, we get the entanglement entropy which is equivalent to Ryu-Takayanagi formula [57].

The great failure in this logic is that when we divide the expression with $n-1$, we get the entanglement Renyi entropy, $S^{(n)}$ which is independent of n. As shown in many calculations, the entanglement Renyi entropy generally depends on n. The point where this proof fails is that the minimizing action may not be the true saddle point of the path integral. It is also speculated, that the argument by Fursaev may be correct at the vicinity of $n = 1$ [58].

3.2.3 Holographic proof of strong subadditivity and Araki-Lieb inequality

Holographic entanglement entropy provides us with a very simple proof for strong subadditivity (1.8) and the Araki-Lieb inequality (1.9) as shown in [60, 61].

Suppose we have arbitrary, not necessarily separate regions A and B with minimal surfaces γ_A and γ_B in the bulk, respectively. Define $r(A)$ as regions of the bulk geometry such that $\partial r(A) = \gamma_A \cup A$. $r(B)$ is defined similarly. Define $r(A \cup B) = r(A) \cup r(B)$ and $r(A \cap B) = r(A) \cap r(B)$. We decompose the surfaces of these regions to the part on the CFT boundary and the one in the bulk such that $\partial r(A \cup B) = m_{A\cup B} \cup A \cup B$ and $\partial r(A \cap B) = m_{A\cap B} \cup (A \cap B)$. Now, $m_{A\cup B}$ is some surface in the bulk with $\partial m_{A\cup B} = \partial(A \cup B)$ but it need not be minimal but is only an upper bound for the minimal surface. The same applies for $m_{A\cap B}$. We can also see that $m_{A\cup B} \cup m_{A\cap B} = \gamma_A \cup \gamma_B$ i.e. they are just rearrangements of each other and thus their area is the same. Now, let $\gamma_{A\cup B}$ and $\gamma_{A\cap B}$ be the minimal surfaces. Using the formula for holographic entanglement entropy, we can easily conclude that

$$S_A + S_B \geq S_{A\cup B} + S_{A\cap B}, \tag{3.10}$$

which is was the desired inequality. The proof is sketched in figure (3.3).

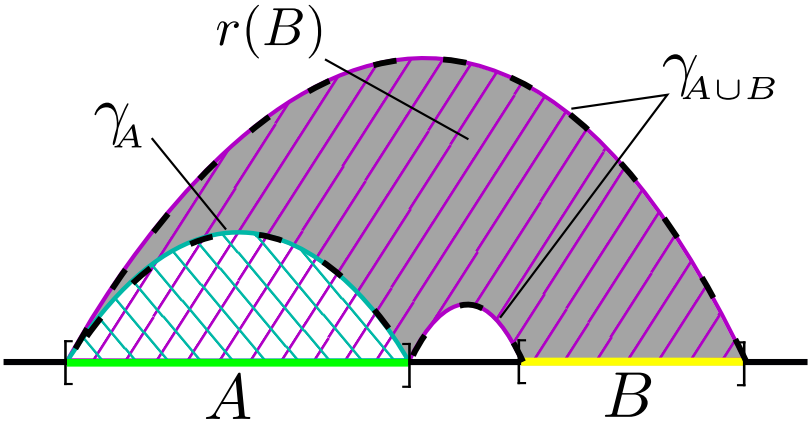

Figure 3.4: A graphical proof of Araki-Lieb inequality. The boundary of the gray region forms a surface for B.

We can prove the Araki-Lieb inequality using similar methods. Suppose we have two separate regions A, B. The latter has the minimal surface γ_B and $A\cup B$ has $\gamma_{A\cup B}$ in the bulk geometry. We define the bulk regions regions $r(B)$ and $r(A\cup B)$ the surfaces of which are the minimal surfaces and the surface on the boundary. In addition, we define $r(A) = r(A\cup B)\setminus r(B)$. We define the surface m_A in the bulk such that $\partial r(A) = m_A \cup A$ and $\partial m_A = \partial A$. We can see that $m_A = \gamma_B \cup \gamma_{A\cup B}$ so the areas are once again additive. Therefore, we can conclude $\text{Area}(\gamma_A) \leq \text{Area}(\gamma_B) + \text{Area}(\gamma_{A\cup B})$ and therefore

$$S_A \leq S_B + S_{A\cup B}. \tag{3.11}$$

which is equivalent to the Araki-Lieb inequality. The proof is sketched in figure (3.4).

There are many more general inequalities which can be found in [61].

3.3 Entanglement entropy using AdS_3/CFT_2 duality

We will now reproduce the results of static cases in the previous chapter using the Ryu-Takayanagi formula. According to the AdS/CFT duality, the relation between the central charge and the gravitational constant is

$$c = \frac{3R}{2G_N^3}. \tag{3.12}$$

The calculations consist mostly of determining the geodesics, which can get quite long and tedious. Therefore, I will not be showing the explicit calculations.

3.3.1 Single interval in an infinite system at zero temperature

For this calculation, we will use the Poincaré coordinates. The CFT is defined on the hypersurface $z = a$. The interval A is defined at $t = t_0$, $-l/2 \leq x \leq l/2$. We can convince ourselves, that the geodesic is constant time. We can argue that the geodesic is symmetric with respect to the midpoint $x = 0$. Therefore, we can parametrize half of the geodesic as a function of z. Now, we can express

the length of the geodesic as

$$2\int_0^{z^*} \mathrm{d}z \frac{\sqrt{1+(x')^2}}{z} \tag{3.13}$$

The minimizing geodesic is $x(z) = -\sqrt{l^2/4 - z^2}$, i.e. a half-circle. The integral diverges at $z = 0$ but we can salvage the situation with a UV regulator $z \geq a$. Therefore, the length of the geodesic is

$$s_{\gamma_A} = 2\int_a^l \mathrm{d}z \frac{l}{z\sqrt{l^2+4z^2}} = 2\log\left(\frac{l}{a}\right) \tag{3.14}$$

Using equations (3.12) and (3.6), the entanglement entropy is

$$S_A = \frac{c}{3}\log\left(\frac{l}{a}\right) \tag{3.15}$$

which is the famous result we derived from the conformal field theories upto a theory specific constant.

3.3.2 Single interval in a finite temperature system

As I mentioned before, the gravity dual of a CFT in a non-zero temperature is an AdS black hole. In 2+1 dimensions, the black hole is a so called non-compact *BTZ black hole* with the metric

$$ds^2 = -(r^2 - m)dt^2 + \frac{dr^2}{r^2 - m} + r^2 dx^2 \tag{3.16}$$

where m is the mass of the black hole. The horizon is at $r = r_H = \sqrt{m}$ and the corresponding Hawking temperature is $\beta^{-1} = \sqrt{m}/2\pi$. When r grows, the metric becomes asymptotically AdS in Poincaré coordinates with $r = 1/z$ up to a rescaling of the metric. Like in the global coordinates, the conformal field theory is now defined at large $r = r_0$. [62]

As before, we need to calculate the geodesic line from $x = 0$ to $x = l$ at time $t = t_0$. The general spacelike geodesics can be found in [62, 63]. The explicit integral for the entanglement entropy is derived later on in chapter 5 in equation (5.42) in a more general context. After inputting the correct values, we find that the length of the geodesic and thus the entanglement entropy are

$$s_{\gamma_A} = 2\log\left(\frac{\beta}{a\pi}\sinh\left(\frac{l\pi}{\beta}\right)\right), \quad S_A = \frac{c}{3}\log\left(\frac{\beta}{a\pi}\sinh\left(\frac{l\pi}{\beta}\right)\right) \tag{3.17}$$

which agrees exactly with our results for conformal field theories.

The inequality $S_A \neq S_{A^\complement}$ in thermal systems has an illuminating interpretation in the compact AdS black hole space. When the interval is still small, the minimizing surface of A is almost the same as in pure AdS space. However, when A grows larger, it starts wrapping around the black hole horizon which contributes to the thermal entropy. We immediately see, that this leads to the inequality of the minimal surfaces of A and its complement. It is also anticipated, that when A grows large enough, the minimal surface will consist of two separate parts: the one wrapped around the whole black hole horizon and one on the boundary. This corresponds to a phase transition. It should be noted that this will only happen in compactified space [28, 82]. This is depicted in figure (3.5)

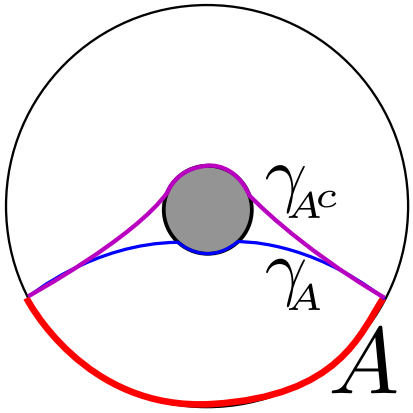

Figure 3.5: A depiction of geodesics in a compact spacetime with a black hole. The black hole prevents the formation of the usual geodesics and also prevents the equality of minimal surfaces for A and its complement.

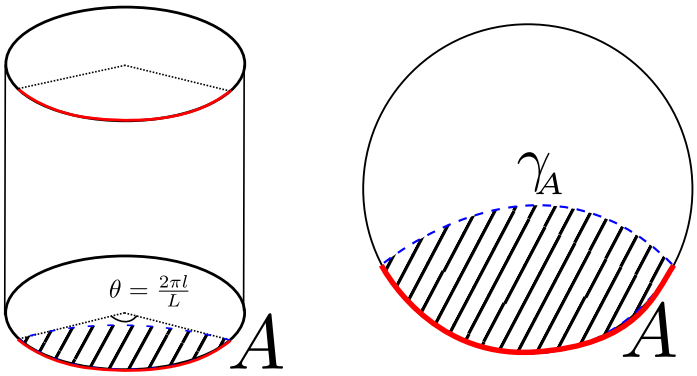

Figure 3.6: A depiction of minimal surfaces in global coordinates. Notice how the lack of black hole allows the minimal surfaces of A and its complement to be equal.

3.3.3 Finite interval in a finite system

Poincaré coordinates are ill-suited for calculations in a finite system as the x coordinate is not bounded. Therefore, we will use global coordinates (3.5) of AdS_3. The conformal field theory is defined on the $\rho = \rho_0$ hypersurface and the interval A is defined at $t = t_0$ and $0 \leq \theta \leq 2\pi l/L$. After a change of coordinates, $\cosh(\rho) = r/r_H$, $\theta = \tau r_H$ and $t = x r_H$, the global metric takes the form

$$ds^2 = R^2(r^2 - r_H^2)d\tau^2 + \frac{R^2 dr^2}{r^2 - r_H^2} - R^2 r^2 dx^2 \tag{3.18}$$

By replacing τ and x with their imaginary counterparts and rescaling the metric, we get the compactified BTZ metric where $\tau \sim t + 2\pi/r_H$. Therefore, we can use our results for BTZ black hole with slight modifications. We just need to replace β with iL and our calculations yield

$$S_A = \frac{c}{3}\log\left(\frac{L}{a\pi}\sin\left(\frac{l\pi}{L}\right)\right) \tag{3.19}$$

which is the same result we got in conformal field theories. The heuristic result can also be derived rigorously from the geodesics of the global coordinates as is done in [28]. The case of global AdS minimal surface has been sketched in figure (3.6)

3.3.4 Massive theories

We can study massive, but almost conformally invariant field theories by introducing an IR cap to Poincaré coordinates. As proposed in [64], this could be done explicitly by considering a metric which has singularities as z approaches an IR cap. The metric is

$$ds^2 = \frac{R^2}{z^2}\left(\frac{dz^2}{f(z)} + f(z)dx^2 - dt^2\right), \quad f(z) = \left(1 + Q\left(\frac{z}{z_0}\right)\log\left(\frac{z}{z_0}\right) - \left(\frac{z}{z_0}\right)^2\right) \tag{3.20}$$

where $0 \leq Q \leq 2$ is a constant. The metric component g_{zz} now diverges at $z = z_0$ which is the IR cap in this theory. However, the divergence is only $z^{-1/2}$ so the geodesic length at the IR boundary may still converge. If the z coordinate of the geodesic is injective, we can find a minimum length for the geodesic as a parameter of the maximum z value, z_m. The length of the geodesic for interval $A = [0, l]$ is then

$$\text{Length}_{\gamma_A} = 2\int_{\varepsilon}^{z_m} \frac{z_m dz}{z\sqrt{z_m^2 f(z) - z^2 f(z_m)}}, \text{ where} \tag{3.21}$$

$$l(z_m) = 2\sqrt{f(z_m)}\int_0^{z_m} \frac{z dz}{f(z)\sqrt{z_m^2 f(z) - z^2 f(z_m^2)}} \tag{3.22}$$

When $z_m \ll z_0$, $l \approx 2z_m$ and we get the usual logarithmic dependence on l. On the other hand, when $l \to \infty$, we lose the injectivity of $z(x)$. We can still use our integrals above with, $z_m \to z_0$, and we get the entanglement entropy

$$S_A = \frac{c}{3}\log\frac{l_{max}}{\varepsilon}, \quad l_{\max} = l(z_0) = \frac{4z_0}{2-Q} \tag{3.23}$$

which agrees with the results of conformal field theories with $\xi = m^{-1} = z_0/(2-Q)$. Interestingly, Q parametrizes the mass gap. The behaviour of entanglement entropy can be understood as follow. When l grows, z has to reach larger and larger values. When z reaches z_0, the metric component of dx^2 vanishes and it becomes favorable to vary the x coordinate there, where the z coordinate stays constant and becomes non-injective. The length of the geodesic does not increase anymore with increasing interval length [64].

3.3.5 Multiple intervals

In the conformal field theory approach, the case of multiple intervals was a difficult problem to attack. However, from the AdS side, the problem becomes surprisingly simple. Let $A = [u_1, v_1] \cup [u_2, v_2]$, i.e. two separate intervals. There are three candidates for the minimizing surface. One would be to have a minimal surface for each interval that is, a disconnected surface, the other two are to connect the end points of the two intervals which correspond to a connected surface. Of the latter two, the mixed geodesics connecting u_1 to u_2 and v_1 to v_2 can be seen to form a connecting surface for u_1 to v_2 and v_1 to v_2. However, the other connected surface is by definition the minimal surface for the latter pair of points and thus the minimum of the two. See figure 3.7.

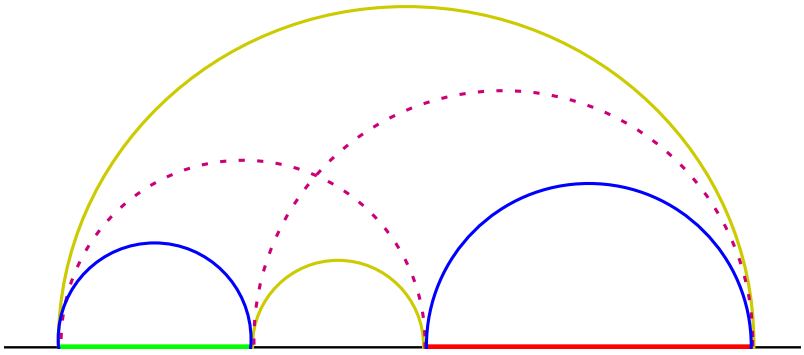

Figure 3.7: The two competing surfaces for two separate intervals. The surface in yellow is the connected surface and the blue geodesics form the disconnected surface. In this figure, it can be seen that the other connecting surface with dashed geodesic lines can be rearranged to a surface similar to the yellow one and thus cannot be the minimal one.

It is easy to see that when the distance between the two interval grows, the disconnected surface provides us with the smaller area. It is expected that when the two intervals are close, the connected surface will be the minimal one. Using our previous results, the two choices give

$$Area_{conn.} = 2R(\log|\frac{v_2-u_1}{\varepsilon}|+\log|\frac{u_2-v_1}{\varepsilon}|) \tag{3.24}$$

$$Area_{disc.} = 2R(\log|\frac{v_1-u_1}{\varepsilon}|+\log|\frac{v_2-u_2}{\varepsilon}|) \tag{3.25}$$

Taking the separation, we get

$$\Delta Area = Area_{conn.} - Area_{disc.} = 2R\log\left|\frac{(v_2-u_1)(u_2-v_1)}{(v_1-u_1)(v_2-u_2)}\right|. \tag{3.26}$$

Whenever the four point ratio $x \equiv (u_1-v_1)(u_2-v_2)/((u_2-u_1)(v_2-v_1)$ is $x<1/2$, the disconnected surface gives the smallest area. In other cases, the connected diagram is the minimal one. If we take the derivative of the entanglement entropy with respect to x, we can see that it is discontinuous at $x=1/2$ which is a sign of phase transition of the first order [23]. When both intervals have length l, the critical distance is $(\sqrt{2}-1)l$.

When considering entanglement entropy of two separate region, the mutual information $I(A,B) = S(A)+S(B)-S(A\cup B)$ is an interesting measure as it is divergence free when the two regions do not share boundaries. In the above case, the mutual information would be

$$I([u_1,v_1],[u_2,v_2]) = \begin{cases} 0, & x<1/2 \\ \frac{c}{3}\log\left(\frac{l_1 l_2}{d(l_1+l_2+d)}\right), & x>1/2 \end{cases}. \tag{3.27}$$

It is rather surprising that the mutual information would vanish completely after the critical distance.

However, we see that the result above is independent of the specific field theory at the boundary. When compared to the results in conformal field theory, the entanglement entropy gets a theory specific correction by the derivative of the function $\mathscr{F}_{n,N}(x_i)$. As pointed out in [58], the holographic entanglement entropy is correct only for large c theories. He also confirmed that the mutual information may vanish abruptly after the critical point in large c theories. It is possible that when we take into account the effects of quantum gravity, the holographic entanglement entropy will give the correct expression.

3.4 Entanglement entropy using AdS$_{d+2}$/CFT$_{d+1}$

Conformal field theories lose much of their predictive power when we consider more than two spacetime dimensions. Fortunately, the simplicity of the Ryu-Takayanagi formula continues to arbitrarily high dimensions. Even if the analytic determination of minimal surfaces proves too difficult, the calculations can easily be done numerically. In the simple cases that we consider in this section, the Ryu-Takayanagi formula correctly reproduces the area law of entanglement entropy.

3.4.1 Infinite strip

We begin with a simple shape. Let $A = [-l/2, l/2] \times [0, L]^{d-1}$ be a d dimensional spatial region of the conformal field theory on $\mathbb{R}^{(1,d)}$ situated at $z = a$ surface of the AdS_{d+2} space. We will be using Poincaré coordinates. If we assume that $l \ll L$ we can greatly simplify the expression for the minimal surface by requiring that z is a function of just one spatial coordinate. Thus, the area functional is

$$\text{Area}(\gamma_A) = R^d L^{d-1} \int_{-l/2}^{l/2} \mathrm{d}x \frac{\sqrt{1+(z')^2}}{z^d}. \tag{3.28}$$

The functional does not depend explicitly on x thus we can regard x as time and use the methods of classical mechanics to find the equation of motion

$$\frac{dz}{dx} = \frac{\sqrt{z_*^{2d} - z^{2d}}}{z^d} \tag{3.29}$$

where we identify the constant z^* as the midpoint of the minimal surface along x. The equation above specifies the minimal surface completely. By separating the x and z variables, we can integrate using Euler beta functions to get an explicit expression for z^*

$$\frac{l}{2} = \int_0^{z^*} \mathrm{d}z \frac{z^d}{\sqrt{z_*^{2d} - z^{2d}}} = \frac{z^*}{2d} \int_0^1 \frac{v^{1/2d-1/2} dv}{\sqrt{1-v}} = z^* \frac{\sqrt{\pi}\Gamma(\frac{d+1}{2d}}{\Gamma(1/2d)} \tag{3.30}$$

Inserting the equation of motion to the area functional, we can integrate explicitly with a UV regulator a. The integral will produce a hypergeometric function and after the dust settles,

$$\text{Area}(\gamma_A) = \frac{2R^d L^{d-1}}{d-1} \left(\frac{1}{a^{d-1}} - \frac{(2\sqrt{\pi}\Gamma((d+1)/2d))^d}{\Gamma(1/2d)^d l^{d-1}} \right). \tag{3.31}$$

And the final expression for entanglement entropy is

$$S_A = \frac{1}{4G_N^{(d+2)}} \left(\frac{2R^d}{d-1} \left(\frac{L}{a}\right)^{d-1} - \frac{2^d \sqrt{\pi}^d R^d}{d-1} \left(\frac{\Gamma((d+1)/2d)}{\Gamma(1/2d)} \right)^d \left(\frac{L}{l}\right)^{d-1} \right). \tag{3.32}$$

We see that the first term is the divergent term proportional to the area. The second term, on the other hand, does not depend on the UV cutoff and depends only on the geometry.

3.4.2 Ball

Next, we consider a d dimensional ball B^d with radius l on the $z=a$ surface of the AdS space. This time, we can express z as a function of the radial coordinate r of the disk. Thus, the area functional is

$$\text{Area}(\gamma_{Ball}) = C_{d-1}R^d \int_0^l \mathrm{d}r \frac{r^d\sqrt{1+(z')^2}}{z^d} \tag{3.33}$$

where C_{d-1} is the surface area of a $d-1$-dimensional sphere. The minimizing equation of motion and the solution are

$$rzz'' + (d-1)z(z')^3 + (d-1)zz' + dr(z')^2 + dr = 0, \quad z^2+r^2 = l^2 \tag{3.34}$$

Like in the case of AdS_3, the minimizing surface is a half sphere. Plugging this into the area functional, the area of the minimal surface with an UV regulation $z > a$ is,

$$\text{Area}(\gamma) = C_{d-1}R^d \int_{a/l}^1 \mathrm{d}y \frac{(1-y^2)^{(d-2)/2}}{y^d} = C_{d-1}R^d\left(\frac{1}{d-1}\left(\frac{l}{a}\right)^{d-1} - \frac{d-2}{2(d-3)}\left(\frac{l}{a}\right)^{d-3} + \ldots\right) \tag{3.35}$$

where we have expanded the numerator as a Taylor series and integrated. We can neglect the $\mathcal{O}(a^n)$ terms. Finally, we get the expression for the entanglement entropy

$$\begin{aligned} S_A &= \frac{2\sqrt{\pi}^d R^d}{4G_N^{(d+2)}\Gamma(d/2)}\Big(p_1\,(l/a)^{d-1} + p_3\,(l/a)^{d-3} + \ldots + \\ &\quad + \begin{cases} p_{d-1}(l/a) + p_d + \mathcal{O}(a/l), & d \text{ even} \\ p_{d-2}(l/a)^2 + q\log(l/a) + \mathcal{O}(1), & d \text{ odd} \end{cases}\Big) \end{aligned} \tag{3.36}$$

where the coefficients are

$$p_1 = (d-1)^{-1}, \; p_3 = -\frac{d-2}{2(d-3)}, \ldots \tag{3.37}$$

$$p_d = \frac{\Gamma(d/2)\Gamma(\frac{1-d}{2})}{2\sqrt{\pi}}, \tag{3.38}$$

$$q = (-1)^{(d-1)/2}(d-2)!!/(d-1)!! \tag{3.39}$$

We notice once again, that the most divergent term is proportional to the surface area of the sphere and it diverges as a^{d-1}. Unlike in the case of infinite strip, we get more than one divergent term. When d is even, we get a finite universal term, p_d, that is independent of the cutoff and the size of the system. This term resembles topological entanglement entropy considered in [65] for 2+1 dimensional topological field theories. When d is odd, we get a logarithmic term which has a universal coefficient q. This was expected based on the results given when discussing the 4D conformal field theory.

3.4.3 Confining quantum field theories

We now consider the AdS dual of a confining quantum field theory with a mass gap. There is no one and only correct dual metric. A metric that has been considered in [66, 67, 68], is the AdS_5

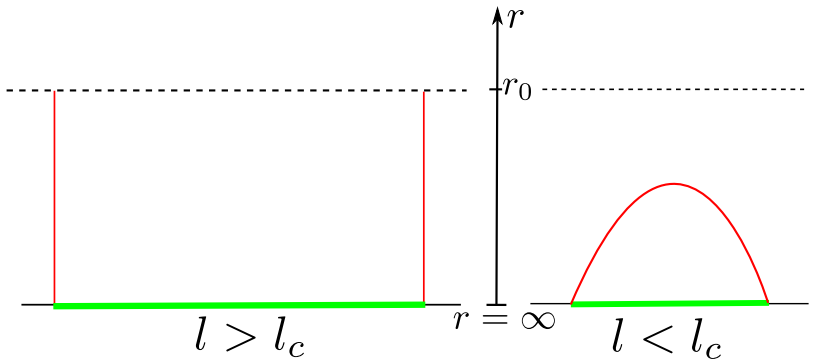

Figure 3.8: On the left, the disconnected surface has the minimal surface area when the width of the strip is too large. On the right, the connected surface is the minimal surface when the width is smaller.

soliton metric which can be obtained from the five dimensional AdS-Schwarzhild metric by two Wick rotations. The metric is

$$ds^2 = \frac{dr^2}{r^2 f(r)} + r^2(f(r)d\chi^2 + dx_1^2 + dx_2^2 - dt^2), \quad f(r) = 1 - \frac{r_0^4}{r^4} \tag{3.40}$$

Here χ is compact with $\chi \sim \chi + L$. However, the dual field theory is not a $3+1$ dimensional confining field theory but a $2+1$ dimensional confinging field theory, more specifically, a pure $SU(N)$ gauge theory. Indeed, this is caused by the anti-periodic boundary conditions of fermions in the original $3+1$ dimensional Super Yang-Mills theory [15], which causes the supersymmetry to break and the theory acquires a mass and become effectively a $2+1$ dimensional confining field theory.

The authors of [66] have considered the strip geometry. They found that there are three competing extremal surfaces. Two are surfaces that connect one end with the other, only one of which is ever the truly minimal. The third candidate is the disconnected surface that starts from the boundary and proceeds along the r axis to r_0, see figure (3.8). There is a definite critical length, l_c, of the interval that separates these two phases and the entanglement entropy is non-analytic at this point corresponding to a phase transition. The connected diagram corresponds to the phase of asymptotic freedom while the disconnected one corresponds to the confined phase. The finite part of the entanglement entropy behaves as

$$S_A \approx \begin{cases} -\frac{N^2}{l^2} & l \to 0 \\ \text{constant} & l \to \infty \end{cases}. \tag{3.41}$$

These have been compared to the entanglement entropy of free Yang-Mills theory and the results agree reasonably well [69].

Chapter 4

Holographic evolution of entanglement entropy

So far, we have reproduced the static results for entanglement entropies of conformal field theories. The calculations for multidimensional cases were relatively simple and straightforward. We now wish to reproduce the time dependent results of conformal field theory using the holographic principle.

4.1 The covariant holographic entanglement entropy proposal

The Ryu-Takayanagi formula was very clear and intuitive. It would be desirable to generalize this method to study time evolution and thermalization of systems via entanglement entropy. The natural generalization would be to let the time coordinate also vary.

The original RT formula was inspired by the Bekenstein bound for entropy. The bound can be violated by time dependent systems e.g. radiating black holes. A generalized, covariant bound was proposed by Bousso [70]. His statement is as follows. Consider a $d+1$ dimensional gravitational system in $\mathscr{M}$. Let $\mathscr{S}$ be a $d-1$-dimensional spacelike surface. We then construct the lightlike

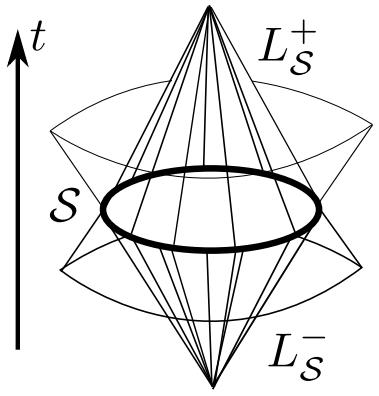

Figure 4.1: A sketch of a light-sheet for a disk in $2+1$ dimensional spacetime. The other lightlike geodesics do not donverge and do not contribute to the light-sheet.

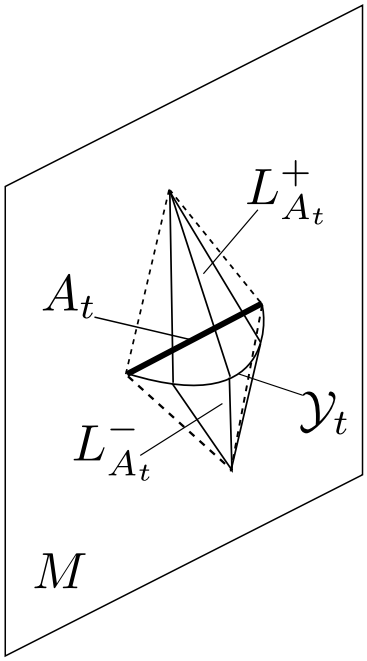

Figure 4.2: Possibly minimal light-sheets form a surface for a single interval.

geodesics starting from $\mathscr{S}$. The geodesics that converge form two null hypersurfaces of dimension d. Together, they form the past and future *lightsheets* of S, $L^{\pm}_{\mathscr{S}}$. See figure (4.1). The *Bousso bound* states that the entropy on the light-sheet is bounded by the area of $\mathscr{S}$ i.e.

$$S_{L_{\mathscr{S}}} \leq \frac{\text{Area}(\mathscr{S})}{4G_N^{(d+1)}}. \tag{4.1}$$

There is no fundamental derivation for the Bousso bound but so far there has been no violation of it and there has been much evidence for it [71].

Hubeny, Rangamani and Takayanagi proposed an application of the Bousso bound to calculate the entanglement entropy in time-dependent systems. Consider a $d+2$ dimensional asymptotically AdS spacetime, $\mathscr{M}$, which has a conformal field theory on its $d+1$ dimensional boundary, M. Let A_t be a d dimensional spacelike region on the boundary and ∂A_t its boundary at time t. We construct the past and future lights sheets of ∂A_t, $\partial L^{\pm}_t$, on M. Now, we extend both of the light-sheets to $d+1$ dimensional hypersurfaces $L^{\pm}_t$ in the bulk AdS space such that they are light-sheets in $\mathscr{M}$. Let $\mathscr{Y}_t$ be the intersection of the bulk-light sheets. The authors proposed that the covariant entanglement entropy of A_t is

$$S_A(t) = \frac{\text{Min}(\text{Area}(\mathscr{Y}_t))}{4G_N^{(d+2)}}, \tag{4.2}$$

where we choose the areawise minimal extension of the light sheets [72]. See figure (4.2).

This definition is difficult to use in any realistic calculations. The authors of [72] argued that the calculation of time-dependent entanglement entropy of region A should reduce to calculating extremal spacelike d-dimensional surfaces in $\mathscr{M}$ such that they share the boundary with A_t. That

is, the simple form for time-dependent entanglement entropy was proposed to be

$$S_A(t) = \frac{\text{Min}(\text{Area}(\gamma_t))}{4G_N^{(d+2)}}, \tag{4.3}$$

where γ_t is the spacelike time dependent extremal surface in $\mathscr{M}$ such that $\partial\gamma_t = \partial A_t$. We choose the extremal surface with the minimal area should there be more than one. This is sometimes called the *Hubeny-Rangamani-Takayanagi* formula or HRT formula.

These two definitions were checked to produce the same results in many situations in [72].

4.2 AdS/Vaidya metric and global quench

4.2.1 AdS/Vaidya metric

The *Vaidya metric* was originally a generalization of the ordinary Schwarzschild metric to the case of emission or absorption of null dust [73]. The usual Schwarzschild metric is

$$ds^2 = -\left(1-\frac{2G_N m}{r}\right)dt^2 + \left(1-\frac{2G_N m}{r}\right)^{-1} dr^2 + r^2(d\theta^2 + sin^2\theta d\phi^2). \tag{4.4}$$

We switch to Eddington-Finkelstein coordinates and introduce the ingoing time

$$t = v - r - 2G_N m \log\left(\frac{r}{2G_N m} - 1\right), \quad dt = dv - \left(1-\frac{2G_N m}{r}\right)^{-1} dr \tag{4.5}$$

Plugging this into the original metric and letting m vary with ingoing time, we get the ingoing Vaidya metric

$$ds^2 = -\left(1-\frac{2G_N m(v)}{r}\right)dv^2 + 2dvdr + r^2(d\theta^2 + sin^2\theta d\phi^2). \tag{4.6}$$

Had we introduced the outgoing time, $t = u + r + 2G_N m \log\left(\frac{r}{2G_N m} - 1\right)$, we would have got the outgoing Vaidya metric which corresponds to a radiating star.

We can evaluate the Ricci tensor and Ricci scalar of the metric and using Einstein equation, we get that the stress energy tensor has only one non-zero component, corresponding to energy density

$$T_{vv} = 2\frac{G_N}{r^2}\frac{dm}{dv}(v). \tag{4.7}$$

The null energy condition requires that for all null vectors N^μ, $T_{\mu\nu}N^\mu N^\nu \geq 0$ and this leads to the requirement that the mass of the black hole is always increasing. Therefore, we can see that the Vaidya metric (4.6) corresponds to a black hole with infalling null dust shell. Specifically, the dust shell is homogeneous.

The Vaidya metric can be generalized to AdS_{d+2} spacetime. The so called AdS/Vaidya metric is

$$ds^2 = \frac{1}{z^2}\left[-\left(1-m(v)z^{d+1}\right)dv^2 - 2dzdv + d\vec{x}^2\right] \tag{4.8}$$

The causal structure of this metric is depicted in figure (4.3). A more familiar form can be achieved with the substitutions $z = r^{-1}$ and $dt = dv - r^{d-1}/(r^{d+1} - m(v))dr$

$$ds^2 = -r^2\frac{r^{d+1} - m(v)}{r^{d+1}}dt^2 - \frac{r^{d+1}}{r^{d+1} - m(v)}\frac{dr^2}{r^2} + r^2 d\vec{x}^2. \tag{4.9}$$

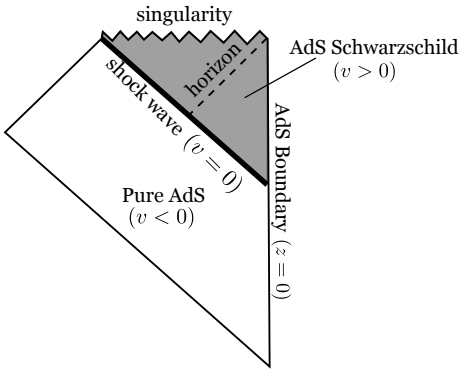

Figure 4.3: The causal structure of the AdS/Vaidya metric in the thin shell limit. The horizon corresponds to the apparent horizon $z_h = M^{1/(d+1)}$ and the singularity to the $z \to \infty$ or $r \to 0$ limit.

We see that if we set $d = 1$ and let the mass be constant m, we get the three dimensional BTZ black hole metric from the previous section. The only non-zero stress energy tensor component is

$$T_{vv} = \frac{d}{2} z^d \partial_v m(v). \tag{4.10}$$

The null energy condition once again requires that the mass of the black hole increases. The Hawking temperature of the black hole in the final state is $T_H = (d+1)m^{1/d}/(4\pi)$ [63].

A common mass function considered is

$$m(v) = m\frac{\tanh\left(\frac{v}{a}\right)+1}{2}. \tag{4.11}$$

This describes the formation of a black hole with mass m by infalling null dust. At early times, the mass of the black hole is still small and the metric corresponds to that of AdS_{d+2}. At late times, the mass is nearly constant and corresponds to the metric of AdS Schwarzshild black hole. The constant a describes, how fast the mass accretes or how thin the dust shell is. In the limit $a \to 0$, the mass function becomes a step function and corresponds to the shock wave limit.

As we saw with global quench in conformal field theories, the entanglement entropy at late times behaved like thermal entropy when there was a global change of the Hamiltonian. Therefore, it is expected that the infalling dust geometry will reproduce the behaviour of the entanglement entropy after a global quench.

4.2.2 Solving the geodesics in the three dimensional AdS/Vaidya metric

We first consider the three dimensional AdS/Vaidya spacetime. It can be seen that both v and r of the geodesic can be parametrized as functions of x. We choose a symmetric strip, $A = [-l/2, l/2]$ and set the boundary conditions $v(-l/2) = v(l/2) = t$ and $r(-l/2) = r(l/2) = \infty$. Thus, the length of the geodesic is

$$L_{m_a} = 2\int_0^{l/2} \sqrt{r^2 + 2r'v' - (r^2 - m(v))v'^2}. \tag{4.12}$$

The functional does not have explicit x dependence and thus has the conserved quantity

$$\frac{r^4}{r_*^2} = r^2 + 2r'v' - (r^2 - m(v))v'^2. \tag{4.13}$$

In addition, we get two equations of motion for the geodesic by minimizing the integral. However, we can only have two independent differential equations and we prefer diferential equations of the first order. Using the conservation equation, we get a simplified form for the other Euler-Lagrange equation of motion

$$r v'' - 2v'r' - r^2 - r^2(v')^2 = 0. \tag{4.14}$$

We can argue that the geodesic is symmetric about its midpoint and the derivatives of r and v should vanish there. Therefore, r_* is the midpoint value of r on the geodesic.

Analytic results

There are no analytical solutions for a generic mass function but we can greatly simplify the problem by considering the thin shell limit, $m(v) = m\theta(v)$. In this case, the geodesics for strips after $t = 0$ start in the thermal black hole background. The components of the metric are greater in the thermal background so the geodesic would prefer to be in the pure AdS background. If the strip is long enough, the geodesic can penetrate the mass shell to reach the pure AdS spacetime. The geodesics in both the BTZ black hole background and pure AdS space are known, so the thin shell limit is solvable by demanding that the geodesic is continuous at the mass shell. The calculations have been done in [63] and the expression for the entanglement entropy in the regime $t < l/2$ is

$$S_A(l,t) = \frac{c}{3}\log\left[\frac{2\sinh(r_H t)}{\varepsilon r_H \sin[\theta(l,t)]}\right], \tag{4.15}$$

where $\theta(l,t) \in [0, \frac{\pi}{2}]$ is given by the relations

$$l = \frac{1}{r_H}\left[\frac{2\cos(\theta)}{\rho\sin(\theta)} + \log\left(\frac{2(1+cos(\theta))\rho^2 + 2\sin(\theta)\rho - \cos(\theta)}{2(1+\cos(\theta))\rho^2 - 2\sin(\theta)\rho - \cos(\theta)}\right)\right], \tag{4.16}$$

$$\rho = \frac{1}{2}\left[\coth(r_H t) + \sqrt{\coth^2(r_H t) - \frac{2\cos(\theta)}{1+\cos(\theta)}}\right]. \tag{4.17}$$

Here r_H is the apparent horizon, $\sqrt{m}$, and ε is a regularization parameter. The parameter $\theta(l,t)$ grows monotonically from 0 to $\frac{\pi}{2}$ during the time evolution. After the saturation time, $t_s = l/2$, the entanglement entropy gains its thermal equilibrium value as in (3.17) [63].

Although there is no closed form for the entanglement entropy, we can reach some general results by studying the result above at different regimes. These results were first analyzed in [76]. At early times, $r_H t \ll 1$ for all l, thus, ρ must be large. In consequence, $\sin(\theta)$ must be small to satisfy the equations above. We get the following expressions for ρ and $\sin(\theta)$,

$$\rho = \frac{1}{r_H t} + \frac{r_H t}{12}, \quad \sin(\theta) = \frac{2}{l r_H}\left(r_H t - \frac{r_H^3 t^3}{12}\right) \tag{4.18}$$

and putting these into the expression for entanglement entropy we get

$$S_A(l,t) = \frac{c r_H^2}{12} t^2 + \frac{c}{3}\log(\frac{l}{\varepsilon}) \tag{4.19}$$

and we see that the entanglement entropy grows quadratically in agreement with our conformal field theory results in eq. (2.52).

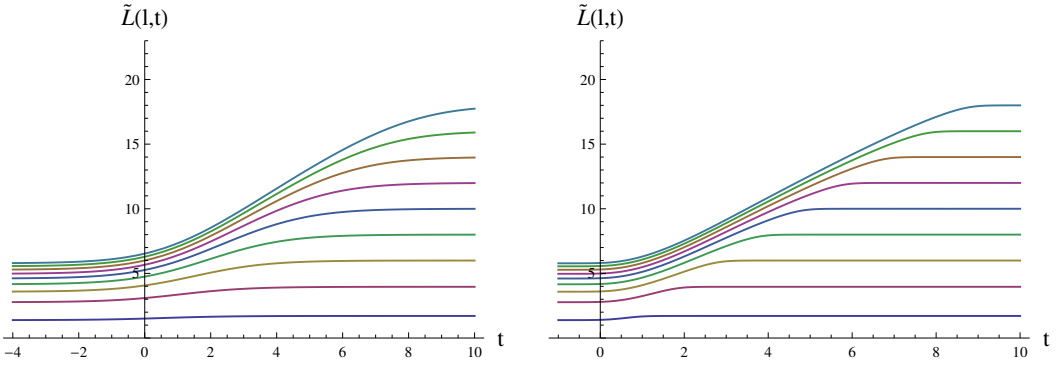

Figure 4.4: Numerical results for a single interval in AdS_3/Vaidya metric. The value mapped is $\frac{6}{c}S_{\text{reg}}$, i.e. it is proportional to entanglement entropy with the vacuum logarithmic divergence removed. On the left side, $a = 2$ and on the right side $a = 1/3$. The length of the interval is $l = 1,\ldots,8$ from the bottom. The figure originally appeared in [74].

When $l \gg r_H t \gg 1$, we wish to recover the linear growth. More specifically, we consider the regime $e^{-t} \ll \phi \ll e^{-2t/5}$. In this case, we can solve ρ and l and get

$$\rho = \frac{1}{2} + \frac{\phi}{4} + \mathcal{O}\left(\frac{e^{-2tr_H}}{\phi}\right), \quad l = \frac{4}{r_H \phi} + t + \log(\phi) + \mathcal{O}. \tag{4.20}$$

Plugging these into the expression (4.15) we get

$$S_A(l,t) = \frac{cr_H}{3}t + \frac{c}{3}\log\left(\frac{l}{\varepsilon}\right) - \frac{c}{3}\log(4) + \mathcal{O}\left(\frac{t}{l}, \frac{\log(l)}{l}, e^{-2r_H t}\right). \tag{4.21}$$

After reminding ourselves that $r_H = 2\pi/\beta$ and $4\tau_0 = \beta_{\text{eff}}$, we see that the first term agrees exactly with the result from conformal field theory.

The authors of [76] have also considered the regime near the critical time. They have expanded the expression for entanglement entropy using $t = t_s - \delta$, where $t_s = l/2$ is the saturation time and $\delta \ll 1$ is an expansion parameter. The authors showed that difference between the entanglement entropy at t and the equilibrium result has a non-trivial power law,

$$S_A(t > l/2) - S_A(t_* - \delta) \propto \delta^{3/2}. \tag{4.22}$$

This is a more physical result than the abrupt change in the conformal field theory result.

Numerical results

It is perhaps more physical to consider the dust shell with finite thickness. These situations cannot be solved analytically but many numerical results exist which have been presented e.g. in [63, 74]. A common feature is that the entanglement entropy starts growing linearly after after the early times. The slope of the linear growth does not depend on the thickness of the shell and the saturation time does not vary much. The authors of [74] estimated that the saturation time is $t_s = l/2 + 2a$.

However, the sharpness of the transition between different regimes of growth differ with different shell thicknesses varies. The greater a i.e. the width is, the smoother the transition. See the figures in (4.4).

4.2.3 The equations of motion in $d+2$ dimensional AdS/Vaidya geometry

As usual, we consider the cases of infinite strips with finite width and spherical regions. For the strip, let $A = [-l/2, l/2] \times [0, L]^{d-1}$. When L is much larger than l, we can parametrize v and r of the minimal surface as functions of $x \in [-l/2, l/2]$, the width parameter. Therefore, the area of the surface is given by the functional

$$\text{Area}_{\gamma_A} = 2L^{d-1} \int_{-l/2}^{0} dx r^{d-1} \sqrt{r^2 + 2r'v' - \left(r^2 - \frac{m(v)}{r^{d-1}}\right) v'^2} \tag{4.23}$$

The integrand does not explicitly depend on x so we have the conservation equation

$$\frac{r^{2d+2}}{r_*^{2d}} = r^2 + 2r'v' - \left(r^2 - \frac{m(v)}{r^{d-1}}\right) v'^2, \tag{4.24}$$

where r_* is a constant and is the midpoint of the minimal surface i.e. $r(0) = r_*$ where $v'(0) = r'(0) = 0$. In addition we need one additional equation of motion to determine the minimizing surface which we obtain by varying the functional with respect to r,

$$v''r - 2r'v' - (d-1)\frac{r^{2d+2}}{r_*^{2d}} - (1 - v'^2)r^2 - (d-1)\frac{v'^2 m(v)}{r^{d-1}} = 0. \tag{4.25}$$

Another shape to consider is the ball. We set $A = B^d(0, l)$ and notice that r and v can be parametrized as functions of $\rho \in [0, l]$, the radial coordinate. The respective area is given by the functional

$$\text{Area}_{\gamma_A} = \text{Area}(S^{d-1}) \int_0^l d\rho \rho^{d-1} r^{d-1} \sqrt{r^2 + 2r'v' - \left(r^2 - \frac{m(v)}{r^{d-1}}\right) v'^2} \tag{4.26}$$

This time, there are no conservation equations as the integrand depends explicitly on ρ. To find the minimizing surface, we would need to calculate the explicit equations of motion for the functional with respect to both r and v. The equations are

$$\frac{d}{d\rho}\left[\frac{\rho^{d-1} r^{d-1} v'}{\sqrt{r^2 + 2r'v' - \left(r^2 - \frac{m(v)}{r^{d-1}}\right) v'^2}}\right] = \rho^{d-1} r^{d-2} \left[\frac{dr^2 - dr^2 v'^2 + 2(d-1)r'v' + \frac{m(v)}{2r^{d-1}} v'^2}{\sqrt{r^2 + 2r'v' - \left(r^2 - \frac{m(v)}{r^{d-1}}\right) v'^2}}\right] \tag{4.27}$$

$$\frac{d}{d\rho}\left[\frac{\rho^{d-1} r^{d-1} \left(r' - \left(r^2 - \frac{m(v)}{r^{d-1}}\right) v'\right)}{\sqrt{r^2 + 2r'v' - \left(r^2 - \frac{m(v)}{r^{d-1}}\right) v'^2}}\right] = \frac{\rho^{d-1} r^{d-1} \frac{m'(v)}{r^{d-1}} v'^2}{\sqrt{r^2 + 2r'v' - \left(r^2 - \frac{m(v)}{r^{d-1}}\right) v'^2}} \tag{4.28}$$

Numerical solutions to the equations of motion have been considered in e.g. [63, 74, 77]. A common feature is the initial quadratic growth followed by the regime of linear growth and after some time, the entanglement entropy reaches equilibrium. The speed of linear growth was found to depend on the system size. Initial analysis found that the saturation time for spherical regions would be the radius of the region [63], but there is a disagreement in larger regions [76]. Also for strip geometry, the saturation time is not linearly depenent on l. The behaviour of entanglement entropy near the saturation time has also been studied. The entanglement entropy for the strip has a discontinuous time derivative at the saturation point [77]. The sphere approaches it with a non-trivial power law [76]. Some examples of the time evolution can be seen in figure (4.5).

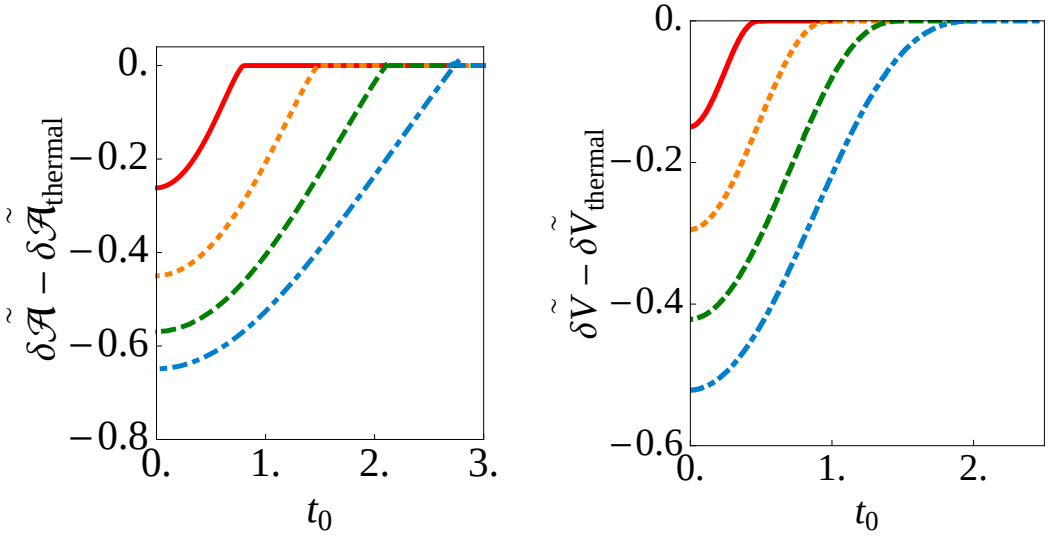

Figure 4.5: Time evolution of renormalized and rescaled entanglement entropy at different dimensions in the thin-shell limit ($a = 0.01$) with $m = 1$. The renormalization is done by subtracting the final value of the entanglement entropy and the rescaling is done by dividing with the volume of the region and setting $4G_N^{(d+2)} = 1$. The figure on the left is the rescaled renormalized surface area of the minimal surface for a strip in AdS_4/Vaidya at lengths $l = 1, 2, 3, 4$. The figure on the right is the rescaled renormalized surface volume of a minimal surface for a sphere in AdS_5/Vaidya geometry with radii $0.5, 1, 1.5, 2$. We see that all the figures exhibit quadratic growth in the early times and then grow linearly in the intermediate times.

4.2.4 Interpretation, significance and discussion

For the two dimensional conformal field theories, we found the surprisingly simple toy model featuring quasiparticles with which we were able to explain the linear growth of entanglement entropy after a global quench. A similar model known as the *entanglement tsunami* has been proposed by Liu and Suh in [75]. Their results apply in the large system limit $l \gg m^{1/(d+1)}$, where m is the final mass of the black hole. According to their analytic results, the entanglement entropy of region A grows quadratically at first,

$$\Delta S_A(t) = \frac{\pi \text{Area}_A}{d} \mathscr{E} t^2 + \cdots, \quad r_H t \ll 1 \quad \mathscr{E} = \frac{d}{16\pi G_N} m, \tag{4.29}$$

where $\mathscr{E}$ is the energy density of the black hole background and Area_A is the area of the region when considering the usual Euclidean metric. After the initial phase, the evolution enters its linear regime where

$$\Delta S_A(t) = v_E s_{\text{eq}} \text{Area}_A t, \quad v_E = \frac{(\eta-1)^{(\eta-1)/2}}{\eta^{\eta/2}}, \quad s_{\text{eq}} = \frac{r_H^{(d-1)}}{4G_N}, \quad \eta = \frac{2d}{d+1}. \tag{4.30}$$

Here, v_E is a dimensionless number which we can interpret as the speed of entanglement propagation. Note, that it does not depend on the shape or size of region we are considering. The other unfamiliar factor is s_{eq} which we can interpret as the entanglement density. This led to the proposal that the entanglement growth can be thought of as a tsunami of quasiparticles starting from the boundary of the region. We could write the equation (4.30) as

$$\Delta S_A(t) = s_{\text{eq}}(\text{Vol}_A - \text{Vol}_{A - v_E t}) \tag{4.31}$$

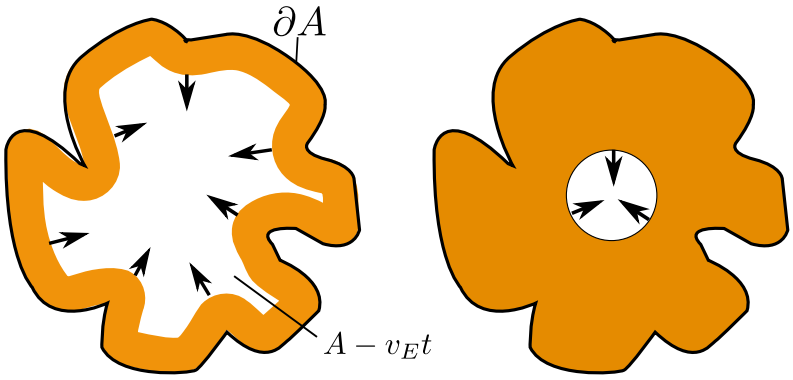

Figure 4.6: The entanglement tsunami at early times and at late times. The entanglement entropy grows linearly at intermediate times as the tsunami does not interact it withself, but at late times, the evolution slows down due to self-interaction.

where $A - v_E t$ is the region A after we have moved each point distance $v_E t$ inwards and Vol is the volume of the region bounded by the surface. The linearity is explained by the fact that for large regions, the shape of the region does not affect the growth of entanglement entropy or the propagation of the tsunami at early times. On the other hand, at late times, the tsunami starts interacting with itself resulting in non-linear growth. The entanglement entropy is considered to be saturated when the tsunami has swept the whole region. This picture is not as intuitive and powerful as the quasiparticle picture for two dimensional conformal field theories, but still relies on the same principle thus making the quasiparticle interpretation more believable. The tsunami propagation has been depicted in figure (4.6).

As stated before, the time evolution of entanglement entropy can be considered as a probe of thermalization in a strongly coupled system which has been quenched out of equilibrium. This has been investigated in e.g. [63]. The physical significance is that the short-distance effects thermalize first and only after that the long-distance effects. This is known as the top-down thermalization. In contrast, perturbative QCD and other weakly coupled systems exhibit bottom-up thermalization [78]. Similar candidates for probes of thermalization are Wilson loops and equal-time two-point functions and they exhibit similar linear growth and saturation. These results have raised interest in (holographic) entanglement entropy in studies of thermalization as an order parameter [63]. The similar behaviour of entanglement entropy after a global quench implies that system is a dual of the null dust shell at least rougly. In addition, this supports the idea global injection of energy as an explanation for the behaviour of entanglement entropy in conformal field theories.

More complicated geometries have also been considered. We could have used a charged AdS black hole as our background [76, 79] or introduced Lifshitz scaling and hyperscaling violation [79, 80]. The latter will be studied in chapter 5.

4.2.5 The time evolution of total entropy

So far, we have limited our discussion to entanglement entropy of subregions during the formation of a black hole. But how does the total entropy behave with the infalling dust shell? Does the

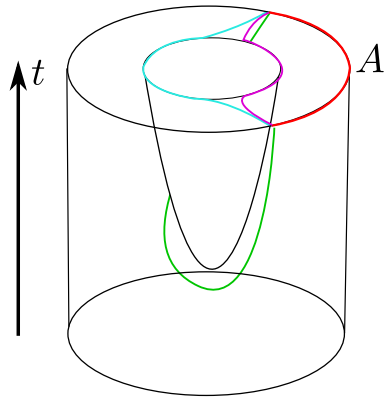

Figure 4.7: An illustration of AdS_3 black hole formation and the deformation of the surfaces.

equality for entanglement entropy of a region and its complement still hold? In the static black hole case, we saw that this is not the case. In our dual conformal field theory, the time evolution was unitary and therefore the total entropy must have remained constant. This is indeed the case also in the gravitational theory if we start from a state without a black hole. The expression for the total entropy is

$$S_{tot} = \lim_{|A^{\complement}|\to 0} (S_A - S_{A^{\complement}}). \tag{4.32}$$

Before the black hole has formed, the entanglement entropies are equal and the total entropy is zero. When the black hole has formed, we can continuously deform the minimal surfaces to early times such that they can be deformed past the spatial region where the black hole is in later times and deformed back to later times. This allows the minimal surfaces to be same both for region A and its complement at all times and thus keeping the total entropy zero and no information is lost according to this approach. This property also has the consequence that total entropy is not a viable measure when detecting black hole formation. Instead, we could use the entanglement entropy [81].

4.3 Falling particle and local quench

We have now seen that the holographic interpretation of entanglement entropy can reproduce the global quench results with an infalling null dust shell. We would still like to reproduce the results of local quench which we could interpret as a local injection of energy. A natural generalization would be to consider a falling massive particle. An alternate approach would be to find a metric that would reproduce the stress energy tensor of the local quench at the boundary. Both approaches will be considered.

4.3.1 The massive falling particle approach

The idea of a falling particle as a dual of local quench is intuitive. To turn this idea into a mathematical expression, we need to consider how a free falling particle affects the surrounding metric via backreaction. There is a crude method by means of perturbation theory considered in [82]. The

perturbative approach starts from the action functional and Einstein equation.

However, there is a more elegant and simple method considered in [44, 82]. We consider the particle motion in pure AdS space in the Poincaré patch that starts its motion at rest from the boundary at $(z,\vec{x},t)=(\alpha,\vec{0},0)$ where α is some small quantity. The geodesic of this particle is relatively easy to solve. The particle will stay at the origin and

$$z(t)=\sqrt{t^2+\alpha^2}. \tag{4.33}$$

The corresponding particle energy is $E=m/\alpha$. Consider now the change of coordinates from the Poincaré patch to global coordinates[1],

$$z = \frac{\alpha}{\sqrt{1+r^2}\cos\tau+r\cos\tau}, \tag{4.34}$$

$$t = \frac{\alpha\sqrt{1+r^2}\sin\tau}{\sqrt{1+r^2}\cos\tau+r\cos\tau}, \tag{4.35}$$

$$x_i = \frac{\alpha\sin\theta\, y_i}{\sqrt{1+r^2}\cos\tau+r\cos\tau}, \tag{4.36}$$

where y_i is the spatial coordinate in spherical coordinates i.e. $y_1=r\cos\phi$, $y_2=r\sin\phi$ in AdS_4. This maps the original metric into

$$ds^2=-(1+r^2)d\tau^2+\frac{dr^2}{1+r^2}+r^2d\Omega_d, \tag{4.37}$$

which is the global metric although with the parameter ranges $\tau,\theta\in[-\pi,\pi]$ where θ is periodical. Coincidentally, the trajectory of the falling particle is now constantly at $r=0$. The AdS metric for a black hole in global coordinates is

$$ds^2=-(r^2+1-M/r^{d-1})d\tau^2+\frac{dr^2}{r^2+1-M/r^{d-1}}+r^2d\Omega_d. \tag{4.38}$$

Note that when $d=1$, we require $M>1$ to have a black hole. The mass of the falling particle, m, is related to the black hole mass term M with [82]

$$m=\frac{d\pi^{(d-1)/2}}{8\Gamma(\frac{d+1}{2})}\frac{M}{G_N^{(d+2)}}. \tag{4.39}$$

Now, the elegance of this method follows. We obtain the backreacted metric of the free falling particle when we apply the inverse coordinate transformations of (4.34)-(4.36) to the global black hole metric. We do not need the explicit metric, in fact, it would only confuse us as it is quite copmlicated. We just need to calculate the extremal surfaces in the black hole metric with specific boundary conditions and then map them to the Poincaré patch to obtain them in the backreacted metric [44].

To assure us that we really do get the correct metric, we write the metric in the Fefferman-Graham gauge

$$ds^2=\frac{dz^2+g_{\mu\nu}(x,z)dx^\mu dx^\nu}{z^2}, \tag{4.40}$$

[1] To cover the whole AdS space, we would also have to consider the same change of coordinates but with a negative sign [44].

and expand the newly introduced tensor around the Minkowski metric tensor

$$g_{ab}(x,z) = \eta_{ab} + t_{\mu\nu}(x) z^{d+1} + \mathcal{O}(z^{d+2}). \tag{4.41}$$

We obtain the holographic energy stress tensor i.e the stress energy tensor of the boundary CFT with [83]

$$T_{\mu\nu} = \frac{(d+1)}{16\pi G_N^{(d+2)}} t_{\mu\nu}. \tag{4.42}$$

When this calculation is done in AdS_3 space, we get

$$T_{\pm\pm}(x_\pm) = \frac{M\alpha^2}{8\pi G_N^{(3)}(x_\pm^2+\alpha^2)^2}, \quad T_{\pm\mp} = 0. \tag{4.43}$$

This is entirely compatible with the stress energy tensor obtained in CFTs when considering local quenches (2.74), we only need to identify $M = 3/4$ [82].

4.3.2 Results in AdS_3 backreacted metric

The inverse transformations in case of $d = 1$ are

$$r = \frac{1}{2z}\sqrt{\alpha^2 + \alpha^{-2}(z^2+x^2-t^2)^2 - 2(z^2-x^2-t^2)}, \tag{4.44}$$

$$\tan\tau = \frac{2t\alpha}{\alpha^2+z^2+x^2-t^2} \tag{4.45}$$

$$\tan\theta = \frac{-2x\alpha}{l^2-t^2-\alpha^2} \tag{4.46}$$

We know that the geodesics in the BTZ black hole metric and their lengths can be calculated analytically. For the global coordinates, this has been done in [44, 82]. Let the region A in the conformal field theory be $[-l_1, l_2]$ where $l_1 > |l_2|$ at time t. The boundary is located at $z = z_0$. We need to calculate the geodesics in the black hole metric with the boundary conditions

$$\tau_\infty^{(i)} = \arctan\left(\frac{2t\alpha}{\alpha^2+l_i^2-t^2}\right), \tag{4.47}$$

$$\theta_\infty^{(i)} = \arctan\left(\frac{-2l_i\alpha}{l_i^2-t^2-\alpha^2}\right), \tag{4.48}$$

$$r_\infty^{(i)} = \frac{1}{2z_0}\sqrt{\alpha^2 + \alpha^{-2}(z_0^2+l_i^2-t^2)^2 - 2(z_0^2-l_i^2-t^2)}. \tag{4.49}$$

The entanglement entropy for an asymmetric generic equal-time boundary conditions is

$$S_A = \frac{1}{4G_N^{(d+2)}}\left[\log(r_\infty^{(1)} r_\infty^{(2)}) + \log\left(\frac{2(\cos(\sqrt{1-M}\Delta\tau_\infty) - \cos(\sqrt{1-M}\Delta\theta_\infty))}{1-M}\right)\right] \tag{4.50}$$

where $\Delta\tau_\infty = |\tau_\infty^{(2)} - \tau_\infty^{(1)}|$ and $\Delta\theta_\infty = |\theta_\infty^{(2)} - \theta_\infty^{(1)}|$ and $\Delta\theta_\infty$ should be replaced with $2\pi - \Delta\theta_\infty$ if $\Delta\theta_\infty > \pi$ [44].

If we consider a symmetric interval $[-l, l]$, the entanglement entropy reduces to

$$S_A = \frac{1}{2G_N^{(d+2)}}\log\left[\frac{\sin(\sqrt{1-M}\theta_\infty)}{\sqrt{1-M}}\right] \tag{4.51}$$

where $\theta_\infty = |\theta_\infty^{(i)}|$ and $r_\infty = r_\infty^{(i)}$. Once again, θ_∞ must be replaced with $\pi - \theta_\infty$ when $\theta_\infty > \pi/2$. The replacements of $\Delta\theta_\infty$ and θ_∞ correspond to the non-trivial change of minimal surface [44].

The case of a single interval when $t, l \gg \alpha$

We now consider the case $l, t \gg \alpha$ with fixed particle energy $m/\alpha \propto M/\alpha$. First, we consider the symmetric interval $A = [-l, l]$. At all times, the entanglement entropy is constant. Using the relation between gravitational constant and central charge for two dimensional CFTs and making the identification $z_0 = \varepsilon$, the entanglement entropy is

$$S_A = \frac{c}{3}\log\left(\frac{2l}{\varepsilon}\right) \tag{4.52}$$

which can be identified either as the static entanglement entropy of a strip with length $2l$ or a sum of entanglement entropies of two $[0, l]$ intervals on a half line. However, the value agrees with our results for local quenches for conformal field theories.

When we consider an asymmetric interval $[l_1, l_2]$, where $l_2 > |l_1|$, the entanglement entropy will evolve in time. In early times when $t < |l_1|$ and in late times when $t > l_2$, it has the constant value

$$S_A = \frac{c}{3}\log\left(\frac{l_2 - l_1}{\varepsilon}\right), \quad t < |l_1| \text{ or } t > |l_2|. \tag{4.53}$$

After the initial times, the entanglement entropy for times $l_2 > t > |l_1|$ in the case $l_1 > 0$ has the value

$$S_A = \frac{c}{6}\log\left(\frac{(l_2 - l_1)(l_2 - t)(t - l_1)\tilde{M}}{\alpha\varepsilon^2}\right), \quad l_2 > t > l_1 > 0 \tag{4.54}$$

where we have introduced $\tilde{M} = \sin(\sqrt{1-M}\pi)/\sqrt{1-M}$. In the case $l_1 < 0$ it has two different phases

$$S_A = \frac{c}{6} \times \begin{cases} \log\left(\frac{(l_2-l_1)(l_2+t)(t+l_1)\tilde{M}}{\alpha\varepsilon^2}\right), & \text{if } |l_1| < t < \sqrt{-l_1 l_2} \\ \log\left(\frac{(l_2-l_1)(l_2-t)(t-l_1)\tilde{M}}{\alpha\varepsilon^2}\right), & \text{if } \sqrt{-l_1 l_2} < t < l_2 \end{cases}. \tag{4.55}$$

We see that the case $l_1 > 0$ has its maximum at $t = (l_2 - l_1)/2$

$$S_A(t_{max}) = \frac{c}{6}\log\left(\frac{(l_2 - l_1)^3\tilde{M}}{4\alpha\varepsilon^2}\right). \tag{4.56}$$

On the other hand, the $l_1 < 0$ has its maximum at $t = (l_2 - |l_1|)/2$ if $|l_1| < l_2(3 - \sqrt{8})$ and otherwise at $t = \sqrt{-l_1 l_2}$ i.e. the point of non-analyticity.

We see that there is a disagreement with the CFT results in (2.68). However, they share similar features. The entanglement entropy is constant in early times and late time in both cases and the time evolution has a similar shape. In the holographic results for the case $l_1 > 0$, the overall shape of the time development is independent of the specific value of l_1 as long as $l_2 - l_1$ is fixed.

Finally, let us also consider a semi infinite interval with one end at the origin, $A = [0, l]$. For an infinite interval, we assume $l \gg t \gg \alpha$. In that case, the boundary conditions become simple and we get the simple expression

$$S_A = \frac{c}{3}\log\left(\frac{l}{\varepsilon}\right) + \frac{c}{6}\log\left(\frac{t}{\alpha}\right) + \frac{c}{3}\log\left[\frac{1}{\sqrt{1-M}}\sin\left(\pi\sqrt{1-M}\right)\right] \tag{4.57}$$

$$\simeq \frac{c}{3}\log\left(\frac{l}{\varepsilon}\right) + \frac{c}{6}\log\left(\frac{t}{\alpha}\right) \tag{4.58}$$

This is similar to the results we got from conformal field theories but the factors of the logarithms have been reversed [82].

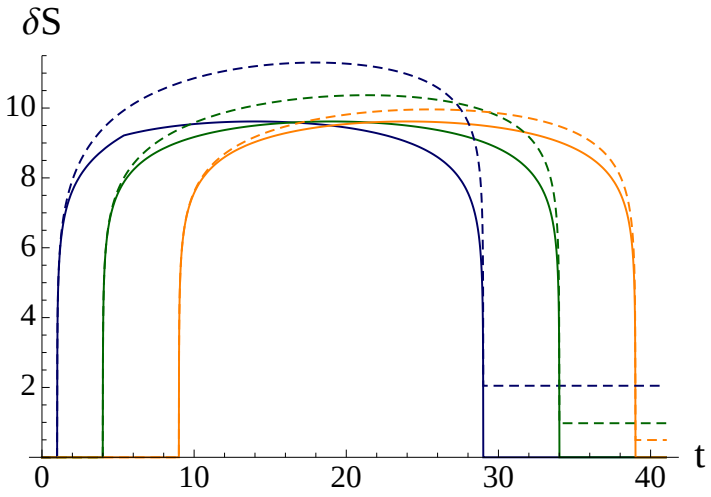

Figure 4.8: The time evolution of entanglement entropy of single interval with early value subtracted and rescaled by setting $4G_N = 1$. The intervals plotted all have length 30 and the starting point is from left to right $l_1 = -1, 4, 9$. The parameters are $M = 3/4, \alpha = 0.001$. For comparison, the universal CFT results are also plotted and we see that the agreement is better at longer distances. The figure originally appeared in [44].

The disagreement between the holographic calculations and the CFT ones can be partly understood if we remember that the original problem on the conformal field theory assumed that the real line is split in two completely unentangled half-lines and that the joining of the two half-lines can be understood to cause a local excitation at the joining site. In our holographic picture, the two half-lines are already entangled and there is only a local injection of energy at the joining site i.e. the position of the falling particle. This explains the factor of $\log(l)$ term. However, this does not explain all the disagreements but we can still say that the results of the falling particle approach are promising [82].

A single interval in more general systems

It would be unsatisfying to leave our discussion of falling particles only considering small particles and extreme cases. By varying M, the entanglement entropy is changed by an additive constant. By varying α, the sharp curves are just smoothened.

The authors of [82] suggested that we can consider even more massive objects with $M > 1$ by just analytically continuing our previous results with $\sqrt{1-M} \to i\sqrt{M-1}$ which changes the cosine and sine functions to their hyperbolic counterparts. The idea is that the falling particle has a finite size which is larger than the horizon of the corresponding black hole and the metric outside is the usual black hole metric while the metric inside has no singularities. This allows us to preserve the equivalence $S_A = S_{A^\complement}$. This changes the entanglement entropy only by an additive constant [82].

Of course, we could also consider falling black holes with $M > 1$. In this case, we also do the analytic continuation but we need to consider two different extremal surfaces. The connected one given by the analytic continuation alone and the disconnected one, where one surface wraps around the horizon and the other connects the two end points using the shortest path. This is most

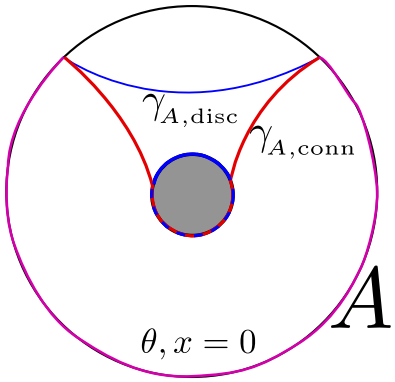

Figure 4.9: An illustration corresponding to a phase transition when the length of the interval grows in the case of falling black hole. When the interval is sufficiently large, the minimal surface disconnects and wraps around the horizon.

simply expressed when discussing the symmetric case for which $A = [-l/2, l/2]$ and [82]

$$S_A = \mathrm{Min}\left(S_A(\theta_\infty), S_A(\pi - \theta_\infty) + \frac{\pi\sqrt{M-1}}{2G_N^{(3)}} \right). \tag{4.59}$$

This has been illustrated in figure (4.9).

4.3.3 Perturbative approach

We can obtain approximative results in multiple dimensions by considering perturbed metrics as done in [82]. The idea is to write the falling particle metric as

$$g_{\mu\nu} = g^{(0)}_{\mu\nu} + g^{(1)}_{\mu\nu} + \mathcal{O}(M^2). \tag{4.60}$$

where the first term is the metric of the pure Poincaré patch and the second term is the perturbation caused by the falling particle of order M^1. The idea is to calculate the minimal surface γ_A in the original metric and calculate the perturbation to its area with

$$\Delta A = \frac{1}{2}\int d^d\xi \sqrt{G^{(0)}}\,\mathrm{Tr}[G^{(1)}(G^{(0)})^{-1}] \tag{4.61}$$

where ξ^μ are the parametric coordinates of the minimal surface γ_A and $G^{(i)}$ are the induced metrics on the surface

$$G^{(i)}_{\alpha\beta} = \frac{\partial X^\mu}{\partial X^\nu}\frac{\partial \xi^\alpha}{\partial \xi^\beta} g^{(i)}_{\mu\nu} \tag{4.62}$$

where X^μ are the coordinates of the surface in the pure Poincaré patch. We typically choose the parametric coordinates to be the spatial coordinates x^i.

We consider the disk with radius l in AdS_4 at the origin which has the minimal surface $z = \sqrt{l^2 - \vec{x}^2}$. Once we have calculated the perturbed metric, we just need to apply the holographic entropy formula to the perturbed area to obtain the change in entanglement entropy. We omit the calculations and just quote the results that can be found in [82].

The expression for the perturbed entanglement entropy in two dimensions is

$$\Delta S_A(d=2) \quad = \quad \frac{\pi M}{4G_N^{(4)}\alpha l}\left[\frac{l^4 - 2l^2t^2 + (\alpha^2+t^2)^2}{\sqrt{l^4 + 2l^2(\alpha^2 - t^2) + (\alpha^2+t^2)^2}} - |t^2 + \alpha^2 - l^2| \right] \tag{4.63}$$

At $t = 0$, the entanglement entropy has the value

$$S_A(t=0, l<\alpha) = \frac{\pi M l^3}{2G_N^{(4)}\alpha(l^2+\alpha^2)} \quad S_A(t=0, l>\alpha) = \frac{\pi M \alpha^3}{2G_N^{(4)} l(l^2+\alpha^2)} \tag{4.64}$$

For $l > \alpha$, the entanglement entropy grows until it reaches its maximum at $t = \sqrt{l^2-\alpha^2}$. If $l < \alpha$ the entanglement entropy is always decreasing. At late times in both cases, the perturbed entanglement entropy decreases asymptotically as

$$\Delta S_A \simeq \frac{\pi M \alpha^3 l^3}{2G_N^{(4)} t^6}. \tag{4.65}$$

We can also calculate the expansions corresponding to large or small l. The expressions are

$$\Delta S_A(l \ll \sqrt{t^2+\alpha^2}) = \frac{\pi M \alpha^3 l^3}{2G_N^{(4)}(t^2+\alpha^2)^3} \tag{4.66}$$

$$\Delta S_A(l \gg \sqrt{t^2+\alpha^2}) = \frac{\pi M \alpha^3}{2G_N^{(4)} l^3} \tag{4.67}$$

The calculations in higher dimensional spaces are straightforward once we have found the perturbed metric. The asymptotic results usually have just different power laws [82].

4.3.4 An alternate approach

For AdS_3 space, there is an alternate way to determine the entanglement entropy. In [83], it was discussed that the general metric tensor in three-dimensional AdS spacetime could be written, upto a gauge transformation, with two unknown functions $L_\pm(x_\pm)$ as

$$ds^2 = l^2\left(\frac{L_+}{2}dx_+^2 + \frac{L_-}{2}dx_-^2 + (\frac{1}{z^2} + \frac{z^2}{4}L_+L_-)dx_+dx_- + \frac{dz^2}{z^2}\right) \tag{4.68}$$

where $x_\pm = x \pm t$ are the light-cone coordinates. It is evident, that when $z \to 0$, the metric approaches asymptotically the pure Poincaré AdS metric. On top of that, the *holographic stress tensor* is determined with

$$T_{\pm\pm}(x_\pm) = \frac{l}{16\pi G_N^{(3)}}L_\pm, \quad T_{\pm\mp} = 0. \tag{4.69}$$

This can be interpreted as the stress energy tensor of the dual conformal field theory. From our previous discussion, we already know, what we want our holographic stress tensor to be so we can obtain our desired metric easily. However, determining the geodesics would be extremely difficult.

However, the author of [84] came up with a method to circumvent the problem. He discovered that if we begin with the pure Poincaré patch metric,

$$ds^2 = l^2\frac{dy_+dy_- + du^2}{u^2}, \tag{4.70}$$

we can do coordinate transformations such that we obtain a metric of the form (4.68) with

$$y_\pm = f_\pm(x_\pm) - \frac{2z^2 f_\pm'^2 f_\pm''}{4f_\pm' f_\mp' + z^2 f_\pm'' f_\mp''}, \quad u = z\frac{4(f_\pm' f_\mp')^{3/2}}{4f_\pm' f_\mp' + z^2 f_\pm'' f_\mp''}. \tag{4.71}$$

The functions $f_\pm(x_\pm)$ are generic functions and they produce the unknown functions of the metric in terms of Schwarzian derivatives

$$L_\pm(x_\pm) = -\frac{\{f_\pm, x_\pm\}}{2} = \frac{3(f''_\pm)^2 - 2f'''_\pm f'_\pm}{4(f'_\pm)^2}. \tag{4.72}$$

Now we need only solve the equation (4.72) for $f_\pm$ when we wish to obtain the holographic stress energy tensor corresponding to a local quench. Two solutions are

$$f_\pm(x_\pm) = x_\pm + \sqrt{x_\pm^2 + \varepsilon^2}, \quad \tilde{f}_\pm(x_\pm) = x_\pm - \sqrt{x_\pm^2 + \varepsilon^2}, \tag{4.73}$$

where ε is some UV regulator.

To evaluate the entanglement entropy of the local quench, we need to solve the geodesic equation in pure AdS space with arbitrary boundary conditions [44]. Like we did before, we get the entanglement entropy by evaluating the length of the geodesic by writing the boundary conditions using the coordinate transformations (4.71). The general geodesic in pure AdS space is a semi-circle with the diameter $\sqrt{(y_\infty^{(2)} - y_\infty^{(1)})^2 + ((t_\infty^{(2)} - t_\infty^{1)})^2}$ where $y_\infty^{(i)}$ and $t_\infty^{(i)}$ are the temporal and spatial boundary conditions. In light-cone coordinates, the length of the geodesic is

$$L_{\gamma_1} = \log\left[\frac{(y_{\infty+}^{(2)} - y_{\infty+}^{(1)})(y_{\infty-}^{(1)} - y_{\infty-}^{(1)})}{u_\infty^{(1)} u_\infty^{(2)}}\right]. \tag{4.74}$$

Assuming that the boundary condition $z_\infty = \varepsilon$ is sufficiently small, we can write the coordinate mapping (4.71) asymptotically as

$$y_{\infty\pm}(x_{\infty\pm}) \simeq f_\pm(x_{\infty\pm}), \quad u_\infty \simeq z_\infty\sqrt{f'_+ f'_-} \tag{4.75}$$

and thus the length of the geodesic γ_1 is

$$L_{\gamma_1} = \frac{1}{2}\log\frac{(f_+(x_{2+}) - f_+(x_{1+}))^2 (f_+(x_{2-}) - f_-(x_{1-}))^2}{\varepsilon^4 f'_+(x_{2+}) f'_+(x_{1+}) f'_-(x_{2-}) f'_-(x_{1-})}. \tag{4.76}$$

This formula, however, is flawed! We notice that the solution $f_\pm$ only gives positive values of $y_\pm$. On the other hand, the solution $\tilde{f}_\pm$ gives only negative values. Therefore, we cannot find all the possible geodesics using just one solution and formula (4.76) is not necessarily the the minimum length. Physically, this can turn up when we consider black holes and the minimum surface is the one wrapping completely around the black hole as discussed using the falling particle approach. Fundamentally, this problem is due to the fact that $f_\pm$ does not have a well-defined inverse-function, the inverse mapping is double-valued [44].

This approach can be salvaged by considering another geodesic, γ_2, where one boundary point is determined using $f_\pm$ and the other using $\tilde{f}_\pm$. This has the length

$$L_{\gamma_2} = \frac{1}{2}\log\frac{(f_+(x_{2+}) - \tilde{f}_+(x_{1+}))^2 (f_+(x_{2-}) - \tilde{f}_-(x_{1-}))^2}{\varepsilon^4 f'_+(x_{2+}) \tilde{f}'_+(x_{1+}) f'_-(x_{2-}) \tilde{f}'_-(x_{1-})} \tag{4.77}$$

and thus the correct expression for entanglement entropy would be

$$S_A = \frac{c}{6}\text{Min}(L_{\gamma_1}, L_{\gamma_2}). \tag{4.78}$$

Physically, this is equivalent to the case of falling particle with $M = 3/4$ as they give the same stress energy tensor [44].

Chapter 5

Lifshitz scaling and hyperscaling violation

In this chapter, we will consider a more exotic and recent model. We will move away from the safe haven known as conformal field theories and consider the gravity duals that exhibit *Lifshitz scaling* and *hyperscaling violation*.

We will first take a quick look at the physical significance of Lifshitz scaling and hyperscaling violation. We will consider its gravity dual in both static cases and in the dynamical case of global quench.

5.1 Arising Lifshitz scaling and hyperscaling violation

In many condensed matter systems, the theory becomes conformally invariant at its critical point. In these cases, the systems stays invariant when we rescale the spatial and temporal coordinates with a constant λ

$$t \to \lambda t, \quad x \to \lambda x. \tag{5.1}$$

There are systems that do not scale as above when at their critical point. Some exhibit Lifshitz scaling where the theory stays invariant when we scale

$$t \to \lambda^{\zeta} t, \quad x \to \lambda x, \tag{5.2}$$

where contant ζ is known as the dynamical critical exponent. In conformal field theories, $\zeta = 1$. For example, the Lifshitz field theory exhibits such scaling with $\zeta = 2$

$$S = \int dx_1 dx_2 dt (\partial_t \phi)^2 - \kappa (\nabla^2 \phi)^2. \tag{5.3}$$

This kind of Lagrangian arises when considering dimer systems [86].

The most relevant example of a metric exhibiting Lifshitz scaling with dynamical critical exponent ζ is the modification of the Poincaré patch of AdS spacetime

$$ds^2 = -\frac{dt^2}{z^{2\zeta}} + \frac{dr^2 + d\vec{x}^2}{z^2} \tag{5.4}$$

where z is scaled as $z \to \lambda z$ thus preserving the metric. These kinds of metrics can be found as solutions to gravitational models with matter fields [86] and have also been found in context of string theory and supergravity [63].

We can go further with our generalizations of scaling behaviour. We can introduce the hyperscaling violation exponent θ such that the metric is not invariant under rescaling of the coordinates. The simplest of such metrics is

$$ds^2 = \frac{1}{z^{2d_\theta/d}}(-z^{2-2\zeta}dt^2 + dz^2 + d\vec{x}^2) \tag{5.5}$$

where $d_\theta = d - \theta$ is the so called effective dimension when considering $d+2$ dimensional AdS spacetime. The metric is rescaled $ds^2 \to \lambda^{2\theta/d} ds^2$ when applying transformations (5.2). This kind of metric arises when considering a gravitational system with N_F gauge fields, F_i, and a scalar dilaton,

$$S = \frac{1}{16\pi G_N^{(d+2)}} \int \sqrt{g} d^{d+2}x \left[R - \frac{1}{2}(\partial\phi)^2 - V(\phi) - \frac{1}{4}\sum_{i=1}^{N_F} e^{\lambda_i \phi} F_i^2 \right]. \tag{5.6}$$

If we consider cases with no potential term, we would have got solutions exhibiting just Lifshitz scaling. In [85], the authors argued that the entropy of a thermal gravitational systems scales like

$$S \sim T^{(d-\theta)/\zeta}. \tag{5.7}$$

Without hyperscaling violation, the entropy would scale with power d/ζ. This is one of the reasons why d_θ is called the effetive dimension and why θ is the hyperscaling violation exponent.

The case $d_\theta = d - 1$ is physically the most important one and is known as the critical value. This gives rise to logarithmic correction to the famous area law of entanglement entropy which has been observed in critical systems with a Fermi surface. In other words, for such $d+1$ dimensional field theories, the entanglement entropy for region A with characteristic length l scales like

$$S_A \sim \left(\frac{l}{\varepsilon}\right)^{d-1} \log\left(\frac{l}{\varepsilon}\right). \tag{5.8}$$

The generalization of Lifshitz scaling and hyperscaling violation to the case of falling shell geometry has been considered in [79, 80]. In the Eddington-Finkelstein geometry, the metric in $d+2$ dimensional spacetime is

$$ds^2 = \frac{1}{z^{2d_{\theta/d}}}\left(-z^{2(1-\zeta)}F(v,z)dv^2 - 2z^{1-\zeta}dvdz + d\vec{x}^2\right) \tag{5.9}$$

where $F(v,z) = 1 + m(v)z^{d_\theta+\zeta}$ in which $m(v)$ is the mass function of the forming black hole. In the case of contant m, the metric can be reduced to

$$ds^2 = \frac{1}{z^{2d_{\theta/d}}}\left(-z^{2(1-\zeta)}F(z)dt^2 + \frac{dz^2}{F(z)} + d\vec{x}^2\right). \tag{5.10}$$

In the static case, the apparent horizon of the black hole is at $z_h = m^{-1/(\zeta+d_\theta)}$ where $F(z_h) = 0$. Thus, the Hawking temperature of the black hole is $T_H = z_h^{1-\zeta}|F'(z_h)|/4\pi$.

Not all values of ζ and θ are allowed. Physically, we can demand that $F(z) \to 1$ (or some constant value) as $z \to \infty$ which leads to the requirement

$$d + \zeta - \theta \geq 0. \tag{5.11}$$

In addition, we require that the null-energy condition is satisfied, i.e. $T_{\mu\nu}N^\mu N^\nu \geq 0$ for each null vector N^μ and the stress energy tensor of the gravitational theory. The condtions for the critical exponents have been considered in [80]. They considered the null-vectors $N_i^\mu = (N_i^v, N_i^z, \vec{N}_i)$

$$N_a^\mu = (0,1,0)\,, \quad N_b^\mu = \left(\frac{-2z^{\zeta-1}}{F(v,z)},1,0\right), \quad N_c^\mu = \left(\pm\frac{z^{\zeta-1}}{\sqrt{F(v,z)}},0,\vec{n}\right), \tag{5.12}$$

for which they got the following conditions

$$\begin{aligned} d_\theta(\zeta-1-\theta/d) &\geq 0 && (5.13)\\ d_\theta[(\zeta-1-\theta/d)F^2-2z^\zeta F_v] &\geq 0 && (5.14)\\ 2(\zeta-1)(d_\theta)+\zeta)F^2+[zF_{zz}-(d_\theta+3(\zeta-1))F_z]zF-z^\zeta d_\theta F_v &\geq 0. && (5.15)\end{aligned}$$

The subindices of F denote partial derivative. When we consider the case with constant m, the last two inequalities reduce to $(\zeta-1)(d_\theta+\zeta)\geq 0$. On the other hand, when we consider the metric with no hyperscaling violation or Lifshitz scaling, we reproduce the condition $m_v \geq 0$. It should be noted, that these are required but not necessarily sufficient conditions for physical parameters.

As usual, the most typical case of the mass function is the same we considered in the previous chapter i.e.

$$m(v) = \frac{m}{2}\left[1+\tanh\left(\frac{v}{v_a}\right)\right]. \tag{5.16}$$

This reduces to a step function as $v_a \to 0$. The equations of motion required for calculating the entanglement entropy do not have an analytic expression unless we consider the step function case and even then, we need to use numerical tools to evaluate the integrals.

5.2 Static cases

In this section, we shortly consider the case where the black hole is static, i.e. $M(v) = M$ or where there is no black hole at all, $M(v) = 0$. We will consider both strips and spherical regions. Since we consider minimal spatial surfaces, our results will not depend on the dynamical critical exponent if we consider cases with $F(z) = 1$.

5.2.1 Static entanglement entropy of a strip

Let the d dimensional spatial region on the boundary be $A = [0,L]^{d-1}\times[-l/2,l/2]$ where $L \gg l$. We assume that the bulk surface γ can be written as a function of $x \in [-l/2,l/2]$ to great accuracy. Thus, the area functional for the bulk surface is

$$\text{Area}_\gamma = 2L^{d-1}\int_0^{l/2} dx \frac{1}{z^{d_\theta}\sqrt{1+\frac{z'^2}{F(z)}}}. \tag{5.17}$$

As usual, the integrand does not explicitly depend of x so we can find the constant of motion

$$z' = -\sqrt{F(z)[(z_*/z)^{d_\theta}-1]} \tag{5.18}$$

where $z(0) = z_*$, i.e. the value of z at the midpoint and also the maximum value of z. When we integrate the above, we get a relation between z_* and l

$$\frac{l}{2} = \int_0^{z_*} \frac{dz}{\sqrt{F(z)[(z_*/z)^{2d_\theta} - 1]}}. \tag{5.19}$$

Now we can insert the equation (5.18) to the area functional and get the minimal surface area

$$\text{Area}_{\gamma_A} = 2L^{d-1} \int_\varepsilon^{z_*} \frac{dz}{z^{d_\theta}\sqrt{F(z)[1-(z/z_*)^{2d_\theta}}} \tag{5.20}$$

where we have introduced the UV regulator ε.

These can be evaluated in an explicit form when $F(z) = 1$ as the integrals become the same we have calculated before in chapter 3. The entanglement entropies are

$$S_A = \begin{cases} \frac{1}{2G_N^{(d+2)}(d_\theta - 1)} \left[\frac{L^{d-1}}{\varepsilon^{d_\theta - 1}} - \frac{L^{d-1}}{l^{d_\theta - 1}} \left(\frac{\pi \Gamma((d_\theta+1)/(2d_\theta))}{\Gamma(1/(2d_\theta))} \right) \right], & \text{if } d_\theta \neq 1 \\ 2L^{d-1} \log(l/\varepsilon), & \text{if } d_\theta = 1 \end{cases} \tag{5.21}$$

We notice that the critical effective dimension $d_\theta = 1$ gives the familiar area law a logarithmic correction also encountered in field theories with a fermi surface [21]. However, our result assumes that region has one side that is significantly smaller than the others and we only have logarithmic divergence as $\varepsilon \to 0$.

5.2.2 Static entanglement entropy of a sphere

We now consider the entangling surface to be a ball of radius R, i.e. $A = B^d(\vec{x}, R)$. As the metric has spherical symmetry with respect to the $\vec{x}$ coordinate, we expect that the z coordinate of the minimal surface can be written as a function $z(\rho)$ where ρ is the radial coordinate of the ball. The area functional of the bulk surface γ can be written as

$$\text{Area}_\gamma = \frac{2\pi^{d/2}}{\Gamma(d/2)} \int_0^R d\rho \frac{\rho^{d-1}}{z^{d_\theta}} \sqrt{1 + \frac{z'^2}{F(z)}} \tag{5.22}$$

where the factor before the integral is the volume of the $d-1$ dimensional unit sphere. This time, there is is an explicit ρ dependence in the integral so we are not able to find any (helpful) constants of motion. Thus, the equation of motion to be solved in order to minimize the functional is

$$2d_\theta \rho F^2 + z[\rho F_z - 2(d-1)z']z'^2 - 2F[\rho z z'' + (d-1)zz' + d_\theta \rho z'^2] = 0. \tag{5.23}$$

with the boundary conditions $z(R) = 0$ and $z'(0) = 0$. Now, even the simple case with $F(z) = 1$ has no analytic solution for general $\theta \neq 0$ and the equations of motion must be solved numerically [80].

The leading order contribution to the entanglement entropy can be computed in the $F(z) = 1$ case if $d_\theta \notin 1, 3, 5, \ldots$. At sufficiently small ε, most of the contribution comes near the points where $\rho = R$ i.e. $z \ll 1$. To take this into account, we write the equation in a dimensionless form with the substitutions $z = R\bar{z}(x)$ and $\rho = R(1-x)$,

$$(1-x)\bar{z}\bar{z}'' + [d_\theta(1-x) - (d-1)\bar{z}\bar{z}'](1 + \bar{z}'^2) = 0, \tag{5.24}$$

where $\bar{z}' = d\bar{z}/dx$. Now, most of the contribution comes from the small x region. We can then make an ansatz in small x, $\bar{z}(x) = \sqrt{x}z_0(1 + z_1 x + z_2 x + \ldots)$ and solve the coefficients,

$$z_0 = \sqrt{\frac{2(d_\theta - 1)}{d-1}}, \quad z_1 = \frac{2d - 2 - (d_\theta - 1)^2}{4(d_\theta - 1)(d_\theta - 3)}. \tag{5.25}$$

Inputting these into the area functional, we obtain the leading order contribution to the entanglement entropy

$$S_A = \frac{2\pi^{d/2}}{\Gamma(d/2)} \left[\frac{1}{d_\theta - 1} \frac{R^{d-1}}{\varepsilon d_\theta - 1} + \ldots \right]. \tag{5.26}$$

The above method fails when the effective dimension is an odd integer. The most important case $d_\theta = 1$ has been considered in [87] for $d = 2$. Their result exhibits the logarithmic correction to the area law,

$$\frac{2\pi}{G_N^{(4)}} \left(R \log\left(\frac{R}{\varepsilon}\right) + \ldots \right). \tag{5.27}$$

This time, the entanglement entropy resembles that of the Fermi surface theory more closely as the radius of the region, R, is indeed a characterictic length of the system. However, we still have only a logarithmic divergence when $\varepsilon \to 0$ whereas the critical theory with a Fermi surface would also exhibit ε^{-1} scaling.

5.3 Evolution of holographic entanglement entropy

We now move on to the considerably more difficult dynamic case. We recall that there were no explicit expressions for the entanglement entropy even in the usual case of AdS/Vaidya metric, save for the analytic expression for the AdS_3/Vaidya metric in thin shell limit. Things are even worse now as almost everything has to be done numerically. We will consider the cases of infinite strip and ball, concentrating more on the former.

Generally, at early times, geometry will resemble that of a pure AdS space with Lifshitz scaling and hyperscaling violation and at late times, it will be that of a black hole also with Lifshitz scaling and hyperscaling violation. The extremal surface will penetrate less and less through the shell to the AdS region as the time evolution goes further. And after some critical time $t = t_c$, shorter geodesics will no longer penetrate the shell and will behave as those in static black hole geometry.

5.3.1 Strip geometry

In dynamic backgrounds, we must consider extremal surfaces and allow the v coordinate to vary. We consider the strip $A = [0, L]^{d-1} \times [-l/2, l/2]$ where $L \gg l$ and assume that both v and z vary only in the direction of $x \in [-l/2, l/2]$ i.e. $(v, z) = (v(x), z(x))$. As boundary constraints for the extremal surface, we require $v(-l/2) = v(l/2) = t$ and $z(-l/2) = z(l/2) = 0$. It is also evident, that both z and v are even functions of x on the extremal surface which leads to the requirement $v'(0) = z'(0) = 0$. With these constraints, we write the area functional of the d dimensional surface γ,

$$\text{Area}_\gamma = 2L^{d-1} \int_0^{l/2} \frac{\sqrt{\mathscr{L}}}{z^{d_\theta}}, \quad \mathscr{L} = 1 - F(v, z) z^{2(1-\zeta)} v'^2 - 2z^{1-\zeta} z' v'. \tag{5.28}$$

We find a constant of motion from the observation that the integrand does not depend on explicitly on x,

$$\left(\frac{z_*}{z}\right)^{2d_\theta} = \mathscr{L}, \tag{5.29}$$

where z_* is the maximal value of $z(0) = z_*$ on the extremal surface. By extemizing the integral with respect to v and v', and z and z', and using the equation above, we find the Euler-Lagrange equations of motion [80]

$$\frac{d}{dx}[z^{1-\zeta}(z^{1-\zeta}Fv' + z')] = z^{2(1-\zeta)}F_v v'^2/2 \tag{5.30}$$

$$\frac{d}{dx}[z^{1-\zeta}v'] = d_\theta \mathscr{L}/z + z^{2(1-\zeta)}F_z v'^2/2 + (1-\zeta)z^{-\zeta}(z' + z^{1-\zeta}Fv')v'. \tag{5.31}$$

These three equations of motions are not independent and only two are needed to solve the functions $v(x)$ and $z(x)$. When the solutions are found, the area of the minimal surface is

$$\text{Area} = 2L^{d-1}\int_0^{l/2} dx \frac{z_*^{d_\theta}}{z^{2d_\theta}}. \tag{5.32}$$

Naturally, the expression for the area is UV divergent. The situation can be salvaged if we regularize, e.g. by setting the boundary conditions $z(-l/2) = z(l/2) = \varepsilon$. To renormalize, a common procedure is to substract either the early time vacuum entropy or the late time thermal entropy.

Thin shell regime

We now consider the thin shell regime where $M(v) = M\theta(v)$. Once again, we now have two distinct but far easier metrics where we need to solve the differential equations. It turns out that we can express the minimal surface as an integral over z and with two parameters.

It is important that when we solve the equations of motion separately, the solution remains continuous. Let x_c the position where the solutions should match i.e. where the geodesic crosses the shell. Then $v(x_c) = 0$ and $z(x_c) = z_c$. We can solve the equations of motion separately in regimes $0 \le x \le x_c - \delta/2$ (pure AdS) and $x_c + \delta/2 \le x \le l/2$ (blackhole geometry). The contribution of the remaining area can be evaluated when we integrate the equations of motion (5.30),(5.31) over the remaining area and then take the limit $\delta \to 0$. The non-vanishing contribution to the integrals on the right hand side come from the delta functions arising from F_v terms. When considering the equation (5.31) first, we get the relation $v'(x_c-) = v'(x_c+) \equiv v'_c$. However, the equation (5.30) gives us the non-trivial relation [80]

$$z'(x_c+) - z'(x_c-) = \frac{z_c^{1-\zeta}v'_c}{2}(1 - F(z_c)). \tag{5.33}$$

Considering equation (5.30), we can integarate it as the right hand side vanishes for $x \neq x_c$ thus obtaining

$$z^{1-\zeta}(v'z^{1-\zeta}F + z') = \begin{cases} E_-, & \text{if } 0 \le x < x_c \\ E_+, & \text{if } x_c < x \le l/2 \end{cases}. \tag{5.34}$$

where $E_\pm$ are constants. Remembering that $v'(0) = z'(0) = 0$, we see that $E_- = 0$. Thus, we also see that inside the shell, where $F(v,z) = 1$,

$$v' = -z^{\zeta-1}z', \quad 0 \le x < x_c \tag{5.35}$$

obtaining a useful relation between v' and z'. On the other hand, integrating the equation above from 0 to x_c and, altenatively, taking the limit $x \to x_c-$ give us the relations [80]

$$z_c^\zeta = z_*^\zeta + \zeta v_*, \quad v_c' = -z_c^{\zeta-1}z_-' > 0. \tag{5.36}$$

Consider the geometry outside the shell where the background metric is that of a black hole. First, juggling with equation (5.34), we obtain the useful equation for v'

$$v' = \frac{1}{z^{1-\zeta}F(z)}\left(\frac{E_+}{z^{1-\zeta}} - z'\right), \quad x_c < x \le l/2. \tag{5.37}$$

From the same equation, making use of the equation (5.29), we obtain the equation

$$z'^2 = F(z)\left[\left(\frac{z_*}{z}\right)^{2d_\theta} - 1\right] + \frac{E_+^2}{z^{2(1-\zeta)}}, \quad x_c < x \le l/2. \tag{5.38}$$

This also applies to the interiors of the shell when we modify with $F(z) \mapsto 1$ and $E_+ \mapsto E_- = 0$. We can relate the constant E_+ to $z'(x_c-)$ by taking the difference of equations (5.34) at the shell $x = x_c$. Remembering all the relations we have obtained so far, we get [80]

$$E_+ = \frac{z_c^{1-\zeta}}{2}(1 - F(z_c))z_-' < 0. \tag{5.39}$$

Now, we have plenty of constants and relations and we can finally start wrapping up our results and obtain an expression for the area of the minimal surface. We first assume that $z(x)$ is injective. This is not true in general and we will consider it later. Firstly, we integrate equations (5.38) over both sides of the shell and obtain the relation

$$\frac{l}{2} = \int_{z_c}^{z_*} dz\, z^{d_\theta}(z_*^{d_\theta} - z^{2d_\theta})^{-1/2} + \int_0^{z_c} dz \left\{F(z)\left[\left(\frac{z_*}{z}\right)^{2d_\theta} - 1\right] + \frac{E_+^2}{z^{2(1-\zeta)}}\right\}^{-1/2}. \tag{5.40}$$

Secondly, we use the boundary conditions of v at $x = x_c$ and $x = l/2$ and apply equations (5.37), (5.38) and we are given the expression for t

$$t = \int_0^t dv = \int_{x_c}^{l/2} dx\, v' = \int_0^{z_c} dz\, \frac{z^{\zeta-1}}{F(z)}\left[1 + E_t z^{\zeta-1}\left\{F(z)\left[\left(\frac{z_*}{z}\right)^{2d_\theta} - 1\right] + \frac{E_+^2}{z^{2(1-\zeta)}}\right\}^{-1/2}\right]. \tag{5.41}$$

Thirdly, we obtain the actual expression for the area of the minimal surface using expression (5.32) and making a change of coordinates from x to z and then using (5.38). We finally obtain

$$\text{Area}_{\gamma_A} = 2L^{d-1}z_*^{d_\theta}\left(\int_{z_c}^{z_*} \frac{dz}{z^{d_\theta}}(z_*^{2d_\theta} - z^{2d_\theta})^{-1/2} + \int_\varepsilon^{z_c} \frac{dz}{z^{2d_\theta}}\left\{F(z)\left[\left(\frac{z_*}{z}\right)^{2d_\theta} - 1\right] + \frac{E_+^2}{z^{2(1-\zeta)}}\right\}^{-1/2}\right) \tag{5.42}$$

where the UV regulator ε was explicitly added. It can be removed once we renormalize the entanglement entropy [80].

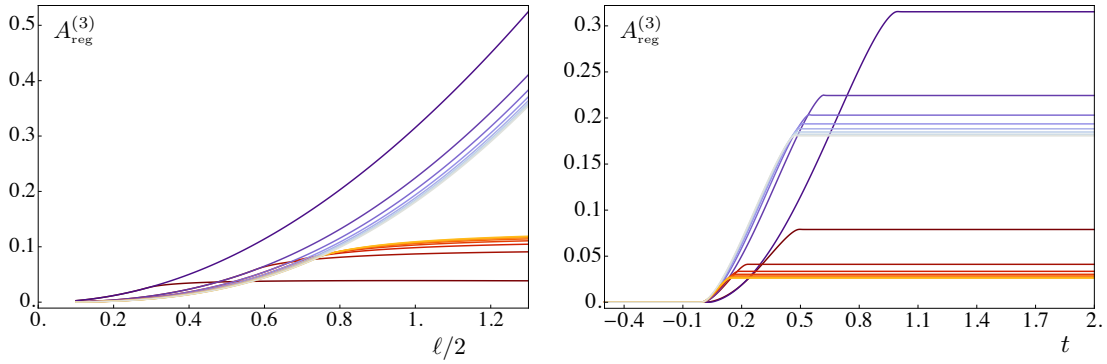

Figure 5.1: The regularized area of the minimal surface for a strip geometry in various dimensions in the thin shell limit ($a = 0.01$) with $m = 1$ as the final mass of the black hole. The vacuum value has been subtracted. Here, $\theta = d - 1$ and $\zeta = 2 - 1/d$, with $d = 1, 2, \ldots, 8$. The darkest curves have $d = 1$ while the lightest have $d = 8$. On the left, the regularized area at a fixed time for various widths, the red curves have $t = 0.15$ and the blue ones have $t = 0.7$. On the right, time evolution of the area for fixed l. The red ones have $l = 1$ while the blue ones have $l = 2$. The figures originally appeared in [80].

However, we originally had 2 parameters l and t, now we have 3: (z_*, z_c, E_+). The solution lies in the fact that we can integrate the geodesic equation of motion inside the shell ($v < 0$) and obtain the parameter $z'(x_c-)$. Using equation (5.38) with replacements $F(z) \mapsto 1$ and $E_+ \mapsto E_- = 0$, we get

$$\begin{aligned} x(z) &= \frac{z_*}{1+d_\theta}\left[{}_2F_1\left(\frac{1}{2},\frac{1+d_\theta}{2d_\theta};\frac{3+d_\theta}{2d_\theta};1\right)-\left(\frac{z}{z_*}\right)^{d_\theta+1}{}_2F_1\left(\frac{1}{2},\frac{1+d_\theta}{2d_\theta};\frac{3+d_\theta}{2d_\theta};\left(\frac{z}{z_*}\right)^{2d_\theta}\right)\right] \\ &= \frac{z_*}{1+d_\theta}\left[\frac{\sqrt{\pi}\Gamma\left(\frac{3d_\theta+1}{2d_\theta}\right)}{\Gamma\left(\frac{2d_\theta+1}{2d_\theta}\right)}-\left(\frac{z}{z_*}\right)^{d_\theta+1}{}_2F_1\left(\frac{1}{2},\frac{1+d_\theta}{2d_\theta};\frac{3+d_\theta}{2d_\theta};\left(\frac{z}{z_*}\right)^{2d_\theta}\right)\right]. \end{aligned} \tag{5.43}$$

Taking the derivative of this expression at $z = z_c$ and inverting it, we get the value of z'_- and thus we can express E_+ with z_c and z_*. Thus, we have the solved the equation of motion for the minimal surface analytically although not in a closed form.

There are several situations where $z(x)$ is not injective. In these cases, the curve of $z(x)$ starts to grow after x_c and forms a symmetric hump [80]. We take this into account with the substitution

$$\int_0^{z_c} dz f(z) \to \int_0^{z_m} dz f(z) + \int_{z_c}^{z_m} dz f(z) \tag{5.44}$$

where $f(z)$ is any of the integrands above. The point $z_m < z_*$ is defined with $z'^2(z_m) = 0$ (5.38). This equation is not algebraically solvable [80].

These geodesics have been studied extensively in general cases using numerical methods. It may be slightly surprising, that the evolution of holographic entanglement entropy behaves similarly to the cases we have considered before. At first, there is a non-trivial power law followed by a regime of linear growth. The figures (5.1) show the behaviour of entanglement entropy explicitly.

5.3.2 Spherical regions

We will briefly touch upon the subject of spherical regions. We will consider the spherical region with radius R, $A = B^d(x, R)$. Due to spherical symmetry, it is obvious that the coordinates v and z

can be expressed as functions of the radial coordinate on the minimal surface in the bulk space. The minimal surface should have the boundary conditions $v(R) = t$, $v'(0) = 0$, and $z(R) = 0$, $z'(0) = 0$. The area functional of the surface is

$$\text{Area}_\gamma = \frac{2\pi^{d/2}}{\Gamma(d/2)} \int_0^R d\rho \frac{\rho^{d-1}}{z^{d_\theta}} \sqrt{\mathscr{L}}, \quad \mathscr{L} = 1 - F(v,z) z^{2(1-\zeta)} v'^2 - 2 z^{(1-\zeta)} z' v'. \tag{5.45}$$

Like in the static case, we cannot find a simple constant of motion, making the analysis more difficult. In order to solve the minimal surface, we must solve the Euler-Lagrange equations of motion arising from the variation of the integral with respect to v and z. They yield [80]

$$\frac{z^{d_\theta}\sqrt{\mathscr{L}}}{\rho^{d-1}} \frac{d}{d\rho} \left[\frac{\rho^{d-1} z^{1-\zeta-d_\theta}}{\sqrt{\mathscr{L}}} (v' z^{1-\zeta} F + z') \right] = \frac{z^{2(1-\zeta)}}{2} F_v v'^2 \tag{5.46}$$

$$\frac{z^{d_\theta}\sqrt{\mathscr{L}}}{\rho^{d-1}} \frac{d}{d\rho} \left[\frac{\rho^{d-1} z^{2(1-\zeta)-d_\theta}}{\sqrt{\mathscr{L}}} v' \right] = \frac{d_\theta}{z} \mathscr{L} + \frac{z^{2(1-\zeta)}}{z^\zeta} (z' + x^{1-\zeta} F v') v'. \tag{5.47}$$

Thin-shell regime

We focus now on the thin-shell limit where the mass function is a step function, $m(v) = m\theta(v)$. However, there is not much to do analytically due to the level of difficulty of the equations of motion to be solved. We are only able to solve v as a function of the others. This analysis was originally considered in [80] and we will point the reader to it for more details.

We can find the solutions for the equations of motion separately inside and outside the shell. To make the complete solution continuous, we introduce the variables $\tilde{v}' = v'/\sqrt{\mathscr{L}}$ and $\tilde{z}' = z'/\sqrt{\mathscr{L}}$. With these, we can integrate over the Euler-Lagrange equations of motion to obtain the conditions for the derivatives of the newly-introduced coordinates at the shell where $\rho = \rho_c$,

$$\tilde{v}'(\rho_c -) = \tilde{v}'(\rho_c +) \equiv \tilde{v}(\rho_c) \tag{5.48}$$

$$\tilde{z}(\rho_c +) - \tilde{z}(\rho_c -) = \frac{z_c^{1-\zeta} \tilde{v}'_c}{2} (1 - F(z_c)). \tag{5.49}$$

We can integrate the equation (5.46) over the region where $v \neq 0$ and $F_v = 0$ to obtain two constans of motion for the two separate regions,

$$\frac{\rho^{d-1} z^{1-\zeta-d_\theta}}{\sqrt{\mathscr{L}}} (v' z^{1-\zeta} F + z') = \begin{cases} E_-, & \text{if } 0 \leq \rho < \rho_c \\ E_+, & \text{if } \rho_c < \rho \leq R \end{cases}, \tag{5.50}$$

where we can immediately set $E_- = 0$ as $v'(0) = z'(0) = 0$. In addition, using the relations for the derivatives on the shell, we realize that $\sqrt{\mathscr{L}}$ is continuous across the boundary [80].

Using all that we have learned so far, we find that

$$E_+ = \frac{\rho_c^{d-1} z_c^{2(1-\zeta)-d_\theta}}{2\sqrt{\mathscr{L}(x_c)}} (F(z_c) - 1) v'_c, \tag{5.51}$$

which gives us an expression for v' outside the shell ($\rho > \rho_c$)

$$v' = \frac{z^{\zeta-1}}{F(z)} \left(\frac{A E_+ \sqrt{1 + z'^2/F(z)}}{\sqrt{1 + A^2 E_+^2/F(z)}} - z' \right), \quad A(z,\rho) \equiv \frac{z^{d_\theta+\zeta-1}}{\rho^{d-1}}. \tag{5.52}$$

Finally, we obtain the equation of motion for z on the extremal surface [80]

$$2d_\theta\rho F^2 + z[\rho F_z - 2(d-1)z']z'^2 - 2F[\rho z z'' + (d-1)zz' + d_\theta\rho z'^2] \\ +E_+^2 A^2\rho[z(F_z+2z'') - 2(\zeta-1)(F+z'^2)] = 0. \tag{5.53}$$

We can obtain the expression for t by integrating (5.52) over $R \le \rho < \rho_c$ but there is no such simple expression for R. Finally, the integral for the area of the extremal surface is the sum of contributions from the both regions and it can be written as

$$\text{Area}_{\gamma_A} = \frac{2\pi^{d/2}}{\Gamma(d/2)}\left(\int_0^{\rho_c} d\rho \frac{\rho^{d-1}\sqrt{1+z'^2}}{z^{2d_\theta}} + \int_{\rho_c}^{R} d\rho \frac{\rho^{d-1}\sqrt{1+F(z)z'^2}}{z^{d_\theta}\sqrt{1+A^2E_+^2/F(z)}}\right). \tag{5.54}$$

Notice, how the integral still depends on the derivative of z. We must solve the equation of motion (5.53) numerically before we can make use of the area functional in any way [80].

Numerical solutions have been considered. The entanglement entropy grows with the same power law as for the corresponding strip and then grows linearly in the intermediate times and saturates with a continuous time derivative [80].

5.4 Analytic results of the time evolution

In the recent papers [79, 80], the work of [76] has been generalized to spacetimes with Lifshitz scaling and hyperscaling violation. It is surprising, that such general properties could be generalized to these kinds of spacetimes, too. According to their results, at early times, the entanglement entropy grows according to a power law. That is, for times $0 < t \ll z_h$, the entanglement grows as

$$\Delta S_A(t) = \frac{M\text{Area}_A\zeta^{1+1/\zeta}}{8(\zeta+1)G_N^{(d+2)}}t^{1+1/\zeta}, \tag{5.55}$$

where Area_A is the surface area of A, a general entangling region. Remarkably, the early times growth does not depend on θ but only on ζ, justifying its name, dynamical critical exponent. Also, in the usual AdS space, $\zeta = 1$, the expression reproduces the quadratic growth we discussed in the previous chapter. This growth has been shown to hold numerically in [80].

When sufficient amount of time has passed, the entanglement entropy will grow linearly. The authors of [79, 80] showed that for a strip, $A = [0,L]^{d-1}\times[-l/2,l/2]$, for times $z_h \ll t \ll l$, and if $d_\theta + \zeta \ge 2$, the holographic entanglement entropy grows as

$$\Delta S_A(t) = \frac{L^{d-1}}{2G_N^{(d+2)}}\frac{v_E}{z_h^{d_\theta+\zeta-1}}t \tag{5.56}$$

where v_E can be thought of as the propagation speed of the entanglement tsunami

$$v_E = \frac{(\eta-1)^{(\eta-1)/2}}{\eta^{\eta/2}}, \quad \eta = \frac{2(d_\theta+\zeta-1)}{d_\theta+\zeta}. \tag{5.57}$$

We see that the propagation speed is unity when $\eta = 1$ and approaches zero when $\eta \to \infty$. Interestingly, the linear growth depends only on the sum $d_\theta + \zeta$ and not on the explicit dimension. The linear growth has been show numerically in many situations e.g. in [80].

For the saturation time, t_s, the time after which the extremal surface of a specific region no longer penetrates the shell, the leading order behaviour can be estimated with

$$t_s = \begin{cases} z_h^{\zeta-1}\sqrt{\frac{d_\theta}{2z_hF'(z_h)}}\,l + \dots & \text{strip} \\ z_h^{\zeta-1}\sqrt{\frac{d_\theta}{2z_hF'(z_h)}} - z_h^{\zeta-1}\frac{d-1}{F'(z_h)}\log(R) + \dots & \text{sphere} \end{cases}. \tag{5.58}$$

For the strip, it was assumed that the time derivative of the entanglement entropy was continuous at $t = t_s$. It can be shown that the entanglement entropy approaches the saturation value according to a power law whenever the derivative is continuous at $t = t_s$,

$$\Delta S_A = (t - t_s)^2. \tag{5.59}$$

On the other hand, when the entangling region is a ball, the saturation value is approached smoothly [80].

It is remarkable and quite non-intuitive that the above general and simple results also apply after generalization to Lifshitz scaling and hyperscaling violation even though many of the calculations became much more difficult in the usual cases of holographic entanglement entropy. It would be most interesting to see, whether these kinds of thermalization properties were observed in the dual field theories either in theory or, in the future, even in experiments. It would also be interesting to see the application of falling particle geometry in this generalization, but so far this remains undone.

Chapter 6

Mutual information

We now move on to the final chapter of this thesis. We will discuss mutual information and, in particular, its time evolution in situations. Most emphasis will be put on mutual information of one-dimensional interval and their phase transitions with varying time and separations. In multi-dimensional cases, we will only consider strips which may differ only in their thickness due to the arising difficulties in determining the minimal surface in more complex situations.

We will first make a brief general discussion of mutual information. After that, we will consider static situations where the most important measure is the distance of the two regions. Situations to be considered are the ones that have been solved in a closed form in the holographic picture. After that, we will consider time evolution of the mutual information both from the conformal field theory perspective and from the holographic perspective. This time, we are mostly interested in the possible phase transitions as time grows.

6.1 The significance of mutual information

As a reminder, if we have two separate spatial regions A and B, their corresponding mutual information is defined

$$I(A,B) = S(A) + S(B) - S(A \cup B) \geq 0, \tag{6.1}$$

where the inequality follows from the subadditivity property of the entanglement entropy. Mutual information answers the questions, how much common information do regions A and B have or how much do we learn about B when studying A. If the mutual information is zero, it means that the regions A and B are uncorrelated and that the reduced density matrix factorizes as in $\rho_{A\cup B} = \rho_A \otimes \rho_B$.

In the case of $1+1$ dimensional conformal field theories, mutual information of two disjoint intervals has been shown to contain all the contents of the theory i.e. the conformal dimensions of primary fields and their correlation functions, although only in the cases where it has been evaluated succesfully. As we saw in chapter 2, the entanglement entropy of a single interval could only tell us the central charge of the theory [23].

Mutual information has some very interesting properties. Perhaps the most useful one is that the divergences cancel as long as the two regions have no common boundary. Another noteworthy

property is in the holographic picture, the mutual information tends to have a phase transition. In the static case, when the separation of two regions is grown from very small to very large distances, the mutual information will have a discontinuous derivative at some point. These are, however, only believed to happen in large c conformal field theories.

6.2 Static cases

In the holographic picture, the mutual information is determined by the difference in area of two (or more) competing extremal surfaces, the disconnected and the connected ones. In the disconnected case, the extremal surface is formed by the two disjoint minimal surfaces of the two regions. In the connected case, the minimal surface is one connected surface, forming a bridge between the two regions. In the first case, the mutual information is always zero and in the latter, it is positive. It is clear that the farther the two regions are, the more likely the minimal surface is disconnected. At the critical distance of the two regions, the two possible minimal surfaces are equal and the mutual information may exhibit a phase transition.

6.2.1 Mutual information of strips in pure AdS$_{d+2}$

We have already discussed the case $d = 1$ in chapter 3 and will not rediscuss it here. Hence, $d > 1$. Let $A = [0, L]^{d-1} \times [-l_1 - x/2, -x/2]$ and $B = [0, L]^{d-1} \times [x/2, x/2 + l_2]$ where $L \gg l_i, x$. In this case, the entanglement entropy of the region $A \cup B$ is determined either by the sum of the two separate minimal surfaces or by the connecting surface. The connected surface is given by considering surfaces for strips $[0, L]^{d-1} \times [0, l_2 + l_1 + x]$ and $[0, L]^{d-1} \times [0, x]$ with appropriate translations. Thus, the connected entanglement entropy is

$$S_{A\cup B,\text{conn}} = \frac{L^{d-1}}{4(d-1)G_N^{(d+2)}} \left[\frac{4}{a^{d-1}} - 2^d \pi^{d/2} \left(\frac{\Gamma(\frac{d+1}{2d})}{\Gamma(\frac{1}{2d})} \right)^d \left(\frac{1}{x^{d-1}} + \frac{1}{(x + l_1 + l_2)^{d-1}} \right) \right] \tag{6.2}$$

where we have used our results from chapter 3 for entanglement entropy of a strip (3.32) with $R = 1$ and a is a UV regulator. Thus, the mutual information of the two strips is

$$I(A, B) = \frac{2^d L^{d-1} \pi^{d/2}}{4(d-1)G_N^{(d+2)}} \left(\frac{\Gamma(\frac{d+1}{2d})}{\Gamma(\frac{1}{2d})} \right)^d \text{Max} \left[0, \left(\frac{1}{x^{d-1}} + \frac{1}{(l_1 + l_2 + x)^{d-1}} - \frac{1}{l_1^{d-1}} - \frac{1}{l_2^{d-1}} \right) \right]. \tag{6.3}$$

We see that the divergences have cancelled and this expression is finite as long as $x > 0$. There is a general expression for critical x for $d = 2, 3$. After that, there is no algebraic solution although they can still be found numerically. When $l_1 = l_2 = l$, the critical distances are

$$\begin{aligned} x_1 &= (\sqrt{2} - 1)l = 0,41l, & x_4 &\approx 0,80l, \\ x_2 &= \tfrac{\sqrt{5}-1}{2} l \approx 0,62l, & x_5 &\approx 0,84l, \\ x_3 &= (\sqrt{3} - 1)l \approx 0,73l, & x_6 &\approx 0,87l. \end{aligned}$$

Asymptotically, the critical distance for large dimensions d is $x_d \simeq 2^{1/(d-1)} l$ and this gives a rather good estimate for $d \geq 4$. The slope of mutual information goes abruptly to zero when the critical distance is reached.

The calculations and results are roughly the same in case of hyperscaling violation, d is just replaced with d_θ except for the power of L.

6.2.2 Mutual information for black hole background

The black hole background is dual to a thermal conformal field theory where the transition between disconnected and connected phase is influeced by the temperature, β^{-1}.

Three dimensional BTZ black hole

We now consider disjoint intervals $A = [-l_1 - x/2, -x/2]$ and $B = [x/2, x/2 + l_2]$. The connected surface will connect the farther endpoints of the two regions and the closest endpoints. It corresponds to two geodesics for intervals $[0, l_1 + l_2 + x]$ and $[0, x]$. This leads to the expression of mutual information for inverse temperature β

$$\frac{c}{3}\text{Max}\left(0, \log\left(\frac{\sinh(\pi l_1/\beta)\sinh(\pi l_2/\beta)}{\sinh(\pi x/\beta)\sinh(\pi(l_1+l_2+x)/\beta)}\right)\right) \tag{6.4}$$

It is notable, that in the high temperature limit, the mutual information vanishes. It is physically clear, that when there is too much thermal fluctuation, the information vanishes over long distances. There is an algebraic solution for the critical distance for general intervals found in [23]. The algebraic solution for equal lengths, $l_1 = l_2 = l$, is

$$x_{1,\text{BH}} = \frac{|\text{arcosh}(\sqrt{\cosh(2l\pi/\beta)}|}{\pi}\beta - l < x_{1,\text{vac}}. \tag{6.5}$$

We see that the critical distance is smaller the higher the temperature is, but it is still non-zero at every finite temperature. It also reduces to the zero-temperature value as $\beta \to \infty$. On the other hand, as $l \to \infty$, the critical distance has the limit $x(\infty) = \frac{\log(2)\beta}{2\pi}$, i.e. it is finite! The phase transition still occurs at the critical distance as the derivative is not continuous. Also, the critical distance of the black hole geometry is always less than that of vacuum geometry, also in the case of general intervals [23].

6.3 Time evolution of mutual information

The real world hardly stays still so dynamical systems are arguably more interesting than the ones in equilibrium. I will begin by discussing global quench from the conformal field theory perspective where the case of multiple intervals can be considered somewhat rigorously. After that I will also consider the corresponding results from the infalling shell geometry originally done in [23, 22].

We will then make a slight detour to the falling particle geometry and consider the time evolution after a local quench in one dimension from both the CFT and holographic perspective. This has originally been done in [44].

The culmination of this thesis is to consider the evolution of mutual information in the thin-shell regime with Lifshitz scaling and hyperscaling violation. At the time of writing, this situation has not been considered before.

6.4 Mutual information after a global quench

6.4.1 Conformal field theory perspective

As originally stated in chapter 2, the global quench setting enables us to ignore the full operator content of the theory to reasonable accuracy. However, we can still only consider one-dimensional cases. As a reminder, the entanglement entropy after a global quench for two disjoint intervals was

$$S_{[u_1,u_2]\times[u_3,u_4]} \approx S_A(\infty) + \frac{\pi c}{12\tau_0} \sum_{k,l=1}^{4} (-1)^{k-l-1} \max(u_k - t, u_l + t), \tag{6.6}$$

where $S_A(\infty)$ is the final value of the entanglement entropy i.e. the sum of the lengths of the intervals multiplied with $\frac{\pi c}{12\tau_0}$. We must always translate our system such that $\sum_k u_k = 0$ and choose $u_k < u_{k+1}$ before using the above expression.

Assume now that $A = [-l_1 - x/2, -x/2]$ and $B = [x/2, x/2 + l_2]$ where $l_1 \geq l_2$. When we evaluate the mutual information using the result above, it stays zero until $t = x/2$. After that, it grows linearly until it reaches $t = (x + l_2)/2$ and stays constant till $t = (l_1 + x)/2$. Finally, it goes linearly back to zero at time $t = (x + l_1 + l_2)/2$ after which it remains at zero. The slopes of the linear growth regimes are $\pm\frac{\pi c}{6\tau_0}$. This applies for all l_i and d. As a special case, the case of equal length intervals produces a sharp peak at $t = (l + x)/2$.

It is strange that no matter what the distance is, there are still times, when the mutual information is non-zero. It is also puzzling that after the initial growth, the mutual information would start to drop back to zero. These phenomena can be motivated by using the simple quasiparticle model originally considered in chapter 2. According to it, quasiparticle excitation created at the same site are entangled and they all form after the initial quench at $t = 0$. Now, the two regions have non-zero mutual information, whenever two entangled quasiparticles are at the two regions at the same time. Remembering that the quasiparticles emitted in the CFT always have speed $v = 1$, this toy model explains perfectly the time evolution of mutual information after a global quench.

6.4.2 Global quench using AdS/Vaidya geometry

Even though we were able to reproduce the time evolution of entanglement entropy for a single interval fairly well in chapter 4, the time evolution of mutual information differs significantly. The distance of the two regions plays a significant role this time.

Before doing any calculations, consider some qualitative features first. For early times, the system we are considering is a pure AdS space and for late times, it has a black hole background. We know that the critical distance in the thermal case is shorter than in vacuum for equal intervals, but this is also the case for unequal intervals [23]. This means that whenever the distance of the two regions is greater than x_{vac}, the mutual information will start at zero and it will end at zero but it may still be non-zero in the middle. However, the mutual information should always be zero when x is sufficiently large. On the other hand, if the distance is shorter than x_{BH}, it is expected that the mutual information is always non-zero. If the distance is between the values, $x_{\text{BH}} < d < x_{\text{vac}}$, the mutual information should start at some non-zero value but for times $t > (l_1 + l_2 + d)/2$ it will be zero. This is because the surfaces contributing to the mutual information will be completely in the

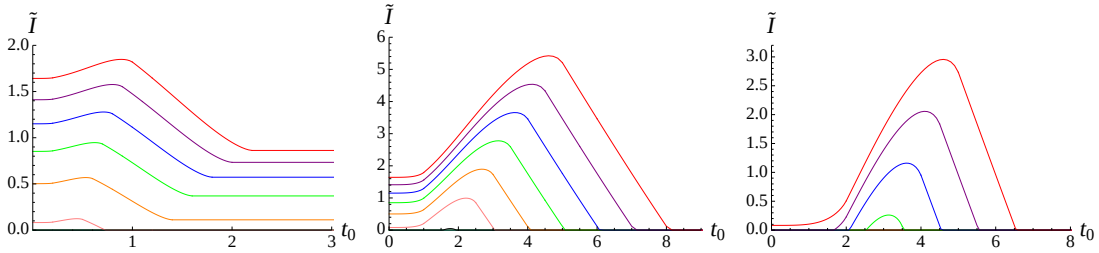

Figure 6.1: Time evolution of (rescaled) mutual information for two equal length intervals with fixed separation. The separations are from left to right $d = 0.4, 2, 4$. The mass of the black hole has been set to unity. The left panel has lengths $l = 0.2, 0.4, \ldots, 2.0$ while the center and right panel have $l = 1, \ldots, 10$. The length increases from the bottom up and the smallest lengths have identically zero mutual information during the evolution. The figures are originally from [22].

black hole geometry and the two regions have effectively reached their final state. All in all, the mutual information starts at its vacuum value and ends up at its lower black hole value.

In the time evolution cases, we should also consider the other possible connected surface, which connects the left boundaries of the strips and the right boundaries of the strips. In static cases, we could argue that it cannot be the minimal surface but no such proof exists in dynamic cases. Nevertheless, in [22], it was shown that this situation does not exhibit the other mixed connected surface as its minimal surface.

In the thin shell limit, a significant factor is whether the potential minimizing geodesic crosses the shell or not. As the quench evolves, the geodesics are less and less likely to cross the shell. Whenever the shell can be crossed, the resulting geodesic will have shorter length than the corresponding black hole geodesic.

The mutual information in the infalling shell geometry was considered in [22, 23] using the thin-shell limit, and we will borrow their results and figures. We see from their figures that the time evolution is much smoother although they still exhibit phase transitions if the mutual information starts from a zero value or if it ends at it. The phase transition may also occur in the finite shell limit. The positions of peaks and and the overall shape of the time evolution does not agree with the conformal field theory results very well. The equal length intervals still produce a peak, there are linear regimes of evolution and the first linear growth starts around $t = x/2$, if it starts at all. In the asymmetric case, the mutual information does not have a regime of constant value but instead decreases steadily until it starts decreasing faster and begins another regime of linear evolution.

The disagreements can be partly understood if we remember that the conformal field theory approach had a finite mass gap which made the long distance correlations irrelevant. This was encoded in the parameter τ_0. There was no such setting in the holographic picture thus making the two approaches slightly different but in a fundamental manner [23]. The quasiparticle picture cannot explain the behaviour of mutual information making it less appealing.

6.5 Mutual information after a local quench

We now move on to the local quench section where our two approaches had some clear disagreements even in the single interval case. This analysis was originally done in [44]. For simplicity, we

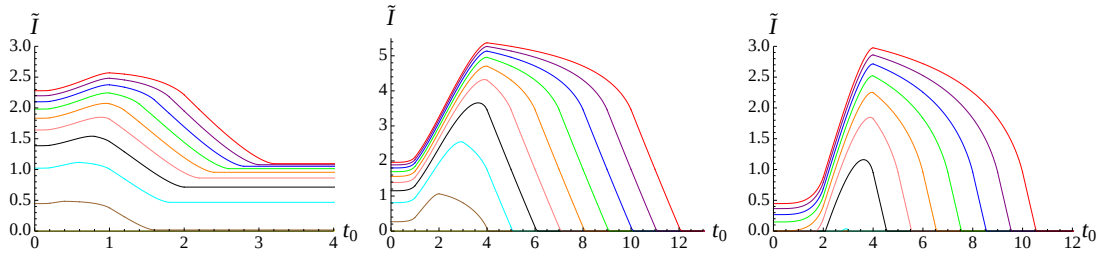

Figure 6.2: Time evolution of mutual information for two intervals with different lengths at fixed separation. The left panel has $l_1 = 2$ and $d = 0.4$, the middle one has $l_1 = 8$,$d = 2$ and the right one has $l_1 = 8$ and $d = 4$. The length of the second interval grows from the bottom up. For the left panel, it is $l_2 = 0.4, 0.8, \ldots, 4.0$ while for the other panels it is $l_2 = 2, 4, \ldots, 20$. Like before, some of the lengths have vanishing identically vanishing mutual information. The figures are originally from [22].

will only consider equal length intervals as they provide us with a sufficiently rich variety of settings themselves.

6.5.1 Conformal field theory perspective

For simplicity, we will omit the non-universal contibutions to the entanglement entropy and focus on the universal parts. First, focus on the symmetric interval with $A = [-(d/2 + l), -d/2]$ and $B = [d/2, d/2 + l]$. Using the results from chapter two, the mutual information evolves to leading order as

$$I(A,B) = \begin{cases} 0 & t < d/2, \\ \frac{c}{3}\log\left[\frac{2(d+l)(d/2+l-t)(t^2-d^2/d)}{\epsilon d l (d/2+l+t)}\right] & d/2 < t < l + d/2, \\ \frac{c}{3}\log\left[\frac{(d+l)^2}{d(d+2l)}\right] & t > l + d/2. \end{cases} \tag{6.7}$$

We see that the mutual information is contant at early and late times and the mutual information has the shape of a hump which is independent of d in the limit $d/l \gg 1$. The maximum of mutual information occurs roughly at $t = (d + l)/2$ and has the value $c/3\log(l/2\epsilon)$ in the limit $d/l \gg 1$, that is, it is independent of their separation in accordance with the quasiparticle picture. Notice also that the one UV regulator, ϵ, still appears at the intermediate times. Physically, this corresponds to the fact, that the intermediate times will dominate when we allow greater energies [44].

For the asymmetric equal length intervals, we choose $A = [-(d-x+l), -(d-x)]$ and $B = [x, x+l]$. This time around, there are five different regimes of evolution, the first and last one corresponding to constant cases where in the first the regions are non-interacting and in the last they are interacting. Assuming that $d - x < x < d - x + l$, the late and early time values are

$$I(A,B)(t < d - x) = 0, \tag{6.8}$$

$$I(A,B)(t > x + l) = \frac{c}{3}\log\left[\frac{(d+l)^2}{d(d+2l)}\right]. \tag{6.9}$$

The intermediate times are much more complex. The values are

$$I(A,B)(d-x<t<x) = \frac{c}{6}\log\left[\frac{(2x-d)(d+l)(x+t)(l+x-t)}{d(l-d+2x)(x-t)(l+x+t)}\right], \tag{6.10}$$

$$I(A,B)(x<t<d-x+l) = \tag{6.11}$$

$$\frac{c}{6}\log\left[\frac{4(x+l)(d+l)^2(d-x+l-t)(t^2-(d-x)^2)(x+l-t)(t^2-x^2)}{\varepsilon^2 d^2(l+x)(l^2-(d-2x)^2)(d-x+l+t)(x+l+t)}\right], \tag{6.12}$$

$$I(A,B)(d-x+l<t<x+l) = \frac{c}{6}\log\left[\frac{(2x-d)(d+l)^3(t^2-(d-x)^2)}{d^2(d+2l)(l-d+2x)(t^2-(d-x+l)^2)}\right]. \tag{6.13}$$

Notice how the UV regulator ε appears only in the middle equation, corresponding to the maximum values of the mutual information of A and B. Once again, it signals that when we allow higher and higher energies, the intermediate times dominate. The mutual information has the shape of a hump when the asymmetry of the intervals is small, but it becomes sharper and sharper until we reach the boundary condition of the validity [44].

When $x > d-x+l$, the timewise midmost section of mutual information becomes constant and has the value

$$I(A,B)(d-x+l<t<x) = \frac{c}{6}\log\left[\frac{(d+l)^2(d-2x)^2}{d(d+2l)((d-2x)^2-l^2)}\right], \tag{6.14}$$

which is independent of the UV regulator ε, i.e. the mutual information is independent of the strength of the quench. This constant behaviour cannot be understood with the quasiparticle picture, as the quasiparticles would never be at A and B simultaneously which would indicate that the mutual information should stay nearly zero the whole time.

Finally, when the two intervals are on the same side, we take the regions to be $A = [x, x+l]$ and $B = [x+l+d, x+2l+d]$ with $x, l, d > 0$. Based on the quasiparticle picture, we would expect that the mutual information would stay close to zero at all times. Like in the case of asymmetric intervals, this is not the case. The mutual information will have a constant value for most of the time but it will still vary quite a bit during the time evolution. The constant values are

$$I(t<x) = \frac{c}{3}\log\left[\frac{(l+d)^2(2x+2l+d)^2}{d(2x+l+d)(2l+d)(2x+3l+d)}\right] \tag{6.15}$$

$$I(l+x<t<d+l+x) = \frac{1}{2}I(0) \tag{6.16}$$

$$I(t>x+2l+d) = \frac{c}{3}\log\left[\frac{(l+d)^2}{d(2l+d)}\right] \tag{6.17}$$

The early and late times values correspond to the universal values of the two regions in semi-infinite line and infinite line, respectively. For the intermediate times, the behaviour is

$$I(x<t<x+l) = \tag{6.18}$$

$$\frac{c}{6}\log\left[\frac{(l+d)^3(2x+2l+d)^3(x+l+d-t)(x+2l+d+t)}{d^2(2x+l+d)(2l+d)(2x+3l+d)^2(x+l+d+t)(x+2l+d-t)}\right] \tag{6.19}$$

$$I(x+l+d<t<x+2l+d) = \tag{6.20}$$

$$\frac{c}{6}\log\left[\frac{(l+d)^3(2x+2l+d)(t-(x+l))(x+l+t)}{d^2(2l+d)(2x+3l+d)(t^2-x^2)}\right] \tag{6.21}$$

It is noteworty, that none of the expressions depend on the UV regulator ε. Also, this is yet another blow for the quasiparticle picture in the case of mutual information. It is clear that there is need for

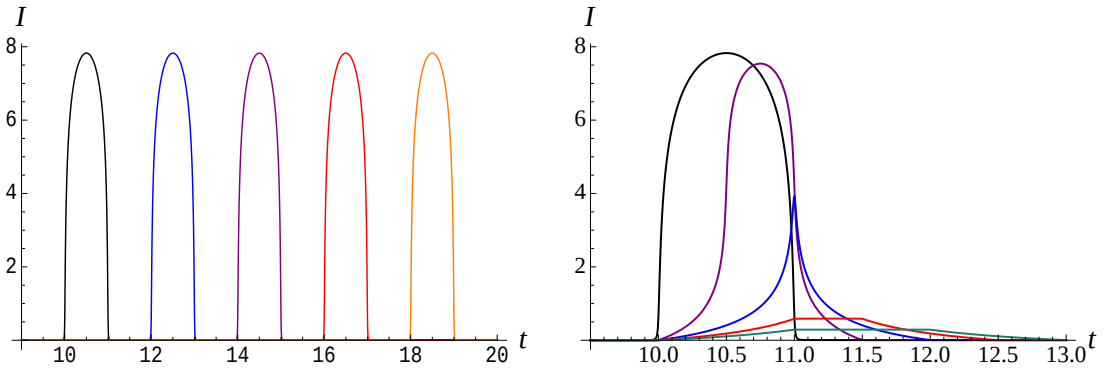

Figure 6.3: Time evolution of universal part of (rescaled) mutual information for two equal-length intervals. On the left, two symmetric intervals with length $l = 1$ and separation $d = 20, 24, 28, 32, 36$ from left to right. On the right we have intervals $[-11, -10]$ and $[10 + j/2, 11 + j/2]$ with $j = 0, 1, 2, 3, 4$. We see the effect of regime $x > d - x + l$ in the three figures from the right. These figures originally appeared in [44].

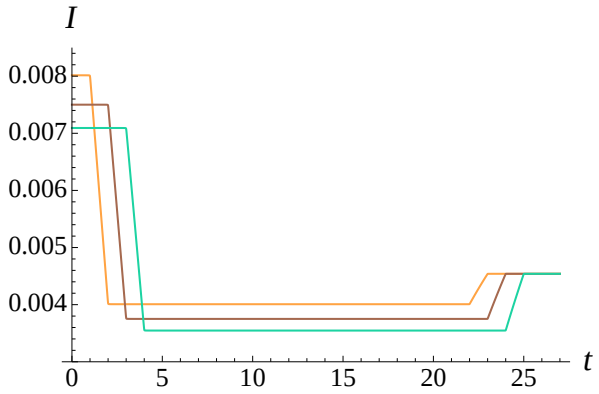

Figure 6.4: Time evolution of universal part of (rescaled) mutual information for two equal-length intervals. These are on the same side of the quench and have separation $d = 20$ and length $l = 1$. The distance from the defect is $x = 1, 2, 3$ from the top down. This figure originally appeared in [44].

a better model of mutual information evolution. One gets a clearer picture of the time evolution by consulting the figures (6.3) and (6.4) where several examples of time evolution have been plotted.

6.5.2 Falling particle perspective

Now we will repeat the analysis done above in the falling particle geometry in the same order. We will be needing our results from chapter 4 for the evolution of entanglement entropy. The analytic results will be mostly quoted from [44] and considered in the case $\alpha \ll 1$. As in the falling shell geometry, we only need to consider the disconnected and connected geodesics as the mixed geodesic turns out to be never minimal.

First, the case of symmetric intervals i.e. $A = [-(l + d/2), -d/2]$ and $B = [d/2, l + d/2]$. As the connected geodesics are symmetric about the interval, their contribution to the entanglement entropy of $A \cup B$ will not evolve in time. We also remember that the early and late times entanglement entropy are equal in the falling particle geometry equalling the vacuum value. Thus, if the separation of the two intervals is $d > d_{\text{vac}}$, the mutual information will vanish for times $t > l + d/2$ and $t < d/2$.

In the intermediate times, the difference between the two candidate geodesics is

$$S_{\text{disc.}} - S_{\text{con.}} = \frac{c}{3}\log\left[\frac{(\frac{d}{2}+l-t)(t-\frac{d}{2})l}{d(d+2l)\alpha}\tilde{M}\right], \frac{d}{2} < t < l+\frac{d}{2} \tag{6.22}$$

If the above is positive at some t, it is also the value of the mutual information at those times. The mutual information vanishes if the above expression is negative. Thus, we get the critical distance for the always vanishing entanglement entropy,

$$\tilde{d}_{sym} = \left(\sqrt{1+\frac{\tilde{M}l}{4\alpha}}\right). \tag{6.23}$$

The final expression for the mutual information for symmetric intervals is

$$I(t) = \begin{cases} \frac{c}{3}\log\left[\frac{l^2}{d(d+2l)}\right] & d < d_{vac} \text{ and } t < \frac{d}{2}, t > \frac{d}{2}+l, \\ \frac{c}{3}\log\left[\frac{l(\frac{d}{2}+l-t)(t-\frac{d}{2})\tilde{M}}{\alpha d(d+2l)}\right] & d < d_{vac} \text{ and } \frac{d}{2} < t < \frac{d}{2}+l, \\ 0 & d_{vac} < d < \tilde{d}_{sym} \text{ and } t < \frac{d}{2}, t > \frac{d}{2}+l, \\ \frac{c}{3}\log\left[\frac{l(d/2+l-t)(t-d/2)\tilde{M}}{\alpha d(d+2l)}\right] & d_{vac} < d < \tilde{d}_{sym} \text{ and } \frac{d}{2} < t < \frac{d}{2}+l, \\ 0 & \text{otherwise.} \end{cases} \tag{6.24}$$

We see that the mutual information is symmetric about its midpoint $t_{mid} = (d+l)/2$ where it also gains its maximum value, $I_max = \frac{c}{3}\log\frac{l^3\tilde{M}}{4\alpha d(d+2l)}$ and the overall shape is a hump. This agrees fairly well with the CFT results especially at long separations. The differences are the height of the hump and the asymmetry of it at shorter distances. At longer distances, the mutual information completely vanishes in the holographic picture but stays constant in the CFT case.

We now consider the asymmetric intervals with equal length, that is $A = [-(d-x+l), -(d-x)]$ and $B = [x, x+l]$. This time, the contribution of connecting geodesics also evolve in time and they have four different regimes of evolution. When we combine this with the fact that the separation provides 3 different options and that the single intervals have their own regimes of growth, we have simply too many options to be put in any sensible form. Hence, we let the figures in (6.5) speak for themselves and only comment on the qualitative features.

Qualitatively, the shapes of the mutual information is the same, but there is a difference in the maximum value of mutual information. The CFT results always have greater maximum value. The shape of the curves seem to agree better when the distance increases.

Finally, consider two intervals on the same side of the defect with $A = [x, x+l]$ and $B = [x+l+d, x+2l+d]$. The mutual information is never vanishing if the distance between the intervals is

$$d < \tilde{d} \equiv \left[\sqrt{1+\left(\frac{4\alpha}{\tilde{M}l}\right)^{2/3}} - 1\right] l. \tag{6.25}$$

In this case, the mutual information is

$$I(A,B) = \frac{1}{4G_N^{(3)}} \begin{cases} \log\left[\frac{l^4}{d^2(2l+d)^2}\right] & t < x, t > x+2l+d \\ \log\left[\frac{l^3(x+l-t)}{d^2(2l+d)(x+2l+d-t)}\right] & x < t < x+l \\ \log\left[\frac{l^4\alpha^2}{d(2l+d)(x+l+l-t)(t-(x+l))(x+2l+d-t)(t-x)\tilde{M}^2}\right] & x+l < t < x+l+d \\ \log\left[\frac{l^3(t-(x+l+d))}{d^2(2l+d)(t-x)}\right] & x+l+d < t < x+2l+d \end{cases}. \tag{6.26}$$

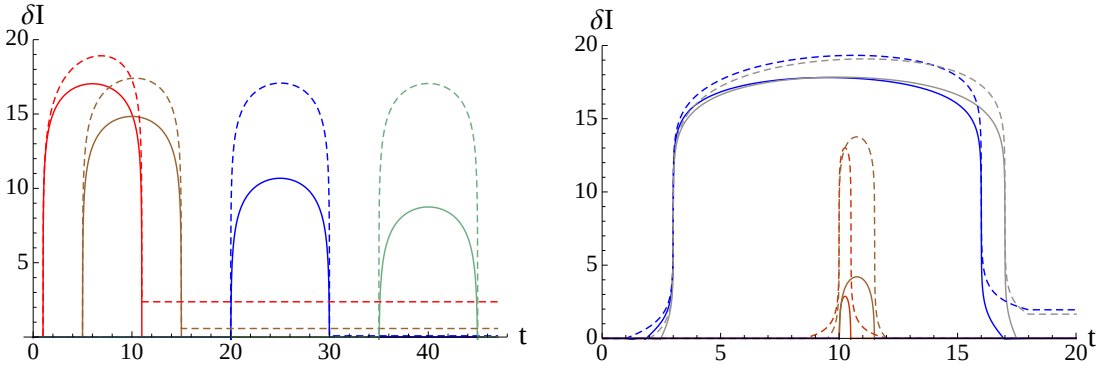

Figure 6.5: Time evolution of (rescaled) holographic mutual information of two equal-length intervals with the universal CFT results in dashed lines. In the left figure, symmetric intervals with $l = 10$ and $d = 2, 10, 40, 70$. On the right, asymmetric intervals with $x = 10$, $l = 2$ and $d = 18.5, 19, 19.5$ at the bottom and $x = 3$, $l = 15$ and $d = 4, 5$ at the top. The curves were calculated with $M = \frac{3}{4}$ and $\varepsilon = \alpha = 0.001$. These figures originally appeared in [44].

On the other hand, if $d > d_1 = (\sqrt{2}-1)l$, then the mutual information vanishes at all times. In the middle i.e. when $\tilde{d} < d < d_1$ the mutual information is

$$I(A,B) = \frac{1}{4G_N^{(3)}} \begin{cases} \log\left[\frac{l^4}{d^2(2l+d)^2}\right] & t < x, t > x+2l+d \\ \log\left[\frac{l^3(x+l-t)}{d^2(2l+d)(x+2l+d-t)}\right] & x < t < \tilde{l}_2 \\ 0 & \tilde{l}_2 < t < \tilde{l}_3 \\ \log\left[\frac{l^3(t-(x+l+d))}{d^2(2l+d)(t-x)}\right] & \tilde{l}_3 < t < x+2l+d \end{cases}, \tag{6.27}$$

where

$$\tilde{l}_2 = l + x + \frac{d^2(2l+d)}{d^2+dl-l^2} \leq l_2 \tilde{l}_3 = x - \frac{l^3}{d^2+dl-l^2} \geq l_3. \tag{6.28}$$

These have been plotted in figure (6.6) with the corresponding CFT results. The results have been scaled such that they would agree at $t = 0$. The general shapes share many similarities but for $\tilde{d} < d < d_1$, the holographic mutual information disappears at intermediate times, which cannot be explained with the quasiparticle picture. There is no such case for the CFT mutual information as it is always positive. And finally, the holographic mutual information vanishes abruptly, when the separation of the two regions is too large, a property that the CFT results do not share as the mutual information vanishes logarithmically with increasing separation.

Even though the results differ quite much, we must remember that the CFT results only contain the universal contributions. In any case, it can be concluded that the toy model of quasiparticles is not enough to explain the time evolution of mutual information.

6.6 Time evolution with Lifshitz scaling and hyperscaling violation

We will now move on to our final topic. We will consider time evolution of holographic mutual information in hyperscaling violating Lifshitz-AdS-Vaidya geometry in the thin shell limit. For the sake of simplicity, most emphasis is on intervals with equal length. The apparent horizon is set at $z_h = 1$ i.e. $M = 1$ and we only consider critical hyperscaling i.e. $\theta = d-1$ with Lifshitz scaling

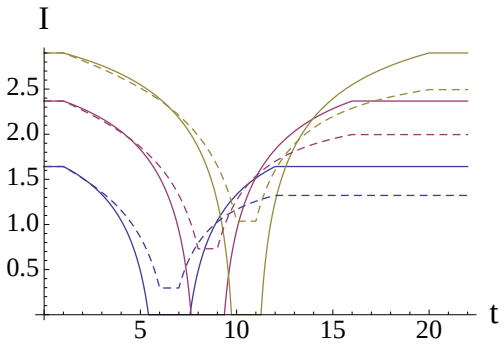

Figure 6.6: Time evolution of (rescaled) holographic mutual information of two equal-length intervals with the universal CFT results in dashed line. In this figure, the intervals are on the same side of the defect. The parameters are $x = 1, l = 10$ and $d = 0.008, 0.5, 0.1$ from the bottom up. Also, $M = 3/4$ and $\varepsilon = \alpha = 0.001$. The CFT results have been matched at $t = 0$ to get comparable results. This figure originally appeared in [44].

$\zeta = 3/2, 2$. We consider intervals with 3 different lenghts and each has five different separations. In addition, we briefly touch upon the subject of intervals with different lengths.

The geodesics must be solved numerically and great care must be taken to regularize them. The easiest methods to solve them is to use the shooting method and use bisection method to search for initial values which produce the correct boundary values. To make things more difficult, sometimes different initial values produce the same boundary values in which case we have competing extremal surfaces. The one with the smallest surface area will be chosen. Often, these are encountered near the saturation point where we usually have to deal with three different geodesics. This *swallow-tail* phenomenon was originally discovered in [77] and has also been discussed in [63]. The code used is a heavily modified from a code originally used in [80].

For equal-length intervals, it turns out that the higher value Lifshitz scaling parameter, ζ, causes the intermediate values and final value to be lower, supposing they are non-zero. Most of the effect is on the speed of the evolution process. For higher ζ, the process settles to its final value faster. Indeed, the name critical dynamical exponent turns out to describe the effect well. The side-by-side comparison can be seen in figure (6.7). It can be seen that the time evolution of mutual information has a similar shape as before with linear regime around its maximum value and constant value at early and late times.

For intervals with different lengths, there are now three different regimes of linear evolution. The change of ζ has no effect on the general shape of the time evolution. The evolution process happens faster for higher ζ and the intermediate and final value are lower for higher ζ. The phase transition can still occur if the mutual information starts or ends at zero-value. The comparison of a few examples can be seen in figure (6.8).

6.7 Discussion

It is unintuitive that mutual information would grow when doing a global quench. After all, the regions in thermal systems have lower mutual information than their vacuum counterparts. It can be partly understood with the quasiparticle picture where pairs of entangled particles are created

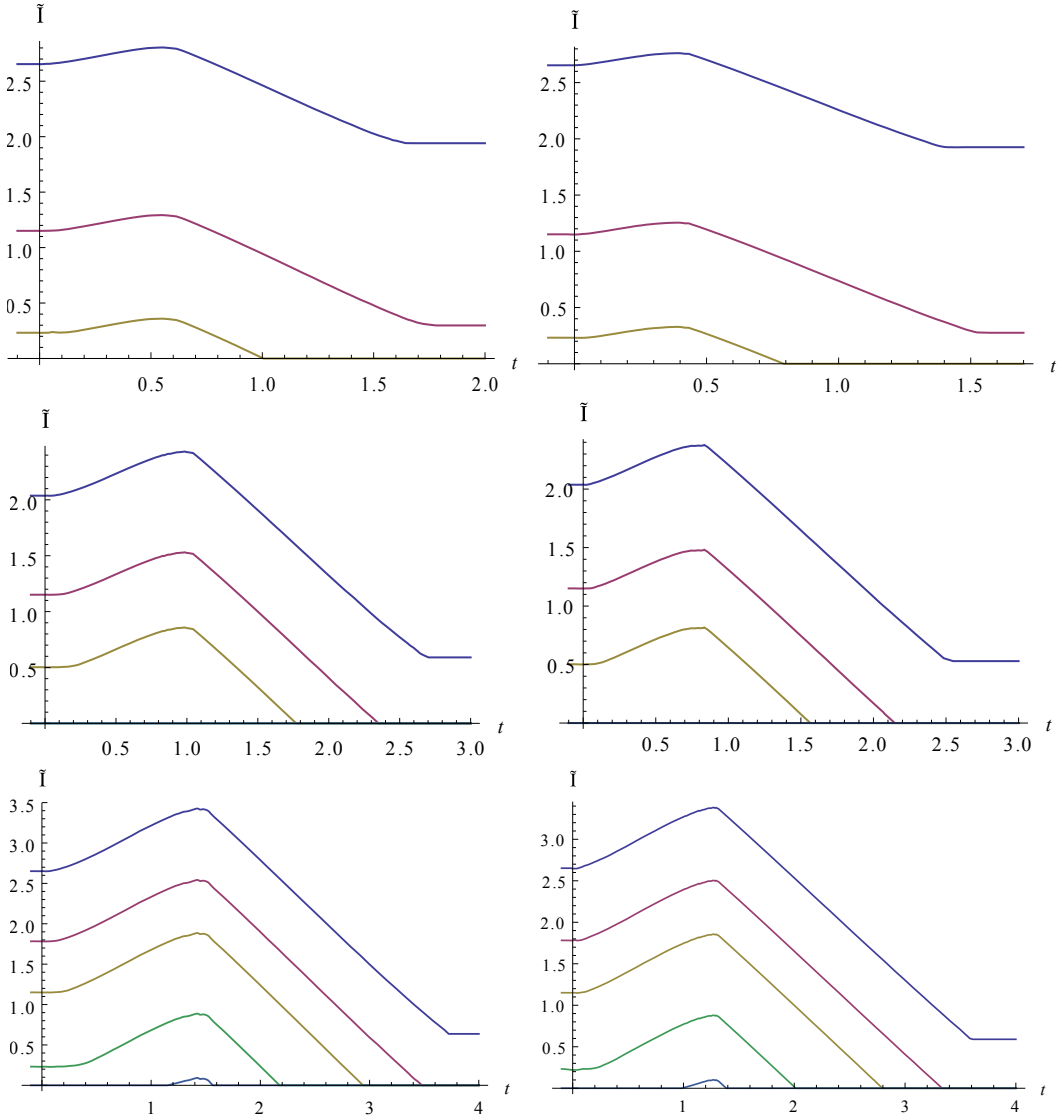

Figure 6.7: The time evolution of (rescaled) mutual information of two equal-length intervals with varying separation. On the left figures, $\zeta = \frac{3}{2}$ while on the right $\zeta = 2$. The top figures have from the top down $l = 2$ ($d = \frac{1}{4}, \frac{1}{2}, \frac{3}{4}, 1, \frac{3}{2}$), the middle ones have $l = 3$ and the bottom figures have $l = 4$ ($d = \frac{1}{2}, \frac{3}{4}, 1, \frac{3}{2}, 2$). The longest separations are identically zero for the shorter lengths.

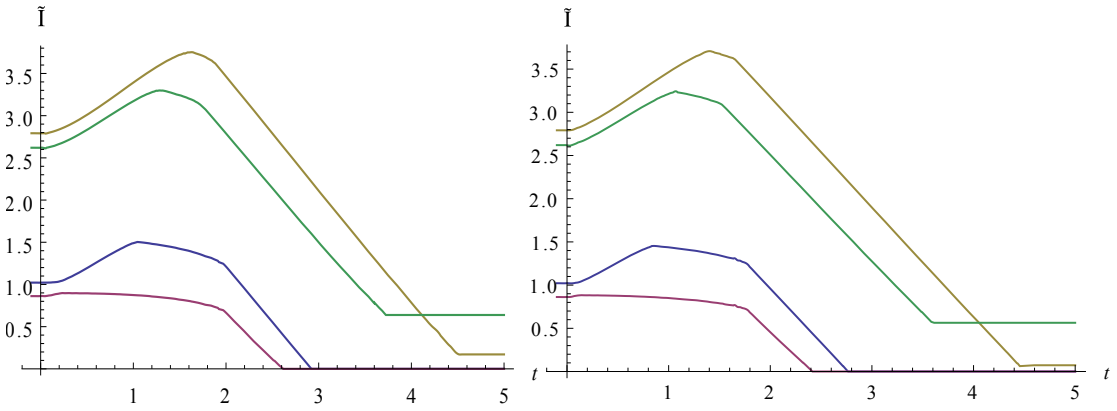

Figure 6.8: Time evolution of (rescaled) holographic mutual information for $d_\theta = 1$ for various intervals of different length and separation with $\zeta = \frac{3}{2}$ on the left and $\zeta = 2$ on the right. The parameters are from the bottom up $(l_1; l_2; d) = (1;5;0.5), (3;5;1), (3.5;4.5;0.5), (4.25;4.75;0.5)$.

everywhere at $t = 0$ and the mutual information of A and B grows if the particles created at the same point are at the two regions simultaneously. However, as seen in the simple case of AdS_3/Vaidya metric, this approach experiences some great difficulties even with the usual AdS_3/Vaidya picture.

Similar arguments can be used to explain the behaviour of mutual information after a local quench or the local energy injection. However, as seen above, this fails in the case where the two regions are on the same side of the defect. Quasiparticle picture would imply that the mutual information would stay constant. This was not the case.

We saw that the holographic picture allows us to calculate the mutual information straightforwardly even though we might not be able to derive an analytic result. For large separations the mutual information becomes identically zero, which would indicate that the two regions would not be entangled. It is not yet clear, whether this also happens in the CFT picture, even though it is known that the explicit expression for mutual information cannot be completely right.

Mutual information in hyperscaling violating Lifshitz-AdS/Vaidya metric had not been considered before. In the special cases that we considered, the results were only surprising in the sense how little the change of critical dynamical exponent affected the intermediate values of mutual information. It would be interesting to consider the time evolution in more diverse situations i.e. with varying value of d_θ.

We saw that the UV divergences were cancelled for almost every situation that we considered. Unfortunately, they did not vanish in (6.22) or (6.24). To remove all divergences we could consider three disjoint regions and their tripartite information as considered in [22, 23]. However, these are yet to be considered for local quenches or for Lifshitz scaling and hyperscaling violating spacetimes.

Chapter 7

Conclusions and discussion

7.1 A review

In this thesis, we have studied entanglement entropy in numerous static and dynamic cases in conformal field theories and, more importantly, from the holographic perspective. In the final chapter, we also considered mutual information mostly from a holograhic point of view, critical distances corresponding to it and also its time evolution.

In the 2D conformal field theory approach, we saw how we could study many different systems by considering different geometries. The replica trick approach with the use of Riemann surfaces was discovered to be an essential part of a mathematical toolbox for calculating entanglement entropies. Often, it was useful to use twist fields in the calculations. Even though we considered mostly just cases with a single interval, the replica trick is still the standard tool in further studies [34, 35]. When considering multiple intervals in static cases and even just a single finite interval in systems with a boundary, we encountered theory specific functions which made the calculations impossible without specifying the full content of the theory. These functions have been calculated for some theories but their analytic continuation has proven to be difficult and they are one of the biggest obstacles in general conformal field theory calculations.

In the static cases, we encountered the logarithmic scaling of the entanglement entropy which was prominent in many of our results. We could easily modify the results to study either finite temperature or finite length and systems with a small mass gap. These results had been confirmed for some lattice models [8].

However, when we considered the time evolution of entanglement entropy, we got some interesting results. In the case of global quench, we changed the time evolution controlling Hamiltonian globally. The entanglement entropy evolved quadratically at the very early times, but soon started a linear growth which lasted until the critical time, $t_c = l/2$ for the single interval in an infinite system and $t_c = l$ for the single interval at the boundary of a semi-infinite system. After the critical time, the entanglement entropy abruptly stopped evolving and gained a constant value which was linear in l corresponding to a value of thermal entropy with an effective temperature $\beta_{\text{eff}} = 4\tau_0$. This was interpreted that the outside region acted as a heat bath for the studied region, emitting quasiparticles which transmitted the entanglement across the system. The quasiparticle model

could also explain the linear growth of entanglement entropy and the non-abrupt change of the growth of it after the critical time, which is observed in lattice systems. The effective temperature is also seen in general two-point functions of the system [41]. Thus, the global quench has the interpretation of a global injection of energy.

The other kind of time evolution considered was the local quench which involved the joining of two semi-infinite real lines to form a single conformal system. Initially, the system has the entanglement entropy of its two half-lines but after the joining, it starts growing logarithmically. In the case of an infinite interval, it continues growing logarithmically forever. In the case of a finite interval, it reaches a peak after some time and then decreases to the entanglement entropy of a finite interval in an infinite system, as is expected. The quasiparticle picture can explain the behaviour of entanglement entropy with quasiparticles emitted from the joining site. As the entanglement entropy reaches its usual conformal field theory value, we can interpret the local quench as a local injection of energy which dissipates into the whole system.

We then considered the holographic approach to calculate entanglement entropy. The holographic conjecture of entanglement entropy i.e. the Ryu-Takayanagi formula transformed the complicated CFT calculations to relatively simple calculations of minimal surfaces in AdS space. We were able to reproduce the static entanglement entropies for a single interval with ease. The dreaded case of multiple intervals was transformed to a case of a multitude of possible minimal surfaces. The expression for multiple intervals cannot be that simple in reality as the expression is independent of the specific field theory. Nevertheless, the holographic entanglement entropy predicts a phase transition in the entanglement entropy as the two intervals get farther from each other, which is also expected in large c conformal field theories [58].

Arguably, the most useful application of the RT formula was the ability to study multidimensional systems as easily as two dimensional systems. They correctly produced the area law and for spherical regions, we got the universal term for the even dimensional spacetimes as predicted by conformal field theories. Unfortunately, these results have not been verified to be true as there are few exact multidimensional results.

A more interesting case is to study the global and local quenches in the holographic picture. The time dependent background metric forces us to consider extremal geodesics and surfaces. Since a black hole corresponds to a thermal state and a global quench to an injection of energy, the global quench in the holographic picture should correspond to a formation of a black hole i.e. the AdS/Vaidya metric. We recovered the quadratic growth at the early times and the linear growth at the intermediate times. For $1+1$ dimensions, the time derivative of entanglement entropy was continuous. In higher dimensions, the spherical regions have a continuous time derivative of the entanglement entropy at the critical time while the strip geometry does not. In addition, the spherical regions exhibited a memory loss regime where the time development of entanglement entropy depended only on the difference between the current time and the saturation time. The quasiparticle model of the conformal field theories has been generalized to higher dimensions in the form of entanglement tsunami [75]. It correctly reproduces the initial quadratic growth and the linear growth of the intermediate times for general shapes along with the memory loss regime for the spherical regions. The AdS/Vaidya geometry has found its applications in study of

thermalization, implying top-down thermalization i.e. that the short range modes thermalize first. Similar results hold for analysis with Green functios and Wilson loops.

For the local quench, we tried two different approaches. We studied the metric caused by the falling particle. Many of the qualitative properties were reproduced, including the hump for a single interval. However, there was a clear quantitative disagreement with the universal terms of the CFT results. For $1+1$ dimensions, we obtained the metric caused by a massive falling star and a black hole. The falling particle approach was also applicable to multiple dimensions but the calculations require some demanding numerical methods to study the metric extensively. However, some general features have been found analytically.

We also considered another approach for AdS_3, which involved finding a suitable coordinate transformation such that the holographic stress energy tensor would match the one in the boundary CFT. The calculations were somewhat simpler and yielded a special case solution of the falling particle approach.

One chapter was dedicated to studying generalization of AdS/Vaidya metric to include Lifshitz scaling and hyperscaling violation. The former has its counter part in field theories and the latter gives rise to effective dimensions and may be the key to studying systems with a Fermi surface from the holographic perspective as it can reproduce a logarithmic scaling correction to the area law. The study of holographic evolution yielded a general power law for the early growth and linear growth for the intermediate times, generalizing the behaviour of the usual AdS/Vaidya metric.

The final chapter discussed mutual information of two disjoint regions in both static and dynamical cases. All of the studied cases exhibited non-analyticity at some separation or at some point in time. For the static cases, there were a few analytic solutions to critical distances. In the dynamic cases, we compared the CFT results with the holographic results. There were qualitative agreements but the largest disagreement came in the form that mutual information may vanish for the whole time for large distances in the holographic picture where as in conformal field theories it will always be non-zero at some time. As a new result, we studied the mutual information in the hyperscaling violating Vaidya-Lifshitz metric. We found that the time evolution of mutual information varies little with the most obvious effect being the faster evolution with higher ζ.

7.2 Future research topics

There are still numerous open questions in the study of entanglement entropy. In the conformal field theory approach, the case of multiple intervals is still a mystery for the most part. The theory specific functions appearing with n-point functions have been solved for few theories and there is still much research to be done.

The general proof for the holographic entanglement entropy formula remains undone. There is only a proof for the case of spherical entangling surfaces [59]. In addition, it is already known that the formula is only approximate and some higher order corrections to it have been calculated [88]. It would also be interesting to calculate the time evolution of entanglement entropy in the falling particle metric in multiple dimensions. In addition, the generalization of the falling particle metric to the Lifshitz scaling, hyperscaling violating case has not been done yet.

Another approach to studying entanglement entropy is to study the *entanglement negativity*. It is defined as follows. Consider the bipartition of a system in the state $|\psi\rangle = a_{ij}|\phi_i\rangle_A|\chi_j\rangle_B$ and with the density matrix $\rho = \langle\psi||\psi\rangle = a_{i'j'}a_{ij}\langle\phi'_i|\langle\chi'_j||\phi_i\rangle|\chi_j\rangle$. The partial transpose of ρ is defined as $[\rho^{T_2}]_{i'j'ij} = [\rho]_{i'jij'}$ i.e. we exchange the indices corresponding to the other part of the system. The logarithmic entanglement negativity is

$$\mathscr{E} = \log \mathrm{Tr}|\rho^{T_2}|, \tag{7.1}$$

where we take the trace over the absolute values of eigenvalues of the partially transposed density matrix. If the value is negative, the system is entangled. Unfortunately, the reverse is not true. However, due to the simpler form compared to entanglement entropy, there has been interest in it [89].

As a physical application, the entanglement entropy could provide us with a tool to formulate quantum gravity. Before that, it might give us some insight into understanding the black hole entropy which is suspected to be the entanglement entropy of the black hole [16]. As a more down to earth topic, the entanglement entropy has already been applied to study thermalization with success [63]. Another possible application is to study phase transitions in condensed matter systems [14].

Entanglement entropy has never been measured. Its nonlocal nature makes it very difficult if not impossible to measure directly. However, there have been proposals for measurement setups. One such proposal is to have long thin lead bars, first separated, and then connected at time $t = 0$. The idea is to measure the amount of electrons transmitted at the contact point due to quantum noise and then relate the results to entropy. At the lowest order, the theory reproduces the entanglement entropy after a local quench. However, much work still needs to be done before actual measurements can happen [90].

This thesis has barely scratched the surface of vast amount of literature available for entanglement entropy. The concept is relatively new and much work has been done in the past 10 years. We have only considered general, solvable models while much work has also been done for cases where our results do not apply, e.g. [16, 20, 30]. The references of this thesis and the references therein should provide an interested reader with a multitude of more cases, general results and different approaches to the problem.

Bibliography

[1] J. Bekenstein; *Black holes and entropy*, Phys.Rev. D**7**, 2333-2346, (1973).

[2] S. Hawking; *Particle creation by black holes*, Commun.Math.Phys. **43**, 199-220, (1975).

[3] G. 't Hooft; *On the quantum structure of a black hole*, Nucl.Phys. B**256**, 727, (1985).

[4] L. Bombelli, R. Koul, J. Lee, R. Sorkin; *Quantum source of entropy for black holes*, Phys.Rev. D**34**, 373 (1985).

[5] M. Srednicki; *Entropy and Area*, Phys.Rev.Lett. **71** 666-669 (1993). arXiv:hep-th/9303048.

[6] L. Susskind; *Some speculations about black hole entropy in string theory*, (1993). arXiv:hep-th/9309145.

[7] C. Holzhey, F. Larsen, F. Wilczek; *Geometric and renormalized entropy in conformal field theory*, Nucl.Phys. B**424**, 443-467, (1994). arXiv:hep-th/9403108

[8] P. Calabrese, J. Cardy; *Entanglement Entropy and Conformal Field Theory*, J.Phys. A**42**, 504005, (2009). arXiv:0905.4013

[9] B.-Q. Jin, J. Korepin; *Quantum Spin Chain, Toeplitz Determinants and Fisher-Hartwig Conjecture*, Journal of Statistical Physics, **116**, 1-4, 79-95, (2004). arXiv:quant-ph/0304108

[10] A. Its, B.-Q. Jin, V. Korepin; *Entanglement in XY Spin Chain*, Journal Phys. A: Math. Gen. **38**, 2975-2990, (2005). arXiv:quant-ph/0409027.

[11] J. Eisert, T. J. Osborne; *General Entanglement Scaling Laws from Time Evolution*, Phys. Rev. Lett. **97**, 150404, (2006). arXiv:quant-ph/0603114.

[12] I. Peschel; *On the entanglement entropy for a XY spin chain*, J. Stat. Mech. P12005, (2004). arXiv:cond-mat/0410416.

[13] S. Ryu, T. Takayanagi: *Holographic Derivation of Entanglement Entropy from AdS/CFT*, Phys.Rev.Lett. **96**, 181602, (2006). arXiv:hep-th/0603001v2.

[14] K.L. Hur; *Entanglement Entropy, decoherence, and quantum phase transition of a dissipative two-level system*, Annals of Physics **323**, 2208-2240, (2008). arXiv:0711.2301.

[15] T. Takayanagi; *Holographic Entanglement Entropy, Fractional Quantum Hall Effect and Lifshitz-like Fixed Point*, J. Phys.: Conf. Ser. **462**, 012053, (2013).

[16] S. Solodukhin; *Entanglement entropy of black holes*, Living Rev. Relativity **14**, 8, (2011). arXiv:1104.3712.

[17] J. Preskill; *Quantum Computation*, Lecture notes at Caltech, (1999).

[18] E. Lieb, M. Ruskai; *Proof of the Strong Subadditivity of Quantum Mechanichal Entropy*, J. Math. Phys. **14**, 1938–1941 (1973).

[19] H. Araki, E.H. Lieb; *Entropy inequalities*, Comm. Math. Phys. **18**, 2, 160-170, (1970).

[20] J. Eisert, M. cramer, M. Plenio; *Area laws for the entanglement entropy - a review*, Rev.Mod.Phys. **82**, 277, (2010). arXiv:0808.3773.

[21] D. Gioev, I. Klich; *Entanglement entropy of fermions in any dimension and the Widom conjecture*, Phys. Rev. Lett. **96**, 100503, (2006). arXiv:quant-ph/0504151.

[22] V. Balasubramanian, A. Bernamonti, N. Copland, B. Craps, F. Galli; *Thermalization of mutual and tripartite information in strongly coupled two dimensional conformal field theories*, Phys. Rev. D **84**, 105017, (2011). arXiv:1110.0488.

[23] A. Allais, E. Tonni; *Holographic evolution of the mutual information*, JHEP **1201**, 102, (2011). arXiv:1110.1607.

[24] P. Di Francesco, P. Mathieu, D. Senechl; *Conformal Field Theory*, Springer, 2nd ed., (1999)

[25] P. Ginsparg; *Applied Conformal Field Theory*, Lectures given at Les Houches summer session, 1988. arXiv:hep-th/9108028

[26] J. Cardy; *Conformal Invariance and Statistical Mechanics*, Lectures given at Les Houches summer session, 1988.

[27] P. Calabrese, J. Cardy; *Entanglement Entropy and Quantum Field Theory*, J.Stat.Mech **0406**, Springer, (2004). arXiv:hep-th/0405152.

[28] S. Ryu, T. Takayanagi; *Aspects of Holographic Entanglement Entropy*, JHEP **0608**, 045, (2006). arXiv:hep-th/0605073.

[29] J. Cardy, O. Castro-Alvaredo, B. Doyon; *Form factors of branch-point twist fields in quantum integrable models and entanglement entropy*, J. Stat. Phys. **130**, 129, (2007). arXiv:0706.3384.

[30] H. Casini, M. Huerta; *Entanglement entropy in free quantum field theory*, J.Phys. A**42**, 504007, (2009). arXiv:0905.2562.

[31] F. Carlson; *Sur une classe de séries de Taylor*, Dissertation, Uppsala, Sweden, (1914).

[32] Azeyanagi, T. Nishioka, T. Takayanagi; *Near Extremal Black Hole Entropy as Entanglement Entropy via AdS2/CFT1*, Phys.Rev. D**77**, 06400, (2008). arXiv:0710.2956.

[33] M. Caraglio, F. Gliozzi; *Entanglement Entropy and Twist Fields*, JHEP **0811**, 076, (2008). arXiv:0808.4094.

[34] P. Calabrese, J. Cardy, E. Tonni; *Entanglement entropy of two disjoint intervals in conformal field theory*, J.Stat.Mech. **0911**, P11001, (2009). arXiv:0905.2069.

[35] P. Calabrese, J. Cardy, E. Tonni; *Entanglement entropy of two disjoint intervals in conformal field theory II*, J.STat.Mech. **1101**, P01021, (2011). arXiv:1011.5482.

[36] F. Franchini, A. Its, V. Korepin; *Rényi Entropy of the XY Spin Chain*, J. Phys. A **41**, e025302, (2008). arXiv:0707.2534.

[37] R. Weston; *The Entanglement Entropy of Solvable Lattice Models* J. Stat. Mech. L03002, (2006). arXiv:math-ph/0601038.

[38] P. Calabrese, J. Cardy; *Evolution of Entanglement Entropy in One-Dimensional Systems*, J.Stat.Mech. **0504** P04010, (2005). arXiv:cond-mat/0503393

[39] M. Fagotti, P. Calabrese; *Entanglement entropy of two disjoint blocks in XY chains*, J.Stat.Mech. **1004**, P04016, (2010). arXiv:1003.1110

[40] S. Bravyi, M. B. Hastings, and F. Verstraete, *Lieb-Robinson Bounds and the Generation of Correlations and Topological Quantum Order*, Phys. Rev. Lett. **97**, 050401, (2006). quant-ph/0603121.

[41] P. Calabrese, J. Cardy; *Quantum Quenches in Extended Systems*, J.Stat.Mech. **0706** P06008 (2007). arXiv:0704.1880.

[42] S. Sotiriadis, J. Cardy; *Inhomogeneous quantum quenches*, J. Stat. Mech. **0811**, P11003, (2008). arXiv:0808.0116.

[43] P. Calabrese, J. Cardy; *Entanglement and correlation functions following a local quench: a conformal field theory approach*, J.Stat.Mech. **0710**, P10004, (2007). *arXiv:0708.3750*.

[44] C. Asplund, A. Bernamonti; *Mutual information after a local quench in conformal field theory*, (2013). arXiv:1311.4173.

[45] T. Ugajin; *Two dimensional quantum quenches and holography*, (2013). arXiv:1311.2562.

[46] M. Fagotti and P. Calabrese, Evolution of entanglement entropy following a quantum quench: Analytic results for the XY chain in a transverse magnetic field, Phys. Rev. A 78, 010306(R) (2008). arXiv:0804.3559.

[47] A. Zamolodhickov; *"Irreversibility" of the Flux of the Renormalization Group in a 2-D Field Theory*, JETP Lett **43**, 730-732, (1986).

[48] D. Fursaev, S. Solodukhin; *On the Description of the Riemannian Geometry in the Presence of Conical Defects*, Phys.Rev. D**52**, 2133-2143, (1995). arXiv:hep-th/9501127.

[49] G. 't Hooft; *Dimensional Reduction in Quantum Gravity*, (1993). arXiv:gr-qc/9310026.

[50] L. Susskind; *The World as a Hologram*, J.Math.Phys. **36**, 6377-6396, (1995). arXiv:hep-th/9409089

[51] J. Maldacena; *The Large N Limit of Superconformal Field Theories and Supergravity*, Adv.Theor.Math.Phys. **2**, 231-252, (1998). arXiv:hep-th/9711200

[52] E. Witten; *Anti De Sitter Space And Holography*, Adv.Theor.Math.Phys. **2**, 253-291, (1998). arXiv:hep-th/9802150

[53] O. Aharony, S. Gubser, J. Maldacena, H. Ooguri, Y. Oz; *Large N Field Theories, String Theory and Gravity*, Phys.Rept. **323**, 183-386, (2000). arXiv:hep-th/9905111

[54] H. Nastase; *Introduction to AdS-CFT*, lecture notes, (2007). arXiv:0712.0689

[55] S. Hartnoll; *Lectures on holographic methods for condensed matter physics*, Class.Quant.Grav. **26**, 224002, (2009). arXiv:0903.3246.

[56] S. Caroll; *Spacetime and Geometry: An Introduction to General Relativity*, Addison-Wesley, (2003).

[57] D. Fursaev; *Proof of the Holographic Formula for Entanglement Entropy*, JHEP **0609**, 018, (2006). arXiv:hep-th/0606184.

[58] M. Headrick; *Entanglement Renyi entropies in holographic theories*, Phys.Rev.D **82**, 126010, (2010). arXiv:1006.0047.

[59] H. Casini, M. Huerta, R. Myers; *Towards a derivation of holographic entanglement entropy*, JHEP **1105**, 036, (2011). arXiv:1102.0440.

[60] M. Headrick, T. Takayanagi: *A holographic proof of the strong subadditivity of entanglement entropy*, Phys.Rev. D**76**, 106013, (2007). arXiv:0704.3719

[61] M. Headrick; *General properties of holographic entanglement entropy*, (2013). arXiv:1312.6717v1

[62] J. Aparicio, E. Lopez; *Evolution of Two-Point Functions from Holography*, (2011). arXiv:1109.3571.

[63] V. Balasubramanian, A. Bernamonti, J. de Boer, N. Copland, B. Craps, E. Keski-Vakkuri, B. Müller, A. Schäfer, M. Shigemori, W. Staessens; *Holographic Thermalization*, Phys.Rev. D **84**, 026010, (2011). arXiv:1103.2683.

[64] J. Molina-Vilaplana; *Holographic Geometries of one-dimensional gapped quantum systems from Tensor Network States*, JHEP **05**, 024, (2013). arXiv:1210.6759.

[65] A. Kitaev, J. Preskill; *Topological entanglement entropy*, Phys.Rev.Lett. **96**, 110404, (2006). arXiv:hep-th/0510092.

[66] T. Nishioka, T. Takayanagi; *AdS Bubbles, Entropy and Closed String Tachyons*, JHEP **0701**, 090, (2007). arXiv:hep-th/0611035.

[67] M. Ishihara, F-L. Lin, B. Ning; *Refined Holographic Entanglement Entropy for the AdS Solitonsand AdS black Holes*, (2012). arXiv:1203.6153.

[68] F. Haehl; *The Schwarzschild-Black String AdS Soliton: Instability and Holographic Heat Transport*, Class. Quantum Grav. **30**, 055002, (2013). arXiv:1210.5763.

[69] Y. Nakagawa, A. Nakamura, S. Motoki, V.I. Zakharov; *Entanglement entropy of SU(3) Yang-Mills theory*, PoS LAT2009: 188, (2009). arXiv:0911.2596.

[70] R. Bousso; *A Covariant Entropy Conjecture*, JHEP **9907**, 004, (1999). arXiv:hep-th/9905177.

[71] R. Bousso; *The holographic principle*, Rev.Mod.Phys. **74**, 825-874, (2002). arXiv:hep-th/0203101.

[72] V. Hubeny, M. Rangamani, T. Takayanagi; *A Covariant Holographic Entanglement Entropy Proposal*, JHEP **0707**, 062, (2007). arXiv:0705.0016

[73] P. Vaidya; *Newtonian Time in General Relativity*, Nature **171**, 260-261, (1953).

[74] J. Abajo-Arrastia, J. Aparicio, E. Lopez; *Holographic Evolution of Entanglement Entropy*, JHEP **1011**, 149, (2011). arXiv:1006.4090

[75] H. Liu, S.J. Suh; *Entanglement Tsunami: Universal Scaling in Holographic Thermalization*, Phys. Rev. Lett. **112**, 011601, (2014). arXiv:1305.7244

[76] H. Liu, S.J. Suh; *Entanglement growth during thermalization in holographic systems*, (2013). arXiv:1311.1200.

[77] T. Albash, C. Johnson; *Evolution of Holographic Entanglement Entropy after Thermal and Electromagnetic Quenches*, New J.Phys. **13**, 045017, (2011). arXiv:1008.3027.

[78] R. Baier, A. Mueller, D. Schiff, D. Son; *Bottom-up thermalization in heavy ion collisions*, Phys.Lett. B**502**, 51-58, (2000). arXiv:hep-ph/0009237.

[79] M. Alishahiha, A. Astaneh, M. Mozaffar; *Thermalization in Backgrounds with Hyperscaling Violating Factor*, (2014). arXiv:1401.2807.

[80] P. Fonda, L. Franti, V. Keränen, E. Keski-Vakkuri, E. Tonni, L. Thorlacius; *Holographic thermalization with Lifshitz scaling and hyperscaling violation*, (2014). arXiv:1401.6088.

[81] T. Takayanagi, T. Ugajin; *Measuring Black Hole Formations by Entanglement Entropy via Coarse-Graining*, JHEP **1011**, 054, (2010). arXiv:1008.3439.

[82] M. Nozaki, T. Numasawa, T. Takayanagi; *Holographic Local Quenches and Entanglement Density*, (2013). arXiv:1302.5703.

[83] V. Balasubramanian, P. Kraus; *A Stress Tensor for Anti-de Sitter Gravity*, Commun.Math.Phys. **208**, 413-428, (1999). arXiv:hep-th/9902121.

[84] M. Roberts; *Time evolution of entanglement entropy from a pulse*, JHEP **1212**, (2012). arXiv:1204.1982.

[85] L. Huijse, S. Sachdev, B. Swingle *Hidden Fermi surfaces in compressible states of gauge-gravity duality*, Physical Review B **85**, 035121, (2012). arXiv:1112.0573.

[86] S. Kachru, X. Liu, M. Mulligana; *Gravity Duals of Lifshitz-like Fixed Points*, Phys.Rev. D**78**, 106005, (2008). arXiv:0808.1725.

[87] V. Keränen, L. Thorlacius; *Holographic geometries for condensed matter applications*, (2013). arXiv:1307.2882.

[88] J. de Boer, M. Kulaxizi, A. Parnachev; *Holographic Entanglement Entropy in Lovelock Gravities*, JHEP **1107**, 109, (2011). arXiv:1101.5781.

[89] P. Calabrese, J. Cardy, E. Tonni; *Entanglement negativity in quantum field theory*, Phys. Rev. Lett. **109**, 130502, (2012). arXiv:1206.3092.

[90] I. Klich, L. Levitov; *Quantum Noise as an Entanglement Meter*, Phys.Rev.Lett. **102**, 100502, (2009). arXiv:0804.1377.